LITERATURE REVIEW: APPLICATIONS FOR

# Traumatic brain injury

F. Marsili

## 1. NEUROPLASTICITY

ALGIAMED

# Author's choice

Traumatic brain injury (TBI) is a lesion of the brain which occurs as a consequence of trauma following falls (40.5%) or car/motor accidents (14.3%) [1]. Birth brain injuries are a sub-category of TBI with a yearly prevalence of 26.46 per 1000 hospital births [2]. Generally, TBI is associated with older individuals, aged 75 or above. Though children with birth brain damage (birth related or otherwise) cover a relatively small percentage of the total TBI population, the significant impact of TBI on the quality of life of children, of their parents and their extended families, makes the research on the improvement of TBI symptomatology especially relevant [2], [3].

The first few weeks or months of an infant are the most critical: children are born with around 100 billion neurons, which are yet to be connected. Neuroplastic events occur continuously during the first developing phases of a newborn, where connections are build and wired experientially [4]. This fact makes early detection and intervention on newborns with TBI essential.

Electrical stimulation therapies have been demonstrated to have significant effects on recovery from brain injuries, such as stroke, ischaemic events, brain and spinal cord trauma, and TBI [5], [6], [7]. Even though the exact underlying mechanisms of electrical stimulation are yet to be understood, clinical evidence shows its efficacy on neurophysiological reorganisation of cortical areas as well as functional recovery including facilitation of movements and pain relief [8], [9]. It can be concluded that electrical stimulation takes advantage of the neuroplastic ability of peripheral nerves and central neurons to trigger adaptive cascades to counteract the maladaptation occurring as a consequence of injuries or disease.

In this collection of papers, we first explore the concept of neuroplasticity, with particular focus on the significance of cortical organisation in developing brains and the role that electrical stimulation plays in triggering reorganisation of cortical areas in developing as well as adult brains. Following, we focus on the clinical evidence of electrical stimulation in enhancing both functional peripheral recovery (e.g., motor and sensory functions) and cortical adjustments (e.g., plastic changes on sensorimotor cortex).

In summary, TBI is a condition significantly affecting the quality of life of the individuals affected by it. In the case of birth brain injuries, children and their families experience significant and long-term impact on their daily lives. Being able to leverage on the brain's ability to reorganise after maladaptation using neuroplastic processes could have an essential role in the treatment of TBI in infants and children. The following papers explore the role that electrical stimulation could have in enhancing adaptive, neuroplastic responses in TBI: a potential therapeutic application for children with brain injuries.


[1]Shepher Center (2022) Leading causes and statistics for traumatic brain injuries. https://www.myshepherdconnection.org/abi/Introduction-to-Brain-Injury/Statistics-and-Causes

[2] Gupta, Ruby and Cabacungan, Erwin T. (2021) Neonatal birth trauma: analysis of yearly trends, risk factors, and outcomes. *The Journal of Paediatrics* 238(E3): P174-P180. doi: 10.1016/j.jpeds.2021.06.080

[3] Jansheski, Gina (2022) Infant brain damage. https://www.cerebralpalsyguidance.com/birth-injury/infant-brain-damage/

[4] Hampton, Debbie (2019) Age-related decline: how neuroplasticity changes over your brain's lifetime. *The Best Brain Possible: Information and Inspiration for Anyone with a Brain.* https://thebestbrainpossible.com/neuroplasticity-brain-changes-baby/

[5] Hofer, Anna-Sophie and Schwab, Martin E. (2019) Enhancing rehabilitaation and functional recovery after brain and spinal cord trauma with electrical neuromodulation. *Current Opinion in Neurology,* 32(6): p828-p835. doi: 10.1097/WCO.0000000000000750

[6] Bath, Philip M. et al. (2020) Pharyngeal electrical stimulation for neurogenic dysphagia following stroke, traumatic brain injury or other causes: main results for the PHADER cohort study. *EClinical Medicine*, 28:100608. doi: 10.1016/j.eclinm.2020.100608

[7] Bao, Shi-chun et al. (2020) Rewiring the lesioned brain: electrical stimulation for post-stroke motor restoration. *Journal of Stroke,* 22(1): p47-p63. doi: 10.5853/jos.2019.03027

[8] Deer, Timothy R. et al. (2021) Peripherally induced reconditioning of the central nervous system: a proposed mechanistic theory for sustained relief of chronic pain with percutaneous peripheral nerve stimulation. *Journal of Pain Research,* 14: p721-p736. doi: 10.2147/JPR.S297091

[9] Ebrahimzadeh, Masoome et al. (2021) Effect of functional electrical stimulation combined with stationary cycling and sit to stand training on mobility and balance performance in a patient with traumatic brain injury: a case report. *Anaals of Medicine and Surgery,* 72(103122), doi: 10.1016/j.amsu.2021.103122

# 1. Neuroplasticity

**Open access sources:** **Page**

*J Neurophysiol* 89: 3205–3214, 2003;
10.1152/jn.01143.2002.

# Reorganization of Remote Cortical Regions After Ischemic Brain Injury: A Potential Substrate for Stroke Recovery

**S. B. Frost, S. Barbay, K. M. Friel, E. J. Plautz, and R. J. Nudo**

*Center On Aging, Department of Molecular and Integrative Physiology; and Mental Retardation Research Center, University of Kansas Medical Center, Kansas City, Kansas 66160*

Submitted 18 December 2002; accepted in final form 19 February 2003

**Frost, S. B., S. Barbary, K. M. Friel, E. J. Plautz, and R. J. Nudo.** Reorganization of remote cortical regions after ischemic brain injury: a potential substrate for stroke recovery. *J Neurophysiol* 89: 3205–3214, 2003; 10.1152/jn.01143.2002. Although recent neurological research has shed light on the brain's mechanisms of self-repair after stroke, the role that intact tissue plays in recovery is still obscure. To explore these mechanisms further, we used microelectrode stimulation techniques to examine functional remodeling in cerebral cortex after an ischemic infarct in the hand representation of primary motor cortex in five adult squirrel monkeys. Hand preference and the motor skill of both hands were assessed periodically on a pellet retrieval task for 3 mo postinfarct. Initial postinfarct motor impairment of the contralateral hand was evident in each animal, followed by a gradual improvement in performance over 1–3 mo. Intracortical microstimulation mapping at 12 wk after infarct revealed substantial enlargements of the hand representation in a remote cortical area, the ventral premotor cortex. Increases ranged from 7.2 to 53.8% relative to the preinfarct ventral premotor hand area, with a mean increase of 36.0 ± 20.8%. This enlargement was proportional to the amount of hand representation destroyed in primary motor cortex. That is, greater sparing of the M1 hand area resulted in less expansion of the ventral premotor cortex hand area. These results suggest that neurophysiologic reorganization of remote cortical areas occurs in response to cortical injury and that the greater the damage to reciprocal intracortical pathways, the greater the plasticity in intact areas. Reorganization in intact tissue may provide a neural substrate for adaptive motor behavior and play a critical role in postinjury recovery of function.

## INTRODUCTION

Cortical injury, as might occur in stroke, is frequently found to affect the initiation and execution of muscular contraction in the extremities opposite the side of the injury. In particular, fine manipulative abilities and skilled use of the upper extremity are often degraded (Bucy 1944; Hoffman and Strick 1995). In the weeks and months after injury, a gradual return of some motor abilities occurs (Lashley 1924; Travis and Woolsey 1956), although complete recovery of function is rare in humans (Gowland 1987).

There is mounting evidence that the return of function observed after cortical injury is largely attributable to adaptive plasticity in the remaining cortical and subcortical motor apparatus (Chollet et al. 1991; Liepert et al. 2000). In the search for neural substrates for adaptive plasticity, studies to date have focused on cortical motor structures adjacent to the site of injury. For example, both neurophysiologic and neuroanatomic studies in experimental animals (Jenkins and Merzenich 1987; Nudo and Milliken 1996) and both neuroimaging and noninvasive stimulation studies in humans (Cao et al. 1994; Cramer et al. 1997; Traversa et al. 1997; Weiller and Rijntjes 1999) confirm functional, seemingly adaptive alterations in the healthy tissue immediately adjacent to a cortical infarct. These examples of adaptive plasticity are consistent with a long-held belief that functions lost due to cortical injury may be "taken over" by tissue immediately adjacent to the injury (Black et al. 1970).

In addition, a large number of reports, especially from the clinical literature, point to functional alterations in more distant motor structures, either in the same hemisphere as the injury or in the opposite hemisphere (Cao et al. 1998; Nelles et al. 1999; Seitz et al. 1998). Reorganization of remote structures has primarily been derived from positron emission tomography (PET) or functional magnetic resonance imaging (fMRI) studies. While metabolic and hemodynamic alterations are typical in these remote cortical areas after cortical infarct, there is no clear consensus regarding their role in functional recovery.

The motor cortex is composed of several cortical areas that are reciprocally interconnected (He et al. 1993; Stepniewska et al. 1993): the primary motor cortex (M1, area 4) located in the precentral gyrus; the premotor cortex [including ventral premotor cortex (PMV) and dorsal premotor cortex(PMD)], located anterior to M1; the supplementary motor area (SMA), located near the midline anterior to M1; and the cingulate motor areas, located in the cingulate gyrus on the medial surface of the cerebral cortex. It has been argued that each of these cortical motor areas plays a somewhat different role in the control of voluntary movements (Lawrence and Kuypers 1968; Luppino and Rizzolatti 2000). Since these cortical motor areas are interconnected, it is likely that the function of any one area will be affected by damage to one of the other areas. Furthermore, as premotor areas have efferent outputs to the spinal cord independent of M1, aspects of restitution of motor function may depend on the extent to which intact efferent systems can compensate or substitute for damaged motor areas (Strick 1988).

The theory that structures either adjacent or remote from the injured area can assume the function of the damaged cortex,

Address for reprint requests: S. B. Frost, Department of Molecular and Integrative Physiology, University of Kansas Medical Center, 3901 Rainbow Blvd., Kansas City, KS 66160 (E-mail: sfrost@kumc.edu).

The costs of publication of this article were defrayed in part by the payment of page charges. The article must therefore be hereby marked "*advertisement*" in accordance with 18 U.S.C. Section 1734 solely to indicate this fact.

often referred to as vicariation of function or substitution (Munk 1881), has gained additional support due to recent examples of functional plasticity after injury. One study using microelectrode stimulation techniques showed that areas adjacent to damaged portions of motor cortex reorganize after behaviorally contingent electrical stimulation of the ventral tegmentum in rats (Castro-Alamancos et al. 1992). Another study using microelectrode-recording techniques showed that changes in functional representations in somatosensory cortex parallel sensorimotor skill recovery from stroke in adult monkeys, although it is unclear whether improvements reflect a recovery to normal preoperative strategies or the development of new compensatory behavioral strategies (Xerri et al. 1998). Subtle compensatory kinematic strategies have been documented during recovery of motor skill following a very small infarct in the M1 hand area of squirrel monkeys (Friel and Nudo 1998). That study suggests that the recovered behavior will rarely be identical to the preinjury behavior.

Previous studies in this laboratory have shown that following a focal vascular infarct in the M1 hand area of squirrel monkeys, the spared tissue adjacent to the injury undergoes alterations in functional topographic representations during the period of recovery (Nudo and Milliken 1996; Nudo et al. 1996b). Spared hand representations in M1 are retained in animals that undergo motor skill training after the injury, while spared hand representations undergo further loss without training (i.e., during spontaneous recovery).

Numerous neuroimaging studies have suggested that plasticity occurs in remote motor areas after strokes affecting M1 in humans (Chollet et al. 1991; Cramer et al. 1997; see Cramer and Bastings 2000 for review). Metabolic and hemodynamic changes have been documented in premotor cortex (Weiller et al. 1992), SMA (Weiller et al. 1993), and M1 in the intact hemisphere (Cao et al. 1998; Nelles et al. 1999; Seitz et al. 1998). A recent study showed that 30-min induced inhibition of M1 results in increased recruitment curves in the contralateral M1 (Schambra et al. 2003). However, little is known about the detailed neurophysiologic changes in remote motor areas after vascular infarct in M1 that might accompany recovery. Studies in the somatosensory system indicate that damage to the primary somatosensory cortex (S1) results in topographic reorganization in the second somatosensory area (S2) (Pons et al. 1988). If this phenomenon is generalizable to the multiple motor cortical areas, then a general principle of compensatory response to brain injury may be postulated.

It was the goal of this study to examine potential reorganization in the hand representation of a secondary motor area, the ventral premotor cortex (PMV) following an experimentally induced ischemic infarct in the hand representation of M1. PMV was considered a good candidate for contributing to functional recovery after M1 injury due to its direct connections with M1 and its axonal projections to the spinal cord. Tracer injections of M1 in primates have revealed somatotopically distributed dense connections with PMV via intracortical axons (Stepniewska et al. 1993) PMV also contains neurons that project directly to the spinal cord; predominantly to the upper cervical segments (He et al. 1993; Nudo and Masterton 1990). Furthermore, microelectrode stimulation techniques have revealed low-threshold sites for elicitation of movement in PMV (Stepniewska et al. 1993). Recent evidence also suggests functional homology between premotor areas in monkey and human (Rizzolatti et al. 2002).

Using microelectrode stimulation techniques [(intracortical microstimulation (ICMS)], it is possible to elucidate the function of specific cortical motor areas by deriving high-resolution functional maps of topographic motor representations (Donoghue et al. 1992; Gould et al. 1986; Nudo et al. 1992, 1996a; Strick and Preston 1982). While most neurophysiologic studies of functional recovery from damage to M1 have concentrated on reorganization in the adjacent intact tissue (i.e., within M1), one would expect that reorganization in nonprimary motor representations, such as PMV, may also parallel functional recovery after M1 injury.

## METHODS

ICMS techniques were used to derive detailed maps of M1 and PMV hand representations in five adult squirrel monkeys (*Saimiri sciureus*) before and after focal ischemic infarcts in the hand area of M1. First, hand preference and manual dexterity measurements were assessed for each animal using a pellet retrieval task that required skilled use of the hand. Then, ICMS mapping techniques were used to physiologically identify the M1 hand representation contralateral to the preferred hand, i.e., the target for the infarct. The PMV hand representation in the same hemisphere was also examined using the same stimulation techniques to obtain a baseline comparison to postinfarct maps. After derivation of the M1 and PMV hand area representations, a focal ischemic infarct of the electrophysiologically defined M1 hand area was induced. During a 3-mo recovery period, limited periodic assessment of hand preference and manual dexterity was conducted. However, no other repetitive training procedure, or any major intervention designed to encourage use of the more-affected limb, was employed. At the end of the 3-mo time period, a second set of representational maps of the M1 and PMV hand areas were derived in each animal.

### *Behavioral methods*

To assess changes in hand preference and dexterity, random probe trials on an automated Klüver board were periodically conducted. This entailed presentations of flavored food pellets in wells of five different diameters, ranging from 9.5 to 25 mm, in random order. Normal retrieval of food pellets from the smallest well required the insertion of one or two fingers, as well as specific movement combinations (Nudo et al. 1996a). During probe trials for assessment of hand preference, a single 45-mg banana- or chocolate-flavored food pellet was placed randomly into one of the five wells, and the animal was allowed to retrieve it with either hand (i.e., open board probe trials). The mean percent of initial reaches with one hand plus the mean percent of retrievals with one hand (equally weighted) for all five wells was used to determine hand preference (Nudo et al. 1992). Five probe trials for each well size were conducted in each open board session. Additional random probe trials were periodically conducted using a restrictive barrier to isolate each hand and assess unimanual dexterity (a total of 25 trials for each hand; data from the hand ipsilateral to infarct are not presented here). Three sessions, conducted during the week prior to the preinfarct map (1 session every alternate day), were used to determine preinfarct hand preference and dexterity performance. Sessions consisting of probe trials (both open-board and hand-restricted) were continued during the postinfarct period to track recovery. During the first 4 weeks, three sessions were conducted each week; during the final 8 weeks, one session was conducted each week. Videotapes of individual trials were analyzed to determine the total number of finger flexions per retrieval and then averaged for each day. These values were normalized relative to preinfarct flexions per retrieval. As a second measurement of postinfarct performance, the

same videotapes were further analyzed to determine the amount of time that the digits were within each well before a successful retrieval (well time). These values were then normalized relative to the average preinfarct well times. These data were later analyzed using the Dunnett test for pairwise mean comparisons to examine differences between baseline (preinfarct) performance and each weekly mean performance (Keppel 1982).

### *Surgical and electrophysiological procedures*

Details of surgical and electrophysiological procedures have been presented previously (Nudo et al. 1996a). Briefly, all surgical procedures were conducted under aseptic conditions. Under halothane/nitrous oxide gas anesthesia, a craniotomy was performed over the M1 and PMV hand representations. A cylinder was affixed over the opening and filled with warm, sterile silicone oil. Gas anesthesia was then withdrawn, and ketamine was administered. Throughout the experimental procedure, core temperature and vital signs were monitored, and intravenous fluids were given. ICMS mapping procedures were then conducted under ketamine anesthesia. Care was taken to maintain a relatively stable anesthetic state. A glass micropipette filled with 3.5 M NaCl (impedance, ~600 kΩ) was advanced perpendicular to the cortex to a depth of approximately 1750 μm (layer 5). The stimulus consisted of thirteen 200-μs cathodal pulses delivered at 350 Hz and repeated at 1/s. Interpenetration distances of 250 and 500 μm were used in the PMV and M1 hand areas, respectively. Movements evoked by ICMS at near-threshold levels defined movement fields (maximum current, 30 μA). From these neurophysiologic data, representational map boundaries were determined to outline different cortical efferent zones. Each zone contained microelectrode penetration sites at which stimulation evoked a specific movement. Further details of these procedures and discussion of possible sources of variation in ICMS-derived motor maps are found elsewhere (Friel and Nudo 1998; Nudo et al. 1992, 1996a).

### *Map construction and areal measurements*

Representational maps of response zones were generated by a computer algorithm that used the *x-y* location of electrode penetrations to establish unbiased borders midway between adjacent sites with different response representations. The hand representation was defined as cortical regions in which ICMS evoked movement of the distal forelimb at near-threshold current levels. These movements include finger, thumb, wrist, and forearm (supination and pronation) movements, but exclude elbow and shoulder movements.

Due to necrosis and scavenging of the infarcted tissue, histological examination, although useful for verifying that all layers of the infarcted area were destroyed, could not be used to accurately define the volume of the lesion. A less direct method was therefore used to measure the areal extent of the M1 infarct. This method takes advantage of the fact that after vascular electrocoagulation, the ischemic cortex becomes blanched and easily distinguished from noninfarcted tissue. Therefore the postinfarct estimate of intact M1 hand area was derived by superimposing a digital photograph of the postinfarct intact vasculature on the preinfarct photograph 3 mo after the ischemic lesion (Friel and Nudo 1998). Using this estimation technique, the areal extent of the M1 surface destroyed by the infarct and the cortical area spared by the infarct was determined. Data obtained via visual inspection was verified using a laser-Doppler blood flow imaging device (Moor Instruments) (Fig. 1) 1 h after the ischemic infarct to determine the precise area of reduced blood flow. The results of the Doppler blood flow imaging was coincident with the infarct area defined by visual inspection. Comparing the two approaches, boundaries differed by <100 microns, well within the range of our ability to resolve the precise boundary using either technique. PMV hand area measurements were taken from the ICMS maps of PMV before and after the ischemic infarct. Measurement differences were then compared using Fishers LSD Post Hoc analysis (Keppel 1982).

### *Infarct procedure*

After derivation of the baseline M1 and PMV hand representation areas contralateral to the preferred hand, blood vessels supplying the M1 hand representation area were permanently occluded as they entered the cortical surface by using microforceps connected to a bipolar electrocoagulator. This model was not designed to mimic clinical stroke per se, but to provide a reliable method for producing physiologically identified ischemic infarcts. This technique consistently produced focal, columnar infarcts through all six layers of the cerebral cortex. In both this and in previous studies, the infarcts were predictable in size and did not affect the underlying white matter (Nudo and Milliken 1996; Nudo et al. 1996b). At the conclusion of each procedure, gas anesthesia was reintroduced for surgical closing. The animal was then monitored in a temperature-controlled incubator until it was awake and alert. Animals were cared for in accordance with the National Institutes of Health Guide for the Care and Use of Laboratory Animals and with the approval of the Institutional Animal Care and Use Committee. After completion of these experiments, each monkey was given a lethal dose of sodium pentobarbital (100 mg per kg of body weight) and perfused transcardially for histological examination of each lesion.

## RESULTS

### *Behavioral results of infarct in M1*

The infarct initially resulted in a marked deficit in the ability to retrieve food pellets with the hand contralateral to the lesion, especially from the smallest wells. In the first 3 days, there was little voluntary use of the affected limb for either food manipulation or movement about the home cage. The elbow of the affected limb was usually held in an extended position, and only reflexive grasping with the affected hand was observed. In

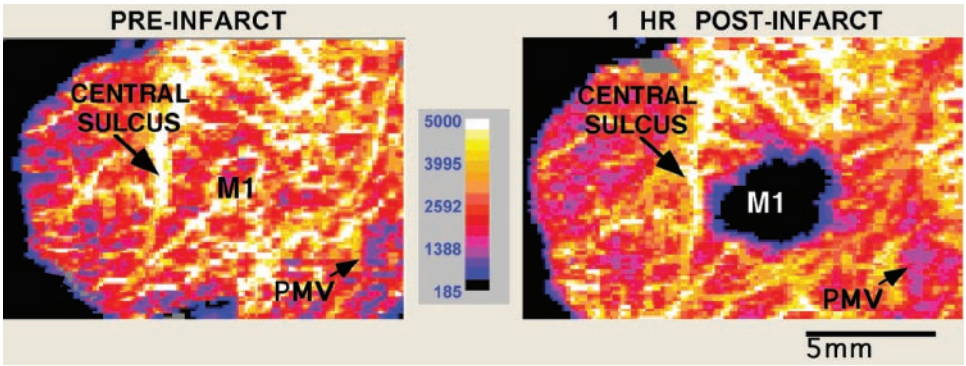


FIG. 1. High-resolution laser-Doppler blood flow images of frontal cortex of a squirrel monkey before and 1 h after an ischemic infarct in the hand area of primary motor cortex. Scale depicts relative perfusion units. After the M1 and PMV hand area representations were physiologically defined using intracortical microstimulation (ICMS), the blood vessels supplying the M1 hand area were occluded as they entered the cortical surface by using microforceps connected to a bipolar coagulator.

the following 7 days, voluntary use of the affected hand gradually returned, although monkeys still had difficulty placing fingers into the smallest wells and were unable to retrieve pellets from the smallest wells with the impaired hand.

By the end of the second week after the infarct, the monkeys were able to retrieve pellets from the smallest well, but manual skill, as measured by the total number of finger flexions per pellet retrieval, was markedly diminished and highly variable across trials. More specifically, the average number of flexions per retrieval from the smallest well in the second week after infarct was 2.5 times that observed in the week before the infarct. This initial postinfarct motor impairment of the contralateral hand was followed by a gradual improvement in performance over 1–3 months. The average flexions per retrieval in week 12 after infarct was reduced to 1.6 times that in the week before infarct, demonstrating some spontaneous recovery, but a lasting residual deficit (Fig. 2*A*; data from the smallest well, well 5, shown). Motor performance indices were not statistically different from baseline values at any week postinfarct despite elevated postinfarct mean values. This is likely due to the relatively small number of monkeys in the study, because some values approached statistical significance.

Although the monkeys were able to retrieve pellets from the smallest well by the end of the second week postinfarct, the amount of time spent in the well for each retrieval was greater than the time spent preinfarct, although the well time was highly variable across animals (Fig. 2*B*). Average well time per retrieval was 5.5 times greater at the end of the second week compared with preinfarct baseline ($P < 0.05$). Well time performance improved in postinfarct week 3, but did not fully return to preinfarct performance levels by week 12. In comparing the flexions per retrieval (motor performance index) and

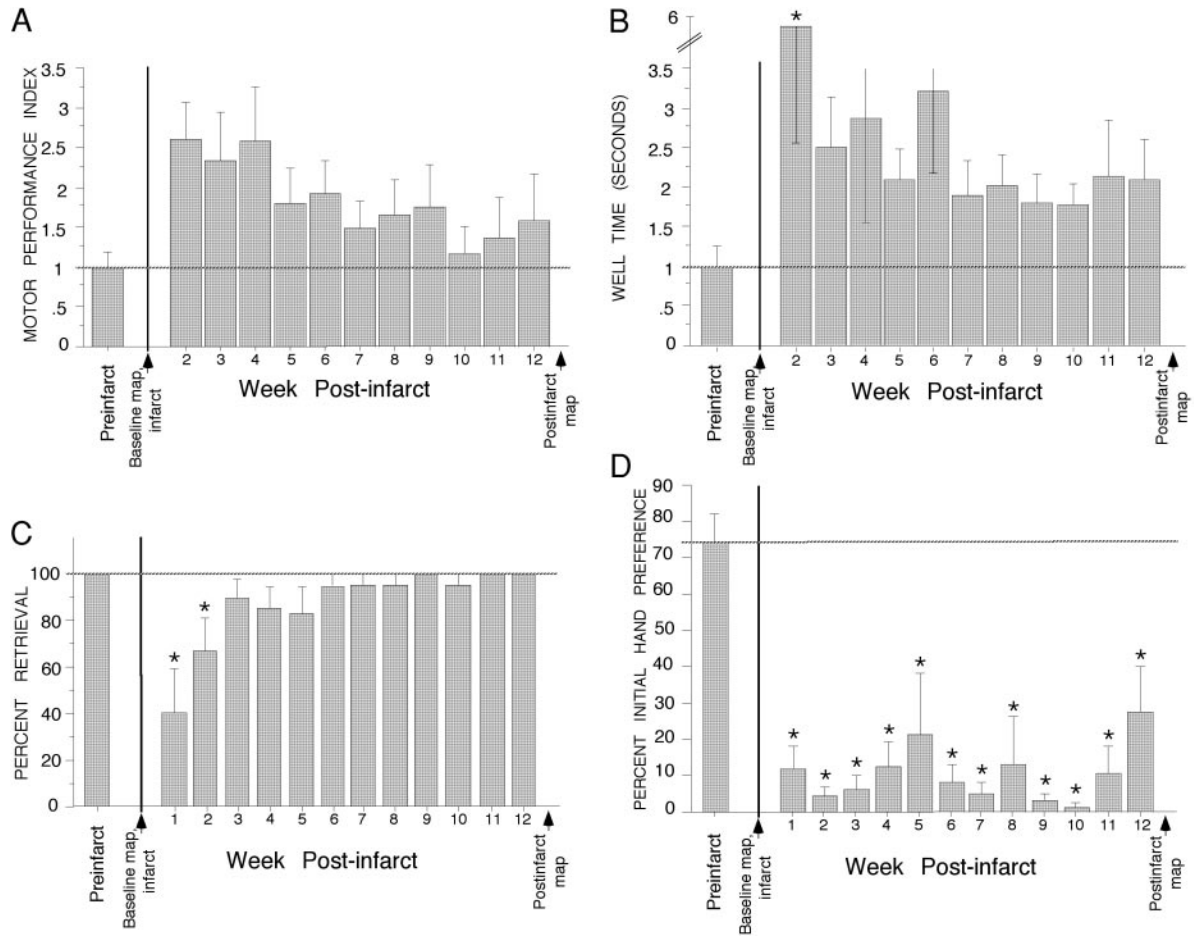


FIG. 2. Effects of ischemic infarct on motor performance and hand preference. *A*: normalized well 5 (smallest well) motor performance of the impaired hand for 4 monkeys in weekly epochs. Evaluation of motor performance was conducted using a Plexiglas barrier that required the monkey to use the impaired hand only. The motor performance index is the number of finger flexions per retrieval divided by the baseline (preinfarct) flexions per retrieval for each animal from the smallest well. Bars represent the mean normalized flexions per retrieval (±SE). One animal (0003) is not included due to insufficient preinfarct data. *B*: normalized well 5 time performance of the impaired hand for the same 4 monkeys. Normalized well time is the amount of time the hand is in the well before a successful retrieval divided by the baseline (preinfarct) well time per retrieval. Bars represent the mean normalized well time per retrieval (±SE). Well time performance for pellet retrieval increased immediately postinfarct ($P < 0.05$), followed by an improvement in performance in postinfarct week 3. Well time performance did not return to preinfarct performance levels through week 12. *C*: percent successfully retrieved pellets from well 5 for all 5 monkeys in weekly epochs. The percentage of successfully retrieved pellets from the smallest well was significantly decreased in postinfarct week 1 (*$P < 0.01$) compared with preinfarct percentage. *D*: percent use of the initially preferred hand for 4 monkeys in weekly epochs. Assessment of hand preference was conducted using an open Klüver board. Bars represent the mean percent use of the preinfarct preferred hand (±SE). The animal with the smallest M1 lesion (9902) did not change hand preference and is not included. Each postinfarct epoch mean differs significantly from the preinfarct mean (*$P < 0.01$).

well time performance across the postinfarct period, the higher mean index values of well time suggest that well time may be a more sensitive measure of motor performance on this task. The percentage of successfully retrieved pellets from the smallest well was significantly decreased in postinfarct week 1 ($P < 0.01$) and week 2 ($P < 0.05$) and gradually returned to the preinfarct level of 100% in each animal (Fig. 2*C*).

Postinfarct hand preference changed to the less-affected hand in the four monkeys with the largest infarcts (based on the percentage of the M1 hand area infarcted). The monkey with the smallest injury to M1 did not change hand preference. In those animals with the largest infarcts, the average use of the initially preferred hand significantly decreased from 74.3 ± 14.8% (SE) in the week before infarct to 4.3 ± 4.8% in the second week after infarct ($P < 0.01$). This change in hand preference was still evident at 12 weeks postinfarct, when the percent use of the initially preferred hand was 30.7 ± 16.6% ($P < 0.01$; Fig. 2*D*).

Postinfarct impairment in performance was also evident in the larger wells (1–4), with each animal showing an increase in motor performance index postinfarct, with a gradual improvement in performance thereafter (Fig. 3). The mean motor performance index for well 3 was significantly higher in week 2 postinfarct ($P < 0.01$) and remained higher than preinfarct performance throughout the 12-wk postinfarct testing period. Performance on well 4 was significantly higher in weeks 2 and 3 postinfarct ($P < 0.05$) and remained higher throughout the 12-wk testing period.

### *Functional reorganization in ventral premotor cortex*

Comparison of ICMS maps of movement representations in PMV before and 12 wk after the infarct revealed substantial enlargement of the hand representation in the PMV cortex ipsilateral to the experimentally induced infarct (Figs. 4 and Fig. 5). ICMS mapping and histological examination of M1 12 wk after the ischemic lesion revealed a decrease in the M1 hand area in all five animals. Partial survival of cortical tissue in the M1 hand area was seen in each monkey. The absolute size of the infarcted M1 area ranged from 6.0 to 16.6 $mm^2$ (Fig. 6). This variation was, in part, due to the variation in size of the preinfarct hand area in individual monkeys. However, the relative size of the infarcted area also varied. Individual percentages of the original M1 hand area that was infarcted ranged from 57 to 96.5%, with a mean loss of 81.3 ± 15.8% (Fig. 7).

ICMS mapping of the PMV hand area at 3 mo postinfarct revealed a net expansion in the PMV hand representation in each monkey, ranging from 0.3 $mm^2$ (i.e., from 3.9 to 4.2 $mm^2$)

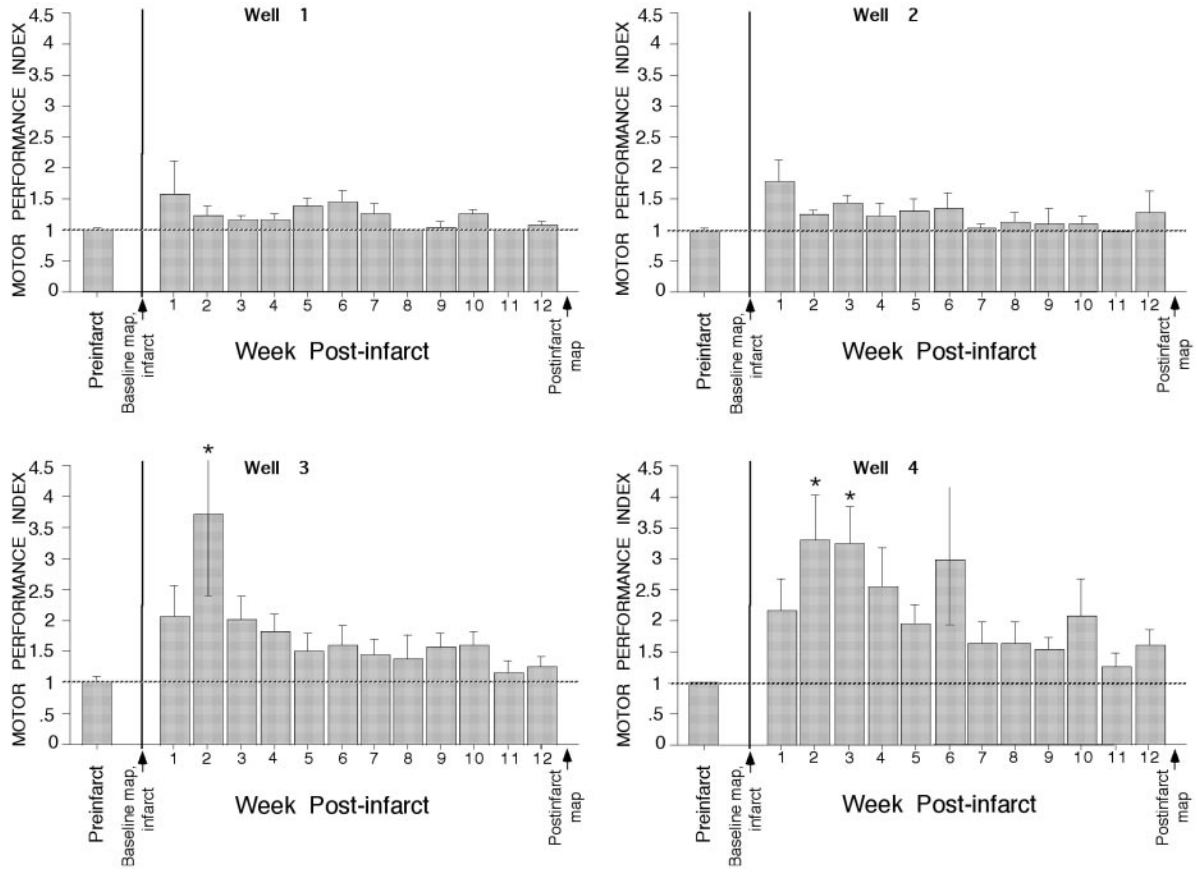


FIG. 3. Effects of ischemic infarct on motor performance for wells 1–4. The normalized motor performance of the impaired hand for 5 monkeys for wells 1–4 in weekly epochs. Evaluation of motor performance was conducted using a plexiglas barrier that required the monkey to use the impaired hand only. The motor performance index is the number of finger flexions per retrieval divided by the baseline (preinfarct) flexions per retrieval for each animal from each well. Bars represent the mean normalized flexions per retrieval (±SE). Each animal had an increase in motor performance index postinfarct, with a gradual improvement in performance thereafter. Mean motor performance index for well 3 was significantly higher in week 2 postinfarct (*$P < 0.01$) and higher for well 4 in weeks 2 and 3 (*$P < 0.05$) compared with preinfarct performance.

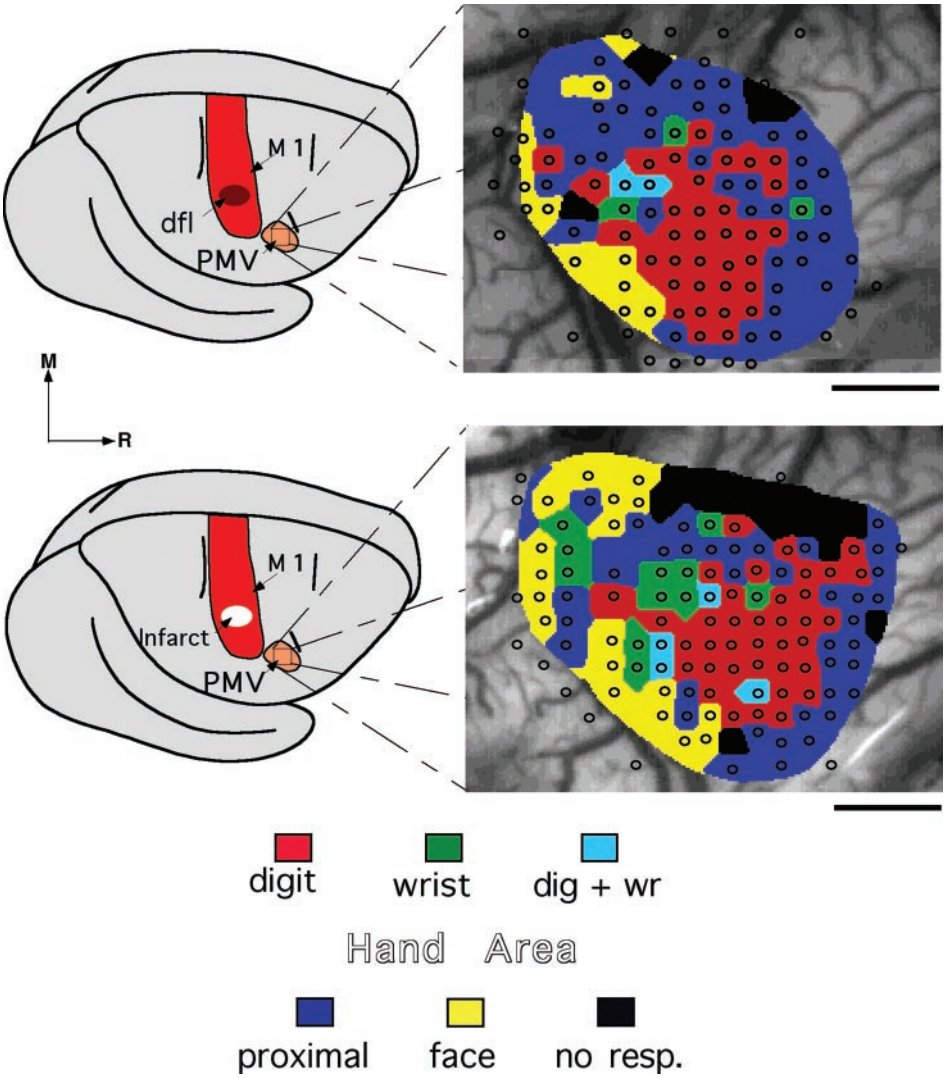


FIG. 4. Reorganization of hand representations in the ventral premotor cortex before and after a focal ischemic infarct in the hand representation of primary motor cortex. *Left*: schematic representation of the forebrain of the squirrel monkey from a lateral view showing the location of the M1 distal forelimb area (dfl) and the location of ventral premotor cortex (PMV). *Right*: results of ICMS mapping of the PMV hand area in 1 monkey (9406) before (*top*) and 12 wk after ischemic infarct in the M1 hand area (*bottom*). Circles represent the location of microelectrode penetrations and colors represent the movement(s) evoked by near-threshold electrical stimulation ($<30$ $\mu$A) at that site. In this animal (9406), the infarct damaged 79% of the preinfarct M1 hand representation area and postinfarct PMV mapping revealed a 45% increase in the PMV hand representation. In each animal, an increase in the area of distal forelimb movement representation occurred 12 wk after infarct in M1. Scale bar = 1 mm.

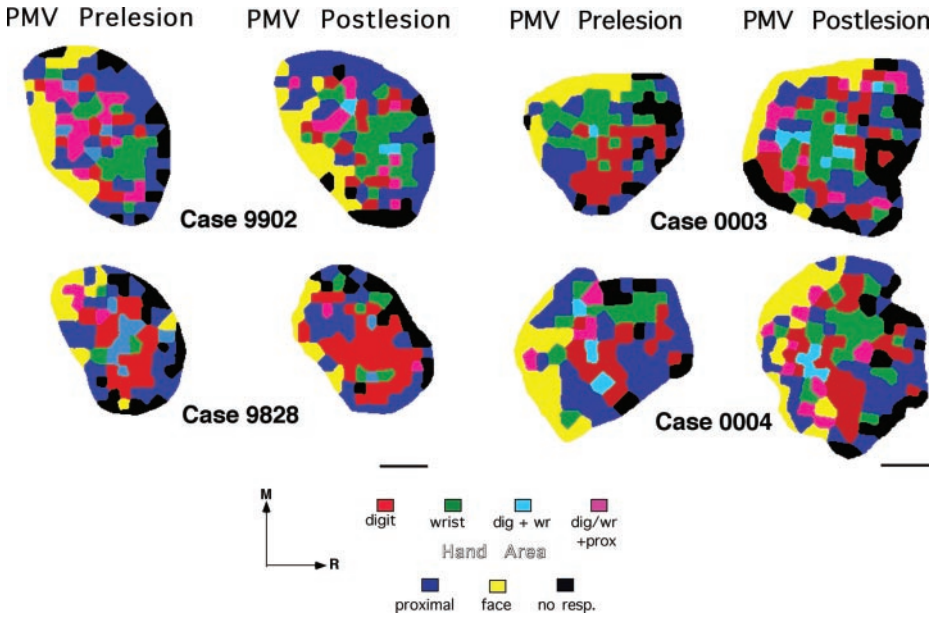


FIG. 5. The results of ICMS mapping of the PMV hand area before and 3 mo after the ischemic infarct in 4 monkeys. ICMS mapping revealed a net expansion in the PMV hand representation in each monkey. Different colors represent the evoked movement(s) of particular body parts at near threshold levels at each penetration site. Scale bars = 1 mm.

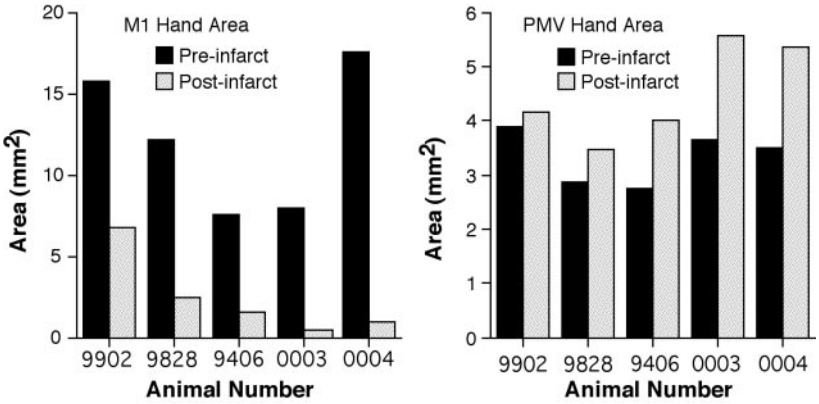


FIG. 6. The results of ICMS mapping of the M1 and PMV hand areas before and 3 mo after the ischemic infarct. *Left*: M1 hand area. The results revealed decreases in the M1 hand area in all 5 animals. Although the entire hand area was targeted for infarct, partial retention of spared hand area was seen in all 5. The decrease in absolute M1 hand area ranged from 6.0 $mm^2$ in 1 animal (9406), to 16.6 $mm^2$ in another (0004). *Right*: PMV hand area. There was an increase in the total area of the hand representation in PMV at 3 mo postinfarct in all 5 animals. This increase ranged from 0.3 (9902) to 1.9 $mm^2$ (0003).

to 1.9 $mm^2$ (i.e., from 3.5 to 5.4 $mm^2$; Fig. 6). These increases ranged from 7.2 to 53.8% relative to the initial PMV hand area, with a mean increase of 36.0 ± 20.8% ($P < 0.05$; Fig. 7). The variation in the sizes of the infarcts in M1 allowed us to examine the relationship between infarct size and degree of reorganization in PMV. This analysis revealed that the increase in the PMV hand representational area was directly proportional to the relative size of the M1 infarct ($R^2 = 0.819$; $P = 0.0348$). The animal that had the smallest infarct in the M1 hand area (also the animal that did not change hand preference after infarct), had the smallest expansion in the PMV hand area representation. The expansion of the PMV distal forelimb representation does not appear to be linked to the size of the initial MI hand area, since the two animals with the largest initial hand areas, 9902 and 0004, had relatively small and large PMV changes, respectively (Figs. 6 and 7). When the PMV hand representation was subdivided into digit and wrist-forearm representations, the digit area increased in four monkeys and decreased in one monkey (−7.1, 15.0, 20.8, 97.1, and 44.0%: in the same order as the individual animal data presented in Figs. 6 and 7), with a mean change of +34.0% (not significant, $P > 0.05$). The wrist-forearm area increased in four monkeys and decreased in one monkey (14.2, −35.8, 245.9, 40.0, and 50.2%) with a mean change of +62.9% (not significant, $P > 0.05$; also in the same order as the individual animal data presented in Figs. 6 and 7). Combination digit and wrist areas were included in both digit as well as wrist areas.

Current thresholds for stimulation of evoked movements were not different from those observed in M1 and were quite low. This may suggest that direct corticospinal connections mediate the movements evoked from stimulation of PMV. Furthermore, stimulation thresholds in PMV did not change postinfarct, suggesting that movements were not mediated transcortically via M1. EMG recordings were not conducted during the mapping procedures, so latencies of EMG responses could not be analyzed.

## DISCUSSION

The changes found in the hand movement representation in PMV following ischemic infarct in the hand representation of M1 indicate that neurophysiologic reorganization of more remote cortical motor areas occurs in response to cortical infarct in M1. Further, since analogous results have been observed in the somatosensory cortex (Pons et al. 1988), it would appear that reorganization of secondary cortical areas is a general feature of injury-induced plasticity. Still further, because the degree of functional expansion in PMV is directly proportional to the amount of damage in M1, a second general principle is suggested. That is, remote reorganization is directly related to the reciprocal connectivity of the various motor areas. The greater the damage to reciprocal intracortical pathways, the greater the plasticity in the secondary, intact area.

Evidence for the contribution of premotor cortex to recovery has come from both human (Fridman et al. 2002; Miyai et al. 1999) and animal (Castro-Alamancos and Borrel 1995; Liu and Rouiller 1999) studies. Neuroimaging studies have reported altered metabolic and hemodynamic changes in premotor cortex after cortical injury in humans (Weiller et al. 1992). Results from a recent transcranial magnetic stimulation study suggest that premotor cortex contributes to functional motor recovery in human stroke patients (Fridman et al. 2002). Miyai et al. (1999) reported that following middle cerebral artery occlusion, recovery in human stroke survivors was improved in those with intact premotor cortex compared with those that had premotor cortex damage. Following damage to M1 and subsequent spontaneous recovery of upper extremity functions in macaque monkeys, Liu and Rouiller (1999) showed that initial

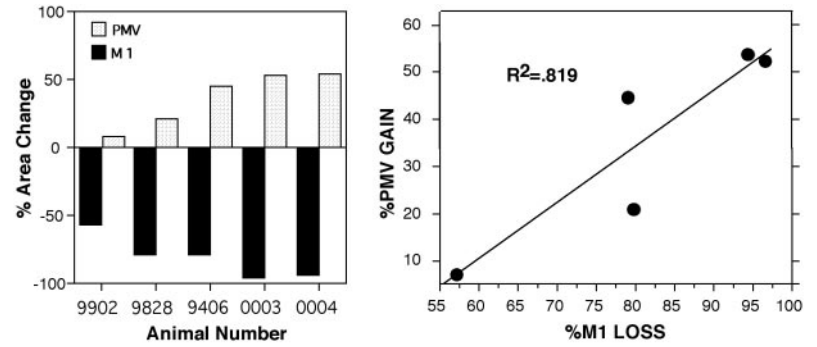


FIG. 7. Relative change in hand area in M1 and PMV 12 wk postinfarct. *Left*: percent change in hand area in M1 and PMV 3 mo postinfarct in 5 animals. The percent of M1 hand area lost ranged from 57.0% (9902) to 96.5% (0003), with a mean of 81.3 ± 15.8%. The percent increase in PMV hand response area ranged from 7.2% (9902) to 53.8% (0004), with a mean of 36.0 ± 20.8%. *Right*: percent increases in PMV hand response area as a function of the percent anatomical loss of M1 hand area 3 mo postinfarct. All 5 animals had an increase in the area of the hand response representation in PMV that was proportional to the amount of M1 hand area lost. In general, the larger the infarct area and greater the percentage of M1 hand response area lost, the larger the increase in the PMV hand response area ($R^2 = 0.819$; $P = 0.0348$).

behavioral deficits were reinstated when PMV and dorsal premotor cortex were pharmacologically inhibited. Other studies have implicated PMV in various aspects of motor planning, execution, and learning in normal human (Winstein et al. 1997) and nonhuman (Kurata and Hoshi 1999) primates. These results suggest that reorganization in PMV and other nonprimary motor areas may provide a neural substrate for adaptive motor behavior and contribute to postinjury recovery of upper extremity motor functions such as manual dexterity.

Many of the cellular and synaptic substrates that support adaptive plasticity in the adult cortex are now well established. Motor learning, or the development of more complex motor behaviors, has been shown to result in both anatomical and physiological changes within sensorimotor cortex. A greater number of synapses per neuron, an increase in dendritic arborizations, and strengthened or enhanced synaptic responses have each been demonstrated following skilled motor learning or exposure to complex environments (Greenough et al. 1985; Jones et al. 1997; Kleim et al. 1996; see Nudo et al. 2001 for review). Similar anatomical changes have been seen in intact contralateral cortex with skilled use training following cortical injury (Kleim et al. 1996; Jones and Schallert 1994; Jones et al. 1999). Motor skill training using a small-object retrieval task has been shown to alter the functional organization of primary motor cortex via an expansion of distal forelimb representations in both rats (Kleim et al. 1998) and primates (Friel and Nudo 1998; Plautz et al. 2000). It seems reasonable to conclude that similar anatomical and physiological changes may occur in connected nonprimary motor and sensory areas in both normal and cortically injured animals.

Several studies have shown that reductions in $GABA_A$ receptor density and a concurrent increase in glutamate *N*-methyl-D-aspartate (NMDA) receptor density occurs in multiple brain areas connectionally related to damaged areas of cortex after infarcts in rodents (Qu et al. 1998a,b; Redecker et al. 2000; Scheine et al. 1996). These changes may act to unmask latent horizontal connections that could contribute to map alterations (Jacobs and Donoghue 1991).

It is now clear that intact motor cortical areas, including those in remote areas interconnected with the damaged motor area, undergo substantial anatomical and neurochemical changes that may contribute to recovery of lost function. The proportional relationship between relative size of the cortical injury and the remote cortical reorganization demonstrated in the present study suggests that post-stroke cortical plasticity is driven by reciprocal intracortical connections between the damaged and intact areas. A direct link between reorganization of PMV and behavioral recovery could not be established in this study due to the variation in M1 lesion size and its relationship with the change in PMV hand area. Future studies should address this issue more directly. In addition to producing similar infarcts with respect to size and location, it will be necessary to determine the correlation (if any) between PMV map expansion and the degree of behavioral recovery. These studies will require similar infarct sizes and a battery of behavioral assessments. Further experiments testing the behavioral consequences of PMV disruption in activity after M1 infarct may also allow for a more direct link between PMV reorganization and motor recovery after M1 injury.

Unlike macaque monkeys, there have been no delineations of sub-areas within PMV in New World monkeys. Studies in owl monkeys have demonstrated a low-threshold hand representation in PMV with stimulation at many sites that evoke movements of multiple joints (Gould et al. 1986; Stepniewska et al. 1993). Large numbers of corticospinal neurons have been found in every primate species studied to date that correspond to the PMV hand area ("Region C" in Nudo et al. 1995; see also Dum and Strick 1991). While it has been reported that the density of corticospinal neurons in macaques approaches that in M1 (Dum and Strick 1991), a comparative study later reported that the density of corticospinal neurons in PMV of squirrel monkeys is higher than in macaques (Nudo et al. 1995). Kakei et al. (2001) showed that most neurons in PMV are extrinsically and directionally tuned regardless of large changes in forearm posture, suggesting that PMV is involved in the spatial guidance of limb movements. PMV may be involved in the transformation of target location in a visual frame of reference into the direction of motor action to acquire the target via its connections with M1. This area, presumed to be F4, appears to code goal-directed actions mediated by spatial locations (Rizzolatti et al. 2002). F5 has been shown in macaques to be involved in motor-action recognition (Umilta et al. 2001) as well as in hand shaping in visuomotor transformations for grasping and manipulation (Fogassi et al. 2001). Human area 44, believed to be homologous to F5 in macaques (Rizzolatti et al. 2002), has been shown to be involved in sensorimotor transformations for grasping and manipulation (Binkofski et al. 1999). Until further behavioral, neurophysiological, and anatomical studies are conducted, it is not yet possible to designate any particular region of squirrel monkey PMV as F4 or F5.

It is feasible that nonprimary motor areas such as PMV contribute to functional recovery following injury in M1. Along these lines, it is important to note that increases in the PMV hand representation reported here occurred in spontaneously recovering animals. In marked contrast, in spontaneously recovering animals after more limited M1 infarcts, the hand representation in the intact, adjacent M1 tissue decreased substantially. It is now of great interest to understand the modulatory effects of behavioral interventions (i.e., physiotherapy) on neurophysiologic reorganization in premotor cortex, such as has been demonstrated for peri-infarct M1 regions (Liepert et al. 2000; Nudo and Milliken 1996; Nudo et al. 1996b). The plastic changes observed here may perhaps be magnified in PMV and other remote areas with appropriate physiotherapeutic and/or pharmacotherapeutic interventions.

We gratefully acknowledge N. Coleman, D. Larson, M. Marucci, S. Delia, and D. Razafsky for assistance on this project. We thank Dr. Elena Zoubina for helpful comments on this manuscript.

This study was supported by National Institutes of Health Grants NS-30853 to R. J. Nudo, National Institutes of Health Institutional Training Grant HD-07523, The University of Kansas Training Program in Biomedical Research to S. B. Frost, American Heart Association Grant 0120624Z to S. B. Frost, NIAAG-14635 (Kansas Claude D. Pepper Center for Independence in Older Americans), and NICHD Center Grant HD-02528.

## REFERENCES

**Binkofski F, Buccino G, Posse S, Seitz RJ, Rizzolatti G, and Freund HJ.** A fronto-parietal circuit for object manipulation in man: evidence from an fMRI-study. *Eur J Neurosci* 11: 3276–3286, 1999.

**Black P, Cianci SN, and Markowitz RS.** Question of transcallosal facilitation of motor recovery: stroke implications. *Trans Am Neurol Assoc* 95: 207–210, 1970.

**Bucy PC.** Effects of extirpation in man. In: *The Precentral Motor Cortex*, edited by Bucy P. Urbana, IL: University of Illinois Press, 1944, p. 353–394.

**Cao Y, D'Olhaberriague L, Vikingstad EM, Levine SR, and Welch KMA.** Pilot study of functional MRI to assess cerebral activation of motor function after poststroke hemiparesis. *Stroke* 29: 112–122, 1998.

**Cao Y, Vikingstad EM, Huttenlocher PR, Towle VL, and Levin DN.** Functional magnetic resonance studies of the reorganization of the human hand sensorimotor area after unilateral brain injury in the perinatal period. *Proc Nat Acad Sci USA* 91: 9612–9616, 1994.

**Castro-Alamancos MA and Borrel J.** Functional recovery of forelimb response capacity after forelimb primary motor cortex damage in the rat is due to the reorganization of adjacent areas of cortex. *Neuroscience* 68: 793–805, 1995.

**Castro-Alamancos MA, García-Segura LM, and Borrell J.** Transfer of function to a specific area of the cortex after induced recovery from brain damage. *Eur J Neurosci* 4: 853–863, 1992.

**Chollet F, DiPiero V, Wise RJ, Brooks DJ, Dolan RJ, and Frackowiak RS.** The functional anatomy of motor recovery after stroke in humans: a study with positron emission tomography. *Ann Neurol* 29: 63–71, 1991.

**Cramer SC and Bastings EP.** Mapping clinically relevant plasticity after stroke. *Neuropharmacology* 39: 842–851, 2000.

**Cramer SC, Nelles G, Benson RR, Kaplan JD, Parker RA, Kwong KK, Kennedy DN, Finklestein SP, and Rosen BR.** A functional MRI study of subjects recovered from hemiparetic stroke. *Stroke* 28: 2518–2527, 1997.

**Donoghue JP, Leibovic S, and Sanes JN.** Organization of the forelimb area in squirrel monkey motor cortex: representation of digit, wrist, and elbow muscles. *Exp Brain Res* 89: 1–19, 1992.

**Dum RP and Strick PL.** The origin of corticospinal projections from the premotor areas in the frontal lobe. *J Neurosci* 11: 667–689, 1991.

**Fridman EA, Hanakawa T, Wu C, and Cohen L.** Contribution of premotor cortex to recovery of motor function after stroke. *Neurology* 58(Suppl 3): A30, 2002.

**Friel KM and Nudo RJ.** Recovery of motor function after focal cortical injury in primates: compensatory movement patterns used during rehabilitative training. *Som Motor Res* 15: 173–189, 1998.

**Fogassi L, Gallese V, Buccino G, Craighero L, Fadiga L, and Rizzolatti G.** Cortical mechanism for the visual guidance of hand grasping movements in the monkey: a reversible inactivation study. *Brain* 124: 571–586, 2001.

**Gould HJ, Cusick CG, Pons TP, and Kaas JH.** The relationship of corpus callosum connections to electrical stimulation maps of motor, supplementary motor, and the frontal eye fields in owl monkeys. *J Comp Neurol* 247: 297–325, 1986.

**Gowland C.** Management of hemiplegic upper limb. In: *Stroke Rehabilitation*, edited by Brandstater M and Basmajian J. Baltimore, MD: Williams and Wilkens, 1987, p. 217–245.

**Greenough WT, Larson JR, and Withers GS.** Effects of unilateral and bilateral training in a reaching task on dendritic branching of neurons in the rat motor-sensory forelimb cortex. *Behav Neurol Biol* 44: 301–314, 1985.

**He SQ, Dum RP, and Strick PL.** Topographic organization of corticospinal projections from the frontal lobe: motor areas on the lateral surface of the hemisphere. *J Neurosci* 13: 952–980, 1993.

**Hoffman D and Strick P.** Effects of a primary motor cortex lesion on step-tracking movements of the wrist. *J Neurophysiol* 73: 891–895, 1995.

**Jacobs KM and Donoghue JP.** Reshaping the cortical motor map by unmasking latent intracortical connections. *Science* 251: 944–947, 1991.

**Jenkins WM and Merzenich MM.** Reorganization of neocortical representations after brain injury: a neurophysiological model of the bases of recovery from stroke. *Prog Brain Res* 71: 249–266, 1987.

**Jones TA, Chu CJ, Grande LA, and Gregory AD.** Motor skills training enhances lesion-induced structural plasticity in the motor cortex of adult rats. *J Neurosci* 19: 10153–10163, 1999.

**Jones TA, Klintsova AY, Kilman VL, Sirevaag AM, and Greenough WT.** Induction of multiple synapses by experience in the visual cortex of adult rats. *Neurobiol Learn Mem* 68: 13–20, 1997.

**Jones TA and Schallert T.** Use-dependent growth of pyramidal neurons after neocortical damage. *J Neurosci* 14: 2140–2152, 1994.

**Kakei S, Hoffman DS, and Strick PL.** Direction of action is represented in the ventral premotor cortex. *Nature Neurosci* 4: 1020–1025, 2001.

**Keppel G.** *Design and Analysis: A Researchers Handbook Second Edition.* Englewood Cliffs, NJ: Prentice-Hall, 1982, p. 144–159.

**Kleim JA, Barbay S, and Nudo RJ.** Functional reorganization of the rat motor cortex following motor skill learning. *J Neurophysiol* 80: 3321–3325, 1998.

**Kleim JA, Lussnig E, Schwartz ER, Comery TA, and Greenough WT.** Synaptogenesis and Fos expression in the motor cortex of the adult rat after motor skill learning. *J Neurosci* 16: 4529–4535, 1996.

**Kurata K and Hoshi E.** Reacquisition deficits in prism adaptation after muscimol microinjection into the ventral premotor cortex of monkeys. *J Neurophysiol* 81: 1927–1938, 1999.

**Lashley KS.** Studies of cerebral function in learning: V. The retention of motor habits after destruction of the so-called motor areas in primates. *Arch Neurol Psychiatr* 12: 249–276, 1924.

**Lawrence DG and Kuypers HGJM.** The functional organization of the motor system in the monkey. I. The effects of bilateral pyramidal lesions. *Brain* 91: 1–14, 1968.

**Liepert J, Bauder H, Wolfgang R, Miltner WH, Taub E, and Weiller C.** Treatment-induced cortical reorganization after stroke in humans. *Stroke* 31: 1210–1216, 2000.

**Liu Y and Rouiller EM.** Mechanisms of recovery of dexterity following unilateral lesion of the sensorimotor cortex in adult monkeys. *Exp Brain Res* 128: 149–159, 1999.

**Luppino G and Rizzolatti G.** The organization of the frontal motor cortex. *News Physiol Sci* 15: 219–224, 2000.

**Miyai I, Suzuki T, Kang J, Kubota K, and Volpe BT.** Middle cerebral artery stroke that includes the premotor cortex reduces mobility outcome. *Stroke* 30: 1380–1383, 1999.

**Munk H.** Uber die Funktionen der Grosshirnrinde. In: *Gesammelte Mitteilungen aus den Jahren* 1877–1880. Berlin: Hirshwald, 1881.

**Nelles G, Spiekramann G, Jueptner M, Leonhardt G, Muller S, Gerhard H, and Diener HC.** Evolution of functional reorganization in hemiplegic stroke: a serial positron emission tomographic activation study. *Ann Neurol* 46: 901–909, 1999.

**Nudo RJ, Jenkins WM, Merzenich MM, Prejean T, and Gedela R.** Neurophysiological correlates of hand preference in primary motor cortex of squirrel monkeys. *J Neurosci* 12: 2918–2947, 1992.

**Nudo RJ and Masterton RB.** Descending pathways to the spinal cord. III: Sites of origin of the corticospinal tract. *J Comp Neurol* 296: 559–583, 1990.

**Nudo RJ and Milliken GW.** Reorganization of movement representations in primary motor cortex following focal ischemic infarcts in adult squirrel monkeys. *J Neurophysiol* 75: 2144–2149, 1996.

**Nudo RJ, Milliken GW, Jenkins WM, and Merzenich MM.** Use-dependent alterations of movement representations in primary motor cortex of adult squirrel monkeys. *J Neurosci* 16: 785–807, 1996a.

**Nudo RJ, Plautz EJ, and Frost SB.** Role of adaptive plasticity in recovery of function after damage to motor cortex. *Muscle Nerve* 24: 1000–19, 2001.

**Nudo RJ, Sutherland DP, and Masterton RB.** Variation and evolution of mammalian corticospinal somata with special reference to primates. *J Comp Neurol* 358: 181–205, 1995.

**Nudo RJ, Wise BM, SiFuentes F, and Milliken GW.** Neural substrates for the effects of rehabilitative training on motor recovery after ischemic infarct. *Science* 272: 1791–1794, 1996b.

**Plautz EJ, Milliken GW, and Nudo RJ.** Effects of repetitive motor training on movement representations in adult squirrel monkeys: role of use versus learning. *Neurobiol Learn Mem* 74: 27–55, 2000.

**Pons TP, Garraghty PE, and Mishkin M.** Lesion-induced plasticity in the second somatosensory cortex of adult macaques. *Proc Natl Acad Sci USA* 85: 5279–5281, 1988.

**Qu M, Buchkremer-Ratzmann I, Schiene K, Schroeter M, Witte OW, and Zilles K.** Bihemispheric reduction of GABAA receptor binding following focal cortical photothrombotic lesions in the rat brain. *Brain Res* 813: 374–380, 1998a.

**Qu M, Mittmann T, Luhmann HJ, Schleicher A, and Zilles K.** Long-term changes of ionotropic glutamate and GABA receptors after unilateral permanent focal cerebral ischemia in the mouse brain. *Neuroscience* 85: 29–43, 1998b.

**Redecker C, Luhmann HJ, Hagemann G, Fritschy JM, and Witte OW.** Differential downregulation of GABAA receptor subunits in widespread brain regions in the freeze-lesion model of focal cortical malformations. *J Neurosci* 20: 5045–5053, 2000.

**Rizzolatti G, Fogassi L, and Gallese V.** Motor and cognitive functions of the ventral premotor cortex. *Curr Opin Neurobiol* 12: 149–154, 2002.

**Schambra HM, Sawaki L, and Cohen LG.** Modulation of excitability of human motor cortex (M1) by 1 Hz transcranial magnetic stimulation of the contralateral M1. *Clin Neurophysiol* 114: 130–133, 2003.

**Schiene K, Bruehl C, Zilles K, Qu M, Hagemann G, Kraemer M, and Witte OW.** Neuronal hyperexcitability and reduction of GABAA-receptor expression in the surround of cerebral photothrombosis. *J Cereb Blood Flow Metab* 16: 906–914, 1996.

**Seitz RJ, Hoflich P, Binkofski F, Tellmann L, Herzog H, and Freund HJ.** Role of the premotor cortex in recovery from middle cerebral artery infarction. *Arch Neurol* 55: 1081–1088, 1998.

**Stepniewska I, Preuss TM, and Kaas JH.** Architectonics, somatotopic organization, and ipsilateral cortical connections of the primary motor area (M1) of owl monkeys. *J Comp Neurol* 330: 238–271, 1993.

**Strick PL.** Anatomical organization of multiple motor areas in the frontal lobe: implications for recovery of function. *Adv Neurol* 47: 293–312, 1988.

**Strick PL and Preston JB.** Two representations of the hand in area 4 of a primate. I. Motor output organization. *J Neurophysiol* 48: 139–149, 1982.

**Traversa R, Cicinelli P, Bassi A, Rossini PM, and Bernardi G.** Mapping of motor cortical reorganization after stroke. A brain stimulation study with focal magnetic pulses. *Stroke* 28: 110–117, 1997.

**Travis AM and Woolsey CN.** Motor performance of monkeys after bilateral partial and total cerebral decortication. *Am Phys Med* 35: 273–310, 1956.

**Umilta MA, Kohler E, Gallese V, Fogassi L, Fadiga L, Keysers C, and Rizzolatti G.** I know what you are doing. a neurophysiological study. *Neuron* 31: 155–165, 2001.

**Weiller C, Chollet F, Friston KJ, Wise RJ, and Frackowiak RS.** Functional reorganization of the brain in recovery from striatocapsular infarction in man. *Ann Neurol* 31: 463–472, 1992.

**Weiller C, Ramsay SC, Wise RJ, Friston KJ, and Frackowiak RS.** Individual patterns of functional reorganization in the human cerebral cortex after capsular infarction. *Ann Neurol* 33: 181–189, 1993.

**Weiller C and Rijntjes M.** Learning, plasticity, and recovery in the central nervous system. *Exp Brain Res* 128: 134–138, 1999.

**Winstein CJ, Grafton ST, and Pohl PS.** Motor task difficulty and brain activity: investigation of goal-directed reciprocal aiming using positron emission tomography. *J Neurophysiol* 77: 1581–1594, 1997.

**Xerri C, Merzenich MM, Peterson BE, and Jenkins W.** Plasticity of primary somatosensory cortex paralleling sensorimotor skill recovery from stroke in adult monkeys. *J Neurophysiol* 79: 2119–2148, 1998.

JOURNAL OF NEUROTRAUMA 30:1137–1146 (July 1, 2013)

DOI: 10.1089/neu.2012.2785

# Cortical Reorganization after Experimental Traumatic Brain Injury: A Functional Autoradiography Study

Neil G. Harris,[1,2] Szu-Fu Chen,[3,4] and John D. Pickard[5,6]


## Abstract

Cortical sensorimotor (SM) maps are a useful readout for providing a global view of the underlying status of evoked brain function, as well as a gross overview of ongoing mechanisms of plasticity. Recent evidence in the rat controlled cortical impact (CCI) injury model shows that the ipsilesional (injured) hemisphere is temporarily permissive for axon sprouting. This would predict that size and spatial alterations in cortical maps may occur much earlier than previously tested and that they might be useful as potential markers of the postinjury plasticity period as well as indicators of outcome. We investigated the evolution of changes in brain activation evoked by affected hindlimb electrical stimulation at 4, 7, and 30 days following CCI or sham injury over the hindlimb cortical region of adult rats. [$^{14}$C]-iodoantipyrine autoradiography was used to quantitatively examine the local cerebral blood flow changes in response to hindlimb stimulation as a marker for neuronal activity. The results show that although ipsilesional hindlimb SM activity was persistently depressed from 4 days, additional novel regions of ipsilesional activity appeared concurrently within SM barrel and S2 regions as well as posterior auditory cortex. Simultaneously with this was the appearance of evoked activity within the intact, contralesional cortex that was maximal at 4 and 7 days, compared to stimulated sham-injured rats, where activation was solely unilateral. By 30 days, however, contralesional activation had greatly subsided and existing ipsilesional activity was enhanced within the same novel cortical regions that were identified acutely. These data indicate that significant reorganization of the cortical SM maps occurs after injury that evolves with a particular postinjury time course. We discuss these data in terms of the known mechanisms of plasticity that are likely to underlie these map changes, with particular reference to the differences and similarities that exist between rodent models of stroke and traumatic brain injury.


**Key words:** autoradiography; blood flow; cortical contusion injury; plasticity

## Introduction

In addition to the well-known cognitive deficits that result from traumatic brain injury (TBI), motor weakness in limb or trunk is a major problem in both adult and young patients,[1,2] even after mild concussive trauma.[3] Motor deficits can persist for many years, despite neurorehabilitative interventions.[4] Although the prolonged time course of recovery holds promising opportunities for therapeutic intervention, the spontaneous restorative processes occurring in the brain after TBI are not completely understood. Mechanisms for the partial motor recovery that occurs after TBI are complex, but are likely to include behavioral compensation as well as anatomical and functional reorganization of the remaining intact brain. These cellular and molecular mechanisms of plasticity underlie changes in somatosensory and motor cortical map representations that occur after injury. Though much of our understanding of these map changes comes from stroke and experimental lesion models, comparatively little progress has been made in the TBI field. Much of this stems from the disparities in injury location between the diseases; TBI is primarily a disparate white matter disease where, instead of functional deficits arising from focal injury sites as occurs in stroke, whole networks can be affected,[5] making it difficult to study systematically. The pathology of TBI is heterogeneous and complex, involving multi-faceted pathologies that reflect the diverse effects of the initial mechanical injury as well as subsequent secondary events. Indeed, the cascade of pathophysiological changes often lasts longer after a diffuse TBI than after focal ischemia.[6] As a result, the known patterns and

[1]UCLA Brain Injury Research Center, Department of Neurosurgery, and [2]Brain Research Institute, David Geffen School of Medicine at UCLA, Los Angeles, California.
[3]Department of Physical Medicine and Rehabilitation, Cheng Hsin General Hospital, Taipei, Taiwan.
[4]Department of Physiology, National Defense Medical Center, Taipei, Taiwan.
[5]Neurosurgery Unit, Cambridge Center for Brain Repair and [6]Wolfson Brain Imaging Center, University of Cambridge, Cambridge, United Kingdom.

mechanisms of plasticity that occur after stroke or lesioning may not be entirely transferable to the TBI field. Though neuronal sprouting and synapse formation occur around focal cortical infarcts and in sensorimotor cortex of the unaffected hemisphere,[7–10] axon sprouting is limited to the pericontused region after experimental TBI and none occurs in the intact cortex.[11] Both experimental and clinical neuroimaging studies after unilateral stroke have shown functional reorganization in both the ipsilesional (injured) and the contralesional (intact) hemisphere in parallel with recovery.[12,13] After TBI, although chronic time-point ipsilesional cortical somatosensory map changes occur after experimental contusion injury and may be related to functional recovery,[14–16] activation in the contralesional hemisphere has only been shown chronically after very severe contusion injury[17] and its role in recovery is unknown. Occurrence of spontaneous, ipsilesional axonal plasticity within the first 2 weeks after TBI,[11] as well as temporary expression of indirect markers of new neuronal connections, such as growth-associated protein 43, microtubule-associated proteins, and polysialylated neural cell adhesion molecule,[18] imply the existence of an earlier, temporary post-traumatic reorganizational state within the brain. This altered state would predict that important cortical map changes occur earlier than previously studied. The eventual postinjury accumulation of growth-inhibitory proteins that mark the end of the growth-promoting period[19] would also predict that further map changes may be stymied, reflecting a reassertion of the normal growth-inhibitory environment of the brain. A determination of how these map changes evolve after TBI is important to determine how future interventional studies may be used to either stimulate or inhibit brain function to promote functional recovery.

In the current study, we have used the controlled cortical impact (CCI) injury rat model, as implemented by us,[20] to investigate the evolution of changes in brain activation after injury over the hindlimb cortical area. $^{14}$C iodoantipyrine (IAP) autoradiography was used to examine the relative local cerebral blood flow (LCBF) changes in response to hindlimb stimulation as a marker for neuronal activity. Here, we present novel findings on temporospatial mappings of the reorganizational response, a hitherto underreported phenomenon after brain trauma, given the importance of the brain's endogenous regenerative potential as a therapeutic target for further enhancement.

## Methods

### *Experimental protocol*

Mild electrical stimulation of the affected (right) hindlimb was used to evoke cerebral activation and was detected by the autoradiographic analysis of the increased LCBF at 4, 7, and 30 days after CCI injury over the left hindlimb, sensory motor cortex ($n = 5$/group), or after sham injury ($n = 3$) of adult male Sprague-Dawley rats (200–300 g body weight). An additional sham group that was not stimulated ($n = 3$) served as a control group to determine a brain region in stimulated animals, where LCBF remained unaffected by stimulation, for use as a normalization region for determining a threshold for increased LCBF. A pilot laser Doppler (LD) cerebral blood flow study was performed in naïve rats ($n = 3$) to determine optimal stimulation parameters for brain activation. All study protocols were approved by the UK Animals Scientific Procedures Act (1986).

### *Pilot study for determining optimal stimulation parameters*

Naïve rats were anaesthetised with 3% isoflurane vaporized in 70% nitrous oxide/30% oxygen and then maintained with 2% isoflurane during surgery. Rats were positioned in a stereotaxic frame, after which a dental trephine drill was used to make a 5-mm craniotomy over the left parietal cortex, 0.5 mm posterior to the coronal suture and 3 mm lateral to the sagittal suture. Using the same α-chloralose sedation anesthesia protocol as used for functional activation (see below), mean arterial blood pressure (MAP) was continuously monitored through the femoral artery, and an LD flowmetry probe (needle-shaped, 0.8 mm), mounted on a micromanipulator and connected to an LD blood-perfusion monitor, was used to monitor LCBF. Care was taken to obtain flow readings only from areas free of large pial vessels. LCBF changes were calculated relative to baseline, defined as the average flow for 3 sec before stimulation. Then, stimulation intensity applied to the hindlimb (see below) was increased from 2 V in steps of 2 V for 1 min and 30 sec. Between each stimulation intensity run, a rest period of 3 min was allowed, during which time the LCBF returns to baseline. Blood gases were measured 20 min after administration of α-chloralose and during the period of stimulation.

### *Brain injury*

Rats were placed under surgical isoflurane anesthesia as described above. The method for induction of CCI injury was performed in the manner described previously.[20–22] Briefly, after reduction of anesthesia to 1.0–1.5% isoflurane and 0.8/0.4 L/min of $N_2O/O_2$, a 2.5-mm-diameter piston was advanced through a 5-mm craniotomy at −0.5 mm posterior to Bregma and 3 mm left-lateral to the sagittal suture and onto the brain at 4 m/sec to a deformation depth of 2 mm below the dura. The bone flap was immediately replaced and sealed, and the scalp was sutured-closed. Rats were placed in a heated cage to maintain body temperature while recovering from anesthesia and soluble paracetamol (1 mg/mL; Cox Pharmaceuticals, Barnstaple, UK) was administered in the drinking water postoperatively.

### *Functional autoradiography*

Under surgical isoflurane anesthesia as before, rats were tracheotomized and then artificially ventilated (Harvard Apparatus, Maidstone, UK) with 1.5% isoflurane in 70% nitrous oxygen/30% oxygen. The left femoral artery was cannulated for monitoring of arterial blood gases and periodic plasma sampling, and the right femoral vein was cannulated for administration of anesthetic agents and isotope infusion. A small-needle electrode was inserted subcutaneously (s.c.) on the right hindpaw, from the medial globular pads extending distally toward the limb. The indifferent electrodes were inserted s.c. at the chest. Tidal volume and ventilation rate were adjusted to maintain normal blood chemistry, and body temperature was kept constant at 37 ± 0.5°C with a homeothermic-controlled heating pad (Harvard Apparatus). Rats were paralyzed by an intravenous (i.v.) bolus of pancuronium (0.6 mg/kg; Organon International, Newhouse, UK), followed by continuous i.v. infusion (0.6 mg/kg/h). Isofluorane anesthsesia was replaced with α-chloralose sedation (50 mg/kg, bolus i.v. infusion; Sigma-Aldrich, Dorset, UK) to prevent the blunting effect of isoflurane on brain activation. Continuous affected (right) hindlimb stimulation was initiated for a 20-min period after discontinuing isoflurane to allow the effects of the isofluorane to dissipate. An optimal stimulation intensity of 8 V (Fig. 1A,B; see Results) with a frequency of 5 Hz and stimulation duration of 0.5 sec was given. Stimulation was begun 30 sec before the beginning of isotope infusion for LCBF autoradiography and continued throughout the measurement of blood samples until the brain was frozen. Autoradiography was performed as described previously[21,22]; briefly, 925 KBq of IAP (Tocris Cookson, Bristol, UK) was infused i.v. over 60 sec using a ramped infusion, and arterial blood samples were collected onto a filter paper every 3 sec. After decapitation, the brain was rapidly excised, frozen in dry ice-cooled isopentane, and subsequently

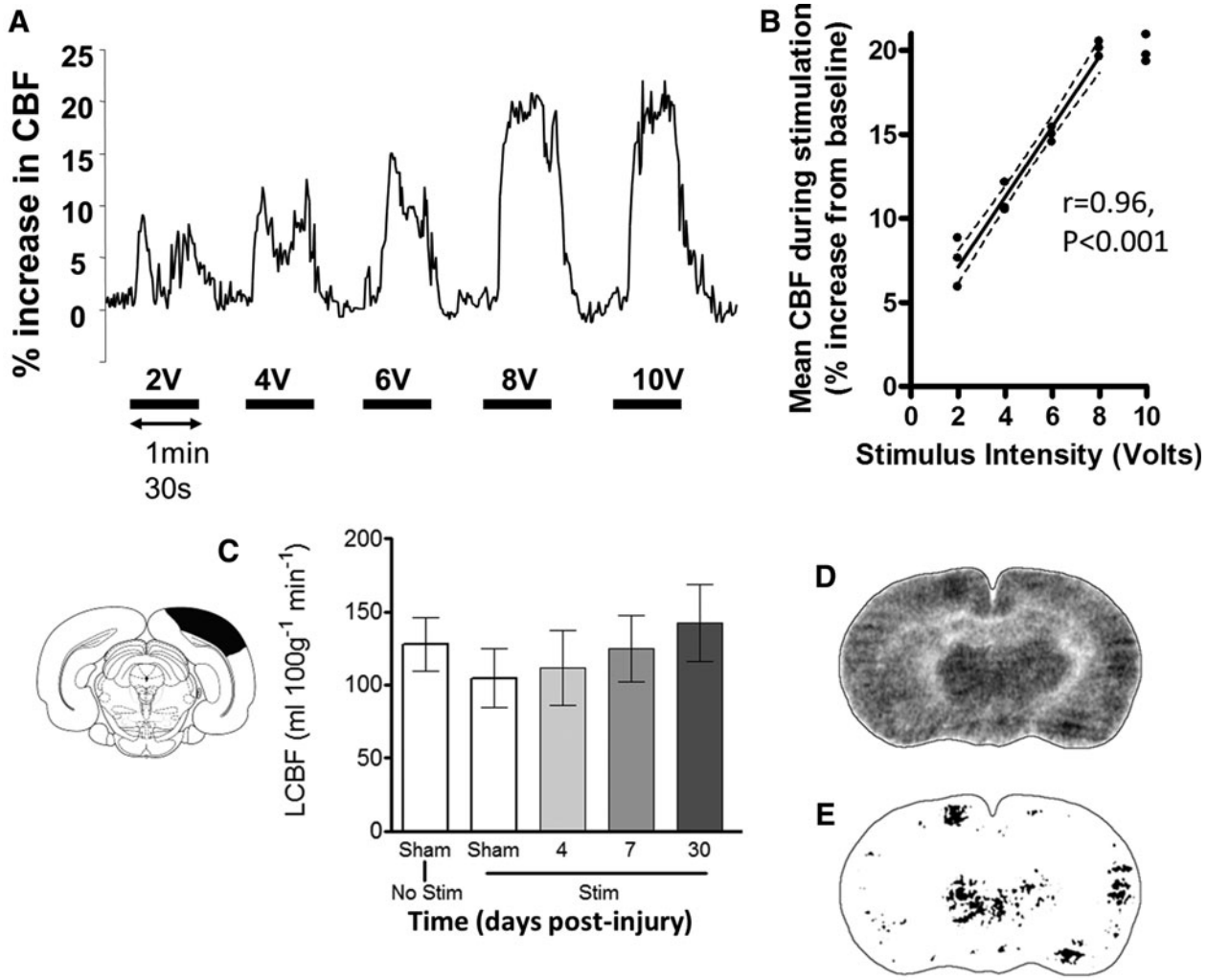


**FIG. 1.** (**A**) Representative laser Doppler flowmetry trace of cerebral blood flow (CBF) from the left hindlimb sensorimotor cortex of a naïve rat showing recorded increases in CBF during periods of electrical stimulation of the contralateral (right) hindlimb. (**B**) CBF increased linearly with stimulus intensity from 2 V to a maximum of 20% above baseline at 8 V (filled circles are individual values from 3 naïve rats; dotted lines represent 95% confidence limits). There was no further increase in CBF at 10 V, compared to 8 V ($p > 0.05$), and so 8 V was used in all autoradiographic experiments. (**C**) Local CBF (LCBF) values obtained by autoradiography did not vary significantly with stimulation in a cortical region at $-6.8$ mm posterior to Bregma, as indicated graphically by the absence of LCBF changes between sham-injured unstimulated (No Stim; $n = 3$), sham-injured stimulated (Stim; $n = 3$), and stimulated brain-injured rats ($p > 0.05$; $n = 5$/group). This region was used as a baseline from which to interrogate images for LCBF changes $>2$ standard deviations (SDs) for assessment of regions of brain activation (see Methods). (**D**) A representative LCBF image from a sham-injured rat analyzed for regions of cortical activation and (**E**) the result of applying a threshold LCBF that is 2 SDs above baseline values in cortex unaffected by stimulation at $-6.8$mm from Bregma. Data are plotted as means ± standard error of the mean.

sectioned at 20 $\mu$m in a cryostat. Brain and plasma IAP concentration were determined using a phosphor imager (Cyclone; PerkinElmer Life Sciences Ltd., Cambridge, UK) and calibrated $^{14}$C standards (Amersham PLC, Little Chalfont, UK), as described previously.[21,22] Blood gases were measured 20 min after administration of $\alpha$-chloralose, during the period of stimulation.

### *Image analysis*

Brain tissue and plasma isotope concentration images of IAP were used to calculate parametric images of LCBF, as described previously.[21,22] To systematically define the region of brain exhibiting increased LCBF as an indicator of brain activation within each brain, the number of pixels was determined with LCBF values greater than 2 standard deviations (SDs) above posterior cortical mean LCBF values at $-6.80$ mm from Bregma and ipsilateral to the stimulated limb (Fig. 1C), a region where LCBF remains unaffected by the stimulation (see Results). The analysis was performed with ImageJ software (National Institutes of Health, Bethesda, MD),[23] which was also used to calibrate and scale the images and convert the ''activated'' pixel numbers to area measurements. Three coronal sections corresponding to Bregma $-1.30$, $-2.3$, and $-5.8$ mm were analyzed per brain, and the sum of each activated brain region for ipsi- and contralesional hemispheres was computed. The rationale for the choice of section levels was based upon the two anterior sections containing hindlimb S1 cortex as well as the likelihood of observing new activations within the posterior cortex, as indicated by initial pilot autoradiographic data. Mean LCBF was obtained from each activated region to test for differences in degree of LCBF enhancement.

The ratio of bilateral hemispheric activation was calculated and expressed as a laterality index for each section by computing the following equation: ipsilesional area − contralesional area/ipsilesional area + contralesional area.

### Statistical analysis

Kolmogorov-Smirnov's test with Lillie's correction and Levene's median test were used to describe distribution of data and determine equality of variances, respectively. Having passed these normality tests, group numerical data were expressed as the means ± standard error of the mean. A one-way analysis of variance (ANOVA) was used to compare physiology data. A two way-way ANOVA (group × region) was used to compare sham- and trauma-group autoradiographic data. Because there were no differences among the different levels of region (anteroposterior level) for any group data, a one-way ANOVA was performed, followed by a Student's/Newman-Keuls' post-hoc method to test for any significant differences among the groups. The laterality index data failed the normality test, and so an ANOVA on ranks was performed, followed by Dunn's method for pairwise multiple comparison procedure. As a result, laterality data are plotted as medians, 25th and 75th percentiles, and minimum/maximum values in a box-and-whiskers plot. Difference between the means were assessed at the probability levels $p < 0.05$, 0.01, and 0.001.

## Results

A pilot experiment using LD flowmetry in 3 naïve rats was initially performed to determine the optimal stimulation parameters for the autoradiographic experiment. There was a linear increase in cerebral blood flow with increasing hindlimb stimulation intensity from 2 V to a maximal 20% change from baseline at 8 V intensity ($r = 0.96$; $p < 0.001$; Fig. 1A,B). No further significant increase was noted at 10 V, and therefore an 8 V stimulus was taken as the optimal intensity and was used for all further experiments. Plasma chemistry values were within normal limits both before and after stimulation, and there was no significant increase in MAP above baseline during the stimulation (Table 1), indicating that the stimulus was not perceived as noxious.[24]

Injured and sham control rats exhibited stable physiological variables, and there was no significant difference between these groups (Table 2). Analysis of LCBF values in a cortical region of interest within the contralesional (opposite to the injury) visual cortex at Bregma −6.80 mm in nonstimulated and hindlimb-stimulated rats showed that the region LCBF remained unaffected by the stimulation paradigm in all groups, compared to unstimulated sham animals ($p > 0.05$; Fig. 1C). As a result, this region was used within each brain to determine the global cortical LCBF threshold, which was greater than 2 SDs above mean baseline LCBF, to systematically determine the region of activation within each cortex (Fig. 1D,E). The mean LCBF within the activated regions was generally between 10 and 20% above baseline LCBF values (Fig. 2). Detectable increases in LCBF above baseline were only observed in sham-injured brains within left cortical regions at Bregma −1.30 and 2.30 mm opposite to the stimulated limb and not in posterior regions at Bregma −5.80 mm, or in right cortical regions ipsilateral to the stimulated limb. In injured brain, the amplitude of the LCBF change at 2 SDs above baseline was not significantly different to sham values or among any other region with raised LCBF in injured brain. However, as indicated below, although LCBF remained unaltered in brain regions normally activated in sham-injured rats (Fig. 3), LCBF increased within additional cortical areas, in posterior ipsilesional regions, at all anteroposterior levels on the contralesional cortex, and at all times examined after injury. These values are plotted against LCBF values obtained from more anterior-activated regions in sham animals (Fig. 2).

As expected, stimulation of the right hindlimb in sham-injured animals resulted in activation within the hindlimb region of the left sensory-motor/primary motor cortex (S1HL/M1) contralateral to the stimulated hindlimb at −1.3 and −2.3 mm from Bregma (Fig. 3A). No activation was observed in the opposite, right hemisphere and none was present in either hemisphere at −5.8 mm, which is outside of the hindlimb sensorimotor representation. As a result of this unilateral activation, sham-group laterality index values, a measure of the degree of bilateral activation, were +1 in all regions examined (Fig. 4B,D,F). Stimulation of the right (affected) hindlimb at 4 days after injury did not result in left, ipsilesional S1HL/M1 cortical activation (Fig. 2B). This pattern of decreased volume of activation was noted not only in the contusion core over the S1HL region, but also in the cortical areas posterior to the injury site at −2.3 mm from Bregma. Despite this, however, there were new areas of ipsilesional cortex activation, which were primarily located lateral and ventral to the S1HL sensorimotor cortex within the whisker barrel and S2 cortical regions, so that the total summed areas of ipsilesional activation were not different from sham-injured animals at any anteroposterior level at 4 days ($p > 0.05$; Fig. 4A,C,E). Clear activation responses were also detected in the opposite, contralesional hemisphere (i.e., ipsilateral to the stimulated paw) that were similar among all anteroposterior levels examined ($p > 0.05$ effect of region; two-way ANOVA), compared to stimulated sham-injured rats, where no contralesional activation was present (Figs. 3B and 4A,C,E). These areas of activation involved various cortical regions, including areas that are not normally involved in sensorimotor function of the hindlimb (e.g., barrel field, forelimb, and auditory cortex regions). As a result, the laterality index was significantly decreased and negative at all anteroposterior levels analyzed, compared to sham ($p < 0.05$, ANOVA on ranks; Fig. 4B,D,F). Although subcortical regions also appeared

Table 1. Physiological Data in Naïve Rats

| | *Before stimulation* | *During stimulation* |
|---|---|---|
| pH | 7.43 ± 0.04 | 7.42 ± 0.01 |
| $PO_2$ (mmHg) | 136.5 ± 6.5 | 130.8 ± 4.5 |
| $PCO_2$ (mmHg) | 40.3 ± 2.3 | 41.1 ± 2.8 |
| MAP (mmHg) | 111 ± 1.5 | 113 ± 1.4 |

Values are expressed as the mean ± standard error of the mean.
MAP, mean arterial pressure.

Table 2. Physiological Data During Hindlimb Stimulation in Rats After TBI or Sham Injury

| | *Sham control* | *TBI* | | |
|---|---|---|---|---|
| | | *Day 4* | *Day 7* | *Day 28* |
| pH | 7.43 ± 0.07 | 7.42 ± 0.03 | 7.42 ± 0.05 | 7.55 ± 0.03 |
| $PO_2$ (mmHg) | 153.5 ± 21.5 | 136.8 ± 12.5 | 135.8 ± 20.4 | 140.0.8 ± 22.9 |
| $PCO_2$ (mmHg) | 40.3 ± 6.7 | 44.0 ± 2.8 | 39.8 ± 8.7 | 36.7 ± 2.5 |

Values are expressed as the mean ± standard error of the mean.
TBI, traumatic brain injury.

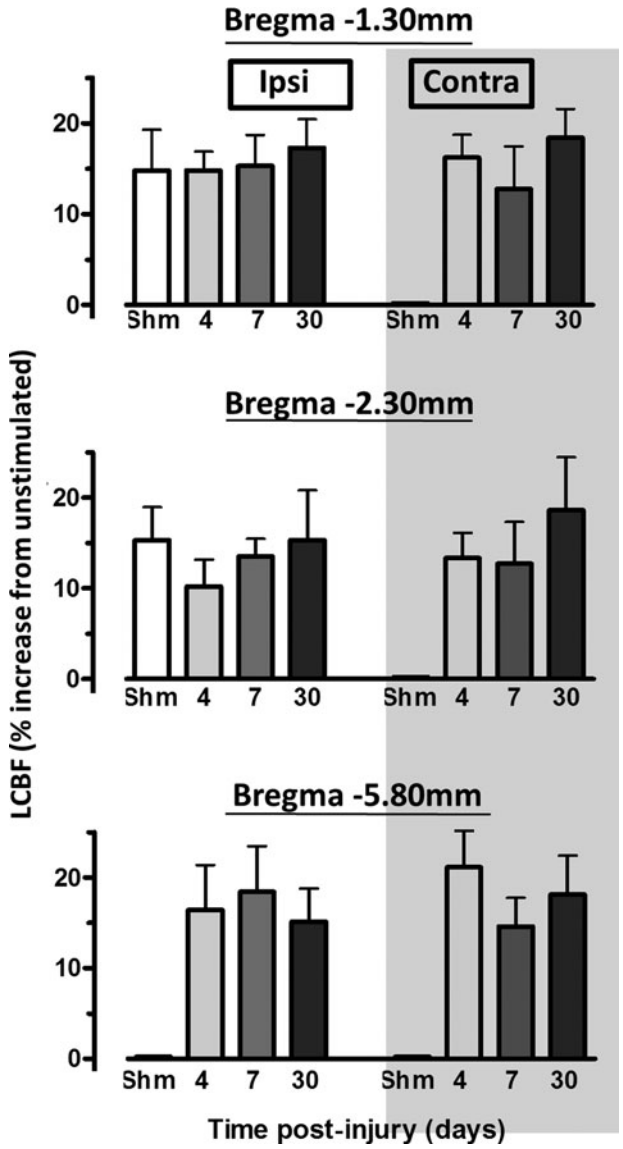


**FIG. 2.** Plots of percent increases in local cerebral blood flow (LCBF) above baseline, unstimulated cortex from activated brain regions that were obtained by image analysis of autoradiographic section images at three anteroposterio levels (see Methods). Cortical LCBF increases were consistently between 10 and 20% above baseline and this did not differ significantly across section levels or between sham (shm) and injured groups ($p > 0.05$). However, in injured rats, detectable increases in evoked LCBF occurred in cortical regions that were not observed in sham animals, in all contralesional regions as well as bilateral posterior regions at Bregma −5.80 mm.

to be activated, the regions were not delineated robustly and reproducibly enough among animals, indicating that the baseline cortical LCBF values used to determine a significant increase in LCBF were not appropriate for determining activation in other brain regions.

The regions of new ipsilesional activation (whisker barrel and S2 cortex) that were present at 4 days postinjury remained activated at 7 days (Fig. 3C) and did not differ among region examined ($p > 0.05$, two-way ANOVA, region effect). Although the areas of ipsilesional activation were larger and approached significance, compared to 4 days ($p = 0.054$, two-way ANOVA, group effect; Fig. 4A,C,E), there was no effect on the laterality index, compared to 4 days ($p > 0.05$), and it remained significantly decreased and negative, compared to the sham-injured group, at all anteroposterior levels ($p < 0.05$, ANOVA on ranks; Fig. 4B,D,F).

Novel areas of ipsilesional activation remained within whisker barrel, S2 cortex (−1.3 and −2.3 mm Bregma), and auditory cortex (−5.8 mm Bregma; Fig. 3D) at 30 days after injury, and these were significantly greater in size, compared to either sham or the 4-day injured groups ($p < 0.01$; Fig. 4A,C,E). However, although contralesional activation remained, it was significantly smaller in size, compared to at 4 and 7 days postinjury ($p < 0.001$), although it was still larger, compared to sham-injured values, where only unilateral activation was present ($p < 0.05$; Fig. 4A,C,E). As a result, the laterality index at 30 days postinjury was positive or at zero in all regions examined, which, over all regions combined, was not significantly different from sham levels ($p > 0.05$, ANOVA on ranks; Fig. 4B,D,F). Clearly, however, the continued presence of some contralesional activation among some rats at 30 days postinjury resulted in variation in the laterality index, indicating that it was not yet completely normalized.

## Discussion

Cortical contusion injury resulting in a lesion over the ipsilateral M1/S1HL sensorimotor cortex was associated with loss of brain activity in these areas. The most novel finding from this study is that there was a shift in brain activation response from its normal position within the lesioned hemisphere to the opposite, contralesional hemisphere. At later times after trauma, this was followed by a shift back to the perilesional cortex, albeit to a different brain region, and some contralesional activation remained.

We measured activation responses by use of IAP autoradiography, which enables us to assess changes in neuronal activity through the measurement of cerebral blood flow (CBF) variations. The use of CBF as an index of neuronal activity is based on the presupposed tight coupling between neuronal activity, metabolism, and CBF.[25] Indeed, several experimental studies have reported a positive linear correlation between electrophysiological and CBF responses.[26,27] The presence of increased LCBF that was limited to hindlimb regions contralateral to the stimulated limb in sham rats in the current study suggests that the protocol used in the experiments was responsive to intact coupling neurovascular coupling.

### *Ipsilesional M1/S1HL cortical activation is depressed acutely*

The absence of activation from within the normal injured M1/S1HL sensorimotor region at Bregma −1.30 mm at 4 days persisted at all times after injury, and this has been reported at even more chronic times after severe CCI injury.[17] The mid-line/anterior region containing motor and at least some S1 cortex remains intact, despite the nearby cavity (Fig. 2), as we have shown previously in the same model using histology,[20] indicating it is not the merely the destruction of tissue that results in inactivation. The status of neurovascular uncoupling in this model is not known, but sensory-evoked potentials are initially absent after acceleration concussion in the rat, after which they are present, but much reduced,[28] so that coupling is likely to be intact by 4 days postinjury in this study. However, there are early perturbations in metabolism and CBF that result in metabolic uncoupling after CCI injury,[21,29] so that the brain may be unable to respond to limb stimulation. Further, there is ample evidence of ionic and/or neurotransmitter perturbations after

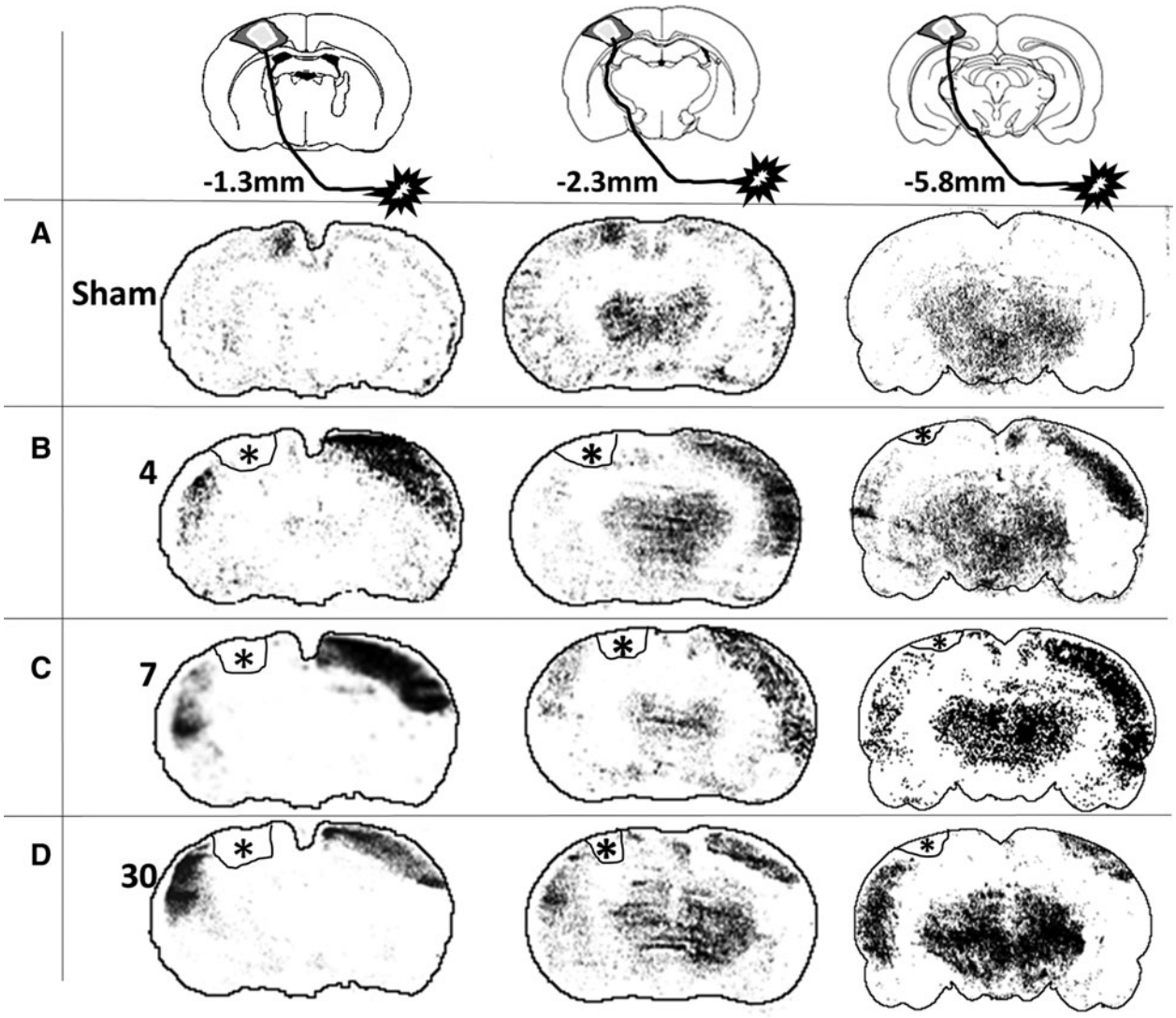


**FIG. 3.** Representative images of local cerebral blood flow (LCBF) autoradiographic coronal sections at three different anteroposterior levels that were acquired during electrical stimulation of the affected (right) hindlimb in (**A**) a sham-injured rat and injured rats at (**B**) 4, (**C**) 7, and (**D**) 30 days after injury. Images were systematically processed (see Methods) to determine the region of increased LCBF corresponding to brain activation (above an unaffected posterior baseline region) and superimposed on the approximate outline of the corresponding atlas section. Hyperintense areas represent LCBF values that are $>2$ standard deviations above a posterior cortical region unaffected by the stimulation. Asterisk represents the location of the impact injury, which has been outlined on these images.

brain injury in the rodent,[30,31] which are also likely to have contributed to the depressed activation in this study. Therefore, at least acutely, the failure of LCBF increase within the ipsilesional cortex might be the result of altered neurovascular coupling after TBI.

The persistent absence of ipsilesional M1/S1HL activation at more chronic postinjury times is similar to the failure to observe whisker-deflected cortical activation for almost 2 months after fluid percussion injury.[16] The absence of activation after CCI injury occurs when cerebral glucose metabolism has normalized in this model,[32] which suggests that either the region has become irreversibly damaged from ensuing tissue atrophy or other local injury mechanisms, or that the region has become chronically disconnected. Disconnection is more likely, because the injured ipsilesional cortex can, in fact, be locally activated by direct stimulation after fluid percussion injury.[33] Ongoing intra- and intercortical and corticothalamic denervation has been shown to be rather more widespread than merely affecting the contused region after rodent CCI injury,[34,35] and axonal damage and disconnection underlying the contusion and mid-line region is evident at this level of injury in this model.[22] Even after more mild CCI injury, there is a persistent reduction in both callosal,[36] as well corticospinal, fiber tracks, as assessed by diffusion tensor imaging,[37] suggesting that ongoing inactivation of gray matter is consistent with deficits in connectivity to other relay centers within the central nervous system (CNS).

### *Ipsilesional activation increases in novel regions chronically*

Despite the disappearance of activation within S1HL regions, ipsilesional activation was clearly evident very soon postinjury within lateral S2 and barrel cortical regions as well as more remote ipsilesional auditory regions at $-5.80$ mm from Bregma. This is

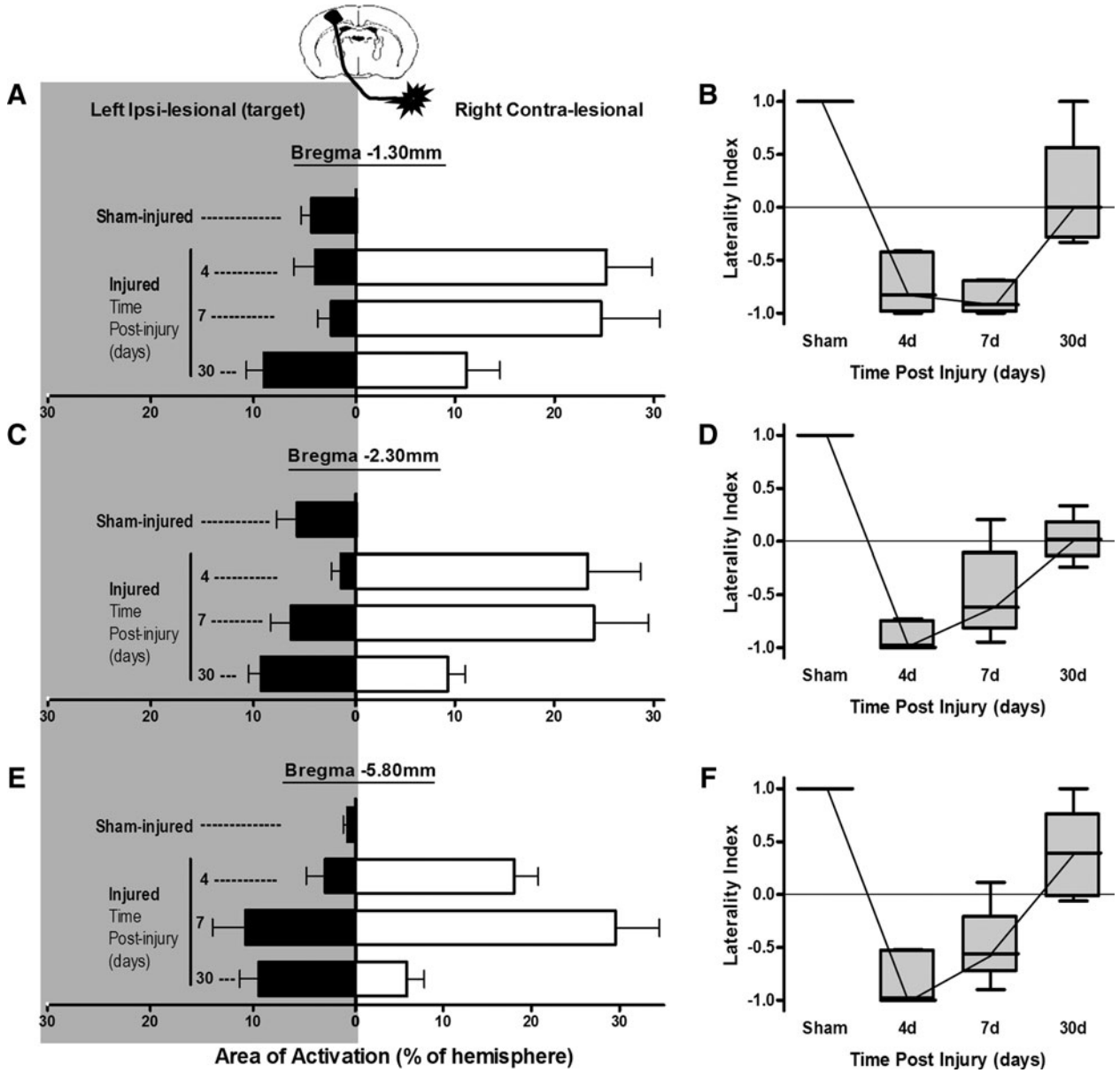


**FIG. 4.** Plots of right (affected) hindlimb evoked, ipsilesional (closed bars), and contralesional (open bars) cortical activation areas (**A, C,** and **E**) and the corresponding laterality index (**B, D,** and **F**] quantified on local cerebral blood flow autoradiographic images at three anteroposterior levels from Bregma (**A** and **B**) −1.30 (**C** and **D**), −2.30, and (**E** and **F**) −5.80 mm in sham- and brain-injured rats at 4, 7, and 30 days after injury. There was no effect of anteroposterior region examined for any parameter ($p > 0.05$; two-way ANOVA), and so group comparison statistics are pooled and are therefore not shown on the individual region plots for clarity. (**A, C,** and **E**) Activation area data are plotted as mean ± standard error of the mean. There was a significant increase in both ipsilesional activation area at 30 days versus sham ($p < 0.01$) and contralesional area at 4, 7, and 30 days versus sham ($p < 0.05$). (**B, D,** and **F**) Laterality index, non-normally distributed data are plotted as median, 25th and 75th percentiles, and minimum/maximum values. A group analysis for pooled regions with a one-way ANOVA on ranks showed a significantly decreased laterality index at 4 and 7 days versus sham ($p < 0.05$), but a significant rise at 30 days, compared to 4 and 7 days ($p < 0.05$), that was overall not different from sham ($p > 0.05$).

different from rodent stroke models of middle cerebral artery occlusion, where ipsilesional activation is reduced or absent until more chronic times,[13] and more similar to changes observed after targeted ministrokes.[38] The sudden appearance of these new regions of activation largely negates the idea that any structural changes are responsible. However, representative autoradiograms (Fig. 3) do show that these regions persist and even enlarge over time, implying that immediate ipsilesional map reorganization is not simply the result of mechanisms governing short-term plasticity, such as temporary changes in receptor densities and/or long-term potentiation- and depression-type mechanisms. Map changes occur even within the first hour after stroke,[38] presumably the result of unmasking of existing horizontal circuits.[39] We have observed similar activation patterns as those described herein using forelimb-evoked blood-oxygen-level–dependent functional magnetic resonance imaging before and after rat CCI injury[40] and with functional micropositron tomography of fluordeoxyglucose uptake (N.G. Harris, unpublished observations, November 2012), so that they

cannot be simply regarded as methodological artefacts. Spontaneous axonal sprouting does occur within the ipsilesional cortex in this model over the first 3 weeks,[11] which may well aid in stabilization of the cortical map changes consolidating the circuit rearrangements. The stimulation protocol employed here is likely to have activated most of the nerves contained within the proximal hindpaw and their branches, so that both sensory and motor representations are observed, as reported for forelimb.[41] Therefore, the new ipsilesional activation may equally represent changes in both afferent (sensory) input as well as efferent (motor) output, because the latter activation will occur through antidromic nerve conduction.[42] In fact, motor control by sensory cortex has been shown to occur in rodent sensory barrel cortex,[43] so that it is plausible that the novel activations do represent both systems and are crucial for the spontaneous behavioral recovery of limb use that occurs in this model.[14,44]

### *"Wrong side" contralesional activation occurs early after TBI*

We observed extensive cortical activation within the contralesional hemisphere as early as 4 days after injury that persisted, in some regions, until 30 days. Similar observations have been made in the rat after suction ablation cortical lesions,[45] middle cerebral artery occlusion stroke,[13] and at 2 months after CCI injury,[17] as well as after clinical stroke.[12,46,47] Though the mechanism for this remapping is uncertain, the short timescale precludes the idea of structural remodeling occurring to reshape the map because, unlike in stroke or lesioning studies,[10,48–51] compensatory structural neuronal plasticity does not occur in the contralesional cortex after CCI injury.[52] However, this does not necessarily rule out that compensatory motor learning associated with over-reliance of the unaffected limb[49,53] might occur to activate contralesional circuits without any major structural remodeling. The extreme asymmetry of limb use early after brain injury[44,52] and the finding that the maladaptive effects of nonparetic limb use depend upon the contralesional cortex[54] would support this as a potential mechanism. It is also plausible that the mechanism of cortical plasticity is driven partly or even solely by CNS-related changes. Past studies have shown that silencing primary somatosensory cortex by cooling results in an immediate expansion of contralateral receptive fields[55] and, after stroke, wrong-sided, contralesional response resulting from affected limb stimulation occurs within 30 min of infarct.[38] There is now increasing evidence for the cooperative, functional interdependence of bilaterally connected cortical regions,[56] so that alteration in output from one cortex significantly alters the other.[57,58] Loss of anatomical connectivity after CCI injury, either by destruction of cortical gray matter or damage to underlying white matter circuitry, results in significant down-regulation of contralesional gamma-aminobutyric acid–mediated alpha-1 receptors.[59] This is consistent with the idea of a loss of transhemispheric inhibition within the contralesional hemisphere from the injured side, and this may be one mechanism that underlies the contralesional activation observed, especially because the near complete normalization of receptors at 4 weeks[59] coincides with the reduction in the size of the contralesional map shown in the present study.

The obvious question that arises from this contralesional activation data is, what is the relevance to outcome? At least after experimental ischemia, this is dependent on the severity or size of the infarct, because subsequent to recovery of forelimb deficits, silencing or lesioning the contralesional cortex reinstates the deficits, but only in rats with the largest strokes,[60,61] indicating the functional importance of the contralesional cortex in motor recovery only in the most severe cases. Similar conclusions are arrived at after CCI injury, where involvement of the contralesional cortex in affected limb control is related to the size of the contusion[40] (Harris and colleagues, submitted). Clinical stroke evidence shows that restoration of the cortical map back to newly reorganized, adjacent motor-associated regions within the ipsilesional hemisphere is required for good outcome.[62–64] We observed a shift of activation back to the ipsilesional hemisphere between 7 and 30 days after trauma to perilesional sites, indicating the injury was not severe enough to prolong wrong-side activation. It remains to be determined whether wrong-side, contralesional activation influences ipsilesional plasticity acutely; whether it is beneficial or detrimental for plasticity. Given the temporal similarities between the postinjury time window in which the ipsilesional hemisphere remains permissive for plasticity,[11,19] and the time when wrong-side activity occurs, further studies are warranted to investigate this.

In conclusion, we have shown that alterations in the cortical hindlimb somatosensory map size and location occur spontaneously after CCI injury. Ensuing novel regions of ipsilesional activity occur in the face of decreasing wrong-sided contralesional involvement, concordant with the known improvement in functional deficits that occur in this model.

## Acknowledgments

This work was supported by a National Institutes of Health/National Institute of Neurological Disorders and Stroke award (#NS055910) and the UCLA Brain Injury Research Center.

## Author Disclosure Statement

No competing financial interests exist.

## References

1. Katz, D.I., Alexander, M.P., and Klein, R.B. (1998). Recovery of arm function in patients with paresis after traumatic brain injury. Arch. Phys. Med. Rehabil. 79, 488–493.
2. Gagnon, I., Forget, R., Sullivan, S.J., and Friedman, D. (1998). Motor performance following a mild traumatic brain injury in children: an exploratory study. Brain Inj. 12, 843–853.
3. Tremblay, S., de Beaumont, L., Lassonde, M., and Théoret, H. (2011). Evidence for the specificity of intracortical inhibitory dysfunction in asymptomatic concussed athletes. J. Neurotrauma 28, 493–502.
4. Hillier, S.L., Sharpe, M.H., and Metzer, J. (1997). Outcomes 5 years post-traumatic brain injury (with further reference to neurophysical impairment and disability). Brain Inj. 11, 661–675.
5. Kasahara, M., Menon, D.K., Salmond, C.H., Outtrim, J.G., Taylor Tavares, J.V, Carpenter, T.A., Pickard, J. D., Sahakian, B.J., and Stamatakis, E.A. (2010). Altered functional connectivity in the motor network after traumatic brain injury. Neurology 75, 168–176.
6. Teasdale, G.M., and Graham, D.I. (1998). Craniocerebral trauma: protection and retrieval of the neuronal population after injury. Neurosurgery 43, 723–737.
7. Stroemer, R.P., Kent, T.A., and Hulsebosch, C.E. (1995). Neocortical neural sprouting, synaptogenesis, and behavioral recovery after neocortical infarction in rats. Stroke 26, 2135–2144.
8. Li, Y.Y., Jiang, N., Powers, C., Chopp, M., and Johansson, B.B. (1998). Neuronal damage and plasticity identified by microtubule-associated protein 2, growth-associated protein 43, and cyclin D1 immunoreactivity after focal cerebral ischemia in rats. Stroke 29, 1972–1980.
9. Carmichael, S.T., Archibeque, I., Luke, L., Nolan, T., Momiy, J., and Li, S. (2005). Growth-associated gene expression after stroke: evidence for a growth-promoting region in peri-infarct cortex. Exp. Neurol. 193, 291–311.

10. Adkins, D.L., Voorhies, A.C., Jones, T.A. (2004). Behavioral and neuroplastic effects of focal endothelin-1 induced sensorimotor cortex lesions. Neuroscience 128, 473–486.
11. Harris, N.G., Mironova, Y.A., Hovda, D.A., and Sutton, R.L. (2010). Pericontusion axon sprouting is spatially and temporally consistent with a growth-permissive environment after traumatic brain injury. J. Neuropathol. Exp. Neurol. 69, 139–154.
12. Cramer, S.C., Nelles, G., Benson, R.R., Kaplan, J.D., Parker, R.A., Kwong, K.K., Kennedy, D.N., Finklestein, S.P., and Rosen, B.R. (1997). A functional MRI study of subjects recovered from hemiparetic stroke. Stroke 28, 2518–2527.
13. Dijkhuizen, R.M., Ren, J., Mandeville, J.B., Wu, O., Ozdag, F.M., Moskowitz, M.A., Rosen, B.R., and Finklestein, S.P. (2001). Functional magnetic resonance imaging of reorganization in rat brain after stroke. Proc. Natl. Acad. Sci. U. S. A. 98, 12766–12771.
14. Nishibe, M., Barbay, S., Guggenmos, D., and Nudo, R. J. (2010). Reorganization of motor cortex after controlled cortical impact in rats and implications for functional recovery. J. Neurotrauma 27, 2221–2232.
15. Hall, K.D., and Lifshitz, J. (2010). Diffuse traumatic brain injury initially attenuates and later expands activation of the rat somatosensory whisker circuit concomitant with neuroplastic responses. Brain Res. 1323C, 161–173.
16. Passineau, M.J., Zhao, W., Busto, R., Dietrich, W.D., Alonso, O., Loor, J.Y., Bramlett, H.M., and Ginsberg, M.D. (2000). Chronic metabolic sequelae of traumatic brain injury: prolonged suppression of somatosensory activation. Am. J. Physiol. Heart. Circ. Physiol. 279, H924–H931.
17. Dunn-Meynell, A.A., and Levin, B.E. (1995). Lateralized effect of unilateral somatosensory cortex contusion on behavior and cortical reorganization. Brain Res. 675, 143–156.
18. Emery, D.L., Raghupathi, R., Saatman, K.E., Fischer, I., Grady, M.S., and McIntosh, T.K. (2000). Bilateral growth-related protein expression suggests a transient increase in regenerative potential following brain trauma. J. Comp. Neurol. 424, 521–531.
19. Harris, N.G., Carmichael, S.T., Hovda, D.A., and Sutton, R.L. (2009). Traumatic brain injury results in disparate regions of chondroitin sulfate proteoglycan expression that are temporally limited. J. Neurosci. Res. 87, 2937–2950.
20. Chen, S., Pickard, J.D., and Harris, N.G. (2003). Time course of cellular pathology after controlled cortical impact injury. Exp. Neurol. 182, 87–102.
21. Chen, S.F., Richards, H.K., Smielewski, P., Johnstrom, P., Salvador, R., Pickard, J.D., and Harris, N.G. (2004). Relationship between flow-metabolism uncoupling and evolving axonal injury after experimental traumatic brain injury. J. Cereb. Blood Flow Metab. 24, 1025–1036.
22. Harris, N.G., Mironova, Y.A., Chen, S.-F., Richards, H.K., and Pickard, J.D. (2012). Preventing flow-metabolism uncoupling acutely reduces axonal injury after traumatic brain injury. J. Neurotrauma 29, 1469–1482.
23. Rasband, W.S. (2008). ImageJ, U.S. National Institutes of Health, Bethesda, MD, http://rsb.info.nih.gov/ij/, 1997–2008.
24. Nordin, M., and Fagius, J. (1995). Effect of noxious stimulation on sympathetic vasoconstrictor outflow to human muscles. J. Physiol. 489, 885–894.
25. Roy, C.S., and Sherrington, C.S. (1890). On the regulation of the blood-supply of the brain. J. Physiol. 11, 85–108.
26. Mathiesen, C., Caesar, K., Akgören, N., and Lauritzen, M. (1998). Modification of activity-dependent increases of cerebral blood flow by excitatory synaptic activity and spikes in rat cerebellar cortex. J. Physiol. 512, 555–566.
27. Ngai, A.C., Jolley, M.A., D'Ambrosio, R., Meno, J.R., and Winn, H.R. (1999). Frequency-dependent changes in cerebral blood flow and evoked potentials during somatosensory stimulation in the rat. Brain Res. 837, 221–228.
28. Shaw, N.A. (1986). Somatosensory evoked potentials after experimental head injury in the awake rat. J. Neurol. Sci. 74, 257–270.
29. Richards, H.K., Simac, S., Piechnik, S., and Pickard, J.D. (2001). Uncoupling of cerebral blood flow and metabolism after cerebral contusion in the rat. J. Cereb. Blood Flow Metab. 21, 779–781.
30. Katayama, Y., Becker, D.P., Tamura, T., and Hovda, D.A. (1990). Massive increases in extracellular potassium and the indiscriminate release of glutamate following concussive brain injury. J. Neurosurg. 73, 889–900.
31. Nilsson, P., Hillered, L., Olsson, Y., Sheardown, M.J., and Hansen, A.J. (1993). Regional changes in interstitial K+ and Ca2+ levels following cortical compression contusion trauma in rats. J. Cereb. Blood Flow Metab. 13, 183–192.
32. Moro, N., Ghavim, S.S., Hovda, D.A., and Sutton, R.L. (2011). Delayed sodium pyruvate treatment improves working memory following experimental traumatic brain injury. Neurosci. Lett. 491, 158–162.
33. Ip, E.Y., Zanier, E.R., Moore, A.H., Lee, S.M., and Hovda, D.A. (2003). Metabolic, neurochemical, and histologic responses to vibrissa motor cortex stimulation after traumatic brain injury. J. Cereb. Blood Flow Metab. 23, 900–910.
34. Hall, E.D., Sullivan, P.G., Gibson, T.R., Pavel, K.M., Thompson, B.M., and Scheff, S.W. (2005). Spatial and temporal characteristics of neurodegeneration after controlled cortical impact in mice: more than a focal brain injury. J. Neurotrauma 22, 252–265.
35. Matthews, M.A., Carey, M.E., Soblosky, J.S., Davidson, J.F., and Tabor, S.L. (1998). Focal brain injury and its effects on cerebral mantle, neurons, and fiber tracks. Brain Res. 794, 1–18.
36. Harris, N., Hovda, D., and Sutton, R. (2009). Acute deficits in transcallosal connectivity endure chronically after experimental brain injury in the rat: a DTI tractography study. J. Neurotrauma 26, A37 (Abstract).
37. Harris, N.G., Verley, D., Hovda, D.A., and Sutton, R.L. (2011). Cyclosporin-a reduces grey matter atrophy and stabilizes axonal integrity, but fails to reinstate brain activation after experimental traumatic brain injury. Abstract. #1204 XXVth International Symposium on Cerebral Blood Flow, Metabolism, and Function, Barcelona, Spain. Available at: http://www.abstractserver.com/brain2011/planner/in.
38. Mohajerani, M.H., Aminoltejari, K., and Murphy, T.H. (2011). Targeted mini-strokes produce changes in interhemispheric sensory signal processing that are indicative of disinhibition within minutes. Proc. Natl. Acad. Sci. U. S. A. 108, E183–E191.
39. Jacobs, K.M., and Donoghue, J.P. (1991). Reshaping the cortical motor map by unmasking latent intracortical connections. Science 251, 944–947.
40. Verley, D., Hovda, D.A., Sutton, R.L., and Harris, N.G. (2011). Time-course of sensorimotor brain activation after traumatic brain injury in the rat. J. Neurotrauma 28, A–81,P220.
41. Cho, Y.R., Pawela, C.P., Li, R., Kao, D., Schulte, M.L., Runquist, M.L., Yan, J.-G., Matloub, H.S., Jaradeh, S.S., Hudetz, A.G., and Hyde, J.S. (2007). Refining the sensory and motor ratunculus of the rat upper extremity using fMRI and direct nerve stimulation. Magn. Reson. Med. 58, 901–909.
42. Ohta, M., and Saeki, K. (1989). Corticotrigeminal motor pathway in the rat—I. Antidromic activation. Comparative biochemistry and physiology. Comp. Physiol. 94, 99–104.
43. Matyas, F., Sreenivasan, V., Marbach, F., Wacongne, C., Barsy, B., Mateo, C., Aronoff, R., and Petersen, C. C.H. (2010). Motor control by sensory cortex. Science 330, 1240–1243.
44. Harris, N., Mironova, Y.A., Hovda, D., and Sutton, R.L. (2010). Chondroitinase ABC enhances pericontusion axonal sprouting but does not confer robust improvements in behavioral recovery. J. Neurotrauma 27, 1–12.
45. Castro-Alamancos, M.A., and Borrell, J. (1995). Functional recovery of forelimb response capacity after forelimb primary motor cortex damage in the rat is due to the reorganization of adjacent areas of cortex. Neuroscience 68, 793–805.
46. Chollet, F., DiPiero, V., Wise, R.J., Brooks, D.J., Dolan, R.J., and Frackowiak, R.S. (1991). The functional anatomy of motor recovery after stroke in humans: a study with positron emission tomography. Ann. Neurol. 29, 63–71.
47. Weiller, C., Chollet, F., Friston, K.J., Wise, R.J., and Frackowiak, R.S. (1992). Functional reorganization of the brain in recovery from striatocapsular infarction in man. Ann. Neurol. 31, 463–472.
48. Luke, L.M., Allred, R.P., and Jones, T.A. (2004). Unilateral ischemic sensorimotor cortical damage induces contralesional synaptogenesis and enhances skilled reaching with the ipsilateral forelimb in adult male rats. Synapse 54, 187–199.
49. Jones, T.A., and Schallert, T. (1994). Use-dependent growth of pyramidal neurons after neocortical damage. J. Neurosci. 14, 2140–2152.
50. Keyvani, K., and Schallert, T. (2002). Plasticity-associated molecular and structural events in the injured brain. J. Neuropathol. Exp. Neurol. 61, 831–840.
51. Jones, T.A., and Schallert, T. (1992). Overgrowth and pruning of dendrites in adult rats recovering from neocortical damage. Brain Res. 581, 156–160.

52. Jones, T.A., Liput, D.J., Maresh, E.L., Donlan, N., Parikh, T.J., Marlowe, D., and Kozlowski, D.A. (2012). Use-dependent dendritic regrowth is limited after unilateral controlled cortical impact to the forelimb sensorimotor cortex. J. Neurotrauma 29, 1455–1468.
53. Kozlowski, D.A., and Schallert, T. (1998). Relationship between dendritic pruning and behavioral recovery following sensorimotor cortex lesions. Behav. Brain Res. 97, 89–98.
54. Allred, R.P., Cappellini, C.H., Jones, T.A. (2010). The ''good'' limb makes the ''bad'' limb worse:experience-dependent interhemispheric disruption of functional outcome after cortical infarcts in rats.Behav. Neurosci. 124, 124–132.
55. Clarey, J.C., Tweedale, R., and Calford, M.B.(1991). Interhemispheric modulation of somatosensory receptive fields: evidence for plasticity in primary somatosensory cortex. Cereb. Cortex 6, 196–206.
56. Shuler, M.G., Krupa, D.J., and Nicolelis, M.A. (2001). Bilateral integration of whisker information in the primary somatosensory cortex of rats. J. Neurosci. 21, 5251–5261.
57. Rema, V., and Ebner, F.F. (2003). Lesions of mature barrel field cortex interfere with sensory processing and plasticity in connected areas of the contralateral hemisphere. J. Neurosci. 23, 10378–10387.
58. Maggiolini, E., Viaro, R., and Franchi, G. (2008). Suppression of activity in the forelimb motor cortex temporarily enlarges forelimb representation in the homotopic cortex in adult rats. Eur. J. Neurosci. 27, 2733–2746.
59. Lee, S., Ueno, M., and Yamashita, T. (2011). Axonal remodeling for motor recovery after traumatic brain injury requires downregulation of $\gamma$-aminobutyric acid signaling. Cell Death Dis. 2, e133.
60. Biernaskie, J., Szymanska, A., Windle, V., and Corbett, D. (2005). Bihemispheric contribution to functional motor recovery of the affected forelimb following focal ischemic brain injury in rats. Eur. J. Neurosci. 21, 989–999.
61. Shanina, E.V, Schallert, T., Witte, O.W., and Redecker, C. (2006). Behavioral recovery from unilateral photothrombotic infarcts of the forelimb sensorimotor cortex in rats: role of the contralateral cortex. Neuroscience 139, 1495–1506.
62. Seitz, R.J., Höflich, P., Binkofski, F., Tellmann, L., Herzog, H., and Freund, H.J. (1998). Role of the premotor cortex in recovery from middle cerebral artery infarction. Arch. Neurol. 55, 1081–1088.
63. Ward, N.S. (2004). Functional reorganization of the cerebral motor system after stroke. Curr. Opin. Neurol. 17, 725–730.
64. Marshall, R.S., Perera, G.M., Lazar, R.M., Krakauer, J.W., Constantine, R.C., and DeLaPaz, R.L. (2000). Evolution of cortical activation during recovery from corticospinal tract infarction. Stroke 31, 656–661.

Address correspondence to:
*Neil G. Harris, PhD*
*Department of Neurosurgery*
*David Geffen School of Medicine at UCLA*
*Box 957039*
*Los Angeles, CA 90095-7039*

*E-mail:* ngharris@mednet.ucla.edu

Cell Communication and Signaling

REVIEW Open Access

# Dual roles of astrocytes in plasticity and reconstruction after traumatic brain injury

Yunxiang Zhou[1†], Anwen Shao[2*†], Yihan Yao[1], Sheng Tu[3], Yongchuan Deng[1] and Jianmin Zhang[2]

## Abstract

Traumatic brain injury (TBI) is one of the leading causes of fatality and disability worldwide. Despite its high prevalence, effective treatment strategies for TBI are limited. Traumatic brain injury induces structural and functional alterations of astrocytes, the most abundant cell type in the brain. As a way of coping with the trauma, astrocytes respond in diverse mechanisms that result in reactive astrogliosis. Astrocytes are involved in the physiopathologic mechanisms of TBI in an extensive and sophisticated manner. Notably, astrocytes have dual roles in TBI, and some astrocyte-derived factors have double and opposite properties. Thus, the suppression or promotion of reactive astrogliosis does not have a substantial curative effect. In contrast, selective stimulation of the beneficial astrocyte-derived molecules and simultaneous attenuation of the deleterious factors based on the spatiotemporal-environment can provide a promising astrocyte-targeting therapeutic strategy. In the current review, we describe for the first time the specific dual roles of astrocytes in neuronal plasticity and reconstruction, including neurogenesis, synaptogenesis, angiogenesis, repair of the blood-brain barrier, and glial scar formation after TBI. We have also classified astrocyte-derived factors depending on their neuroprotective and neurotoxic roles to design more appropriate targeted therapies.

**Keywords:** Astrocyte, Traumatic brain injury, Reconstruction, Neurogenesis, Blood-brain barrier, Glial scar

## Background

Traumatic brain injury (TBI) refers to a sudden trauma caused by traffic accidents, wars, violence, terrorism, falls, and sporting activity [1]. TBI is currently the primary cause of human death in young adults and one of the leading causes of fatality and disability across all ages worldwide, resulting in annual global economic losses of amounting to $US400 billion [2–4]. The high mortality and morbidity of TBI and the substantial economic burden affect the patients, families, and society, and have attracted public attention [5]. To date, more than 1000 clinical trials on TBI have been registered on clinicaltrials.gov. In spite of the immense efforts on the treatment of TBI made in the past few decades, few effective therapies for TBI are available [6–8].

One of the reasons for the failure is because most previous studies have targeted neuronal cells, whereas emerging evidence shows that glial cells also play significant roles in the pathogenesis of TBI [9–11]. Astrocytes, a type of glial cells, are involved in the homeostasis and blood flow control of the central nervous system (CNS) [12]. TBI is known to induce astrocyte activation (reactive astrogliosis), which is involved in tissue remodeling processes such as neurogenesis, synaptogenesis, repair of the blood-brain barrier (BBB), regulation of synaptic plasticity, and formation of glial scar and extracellular matrix (ECM), weighing a lot to the patient outcome [13–15]. However, reports on the effects of reactive astrogliosis are not consistent [10, 16–18]. The current review summarizes the existing knowledge on the role of astrocytes in TBI. We particularly elaborate on the

* Correspondence: 21118116@zju.edu.cn; anwenshao@sina.com
†Yunxiang Zhou and Anwen Shao contributed equally to this work.
[2]Department of Neurosurgery, The Second Affiliated Hospital, School of Medicine, Zhejiang University, Province, Zhejiang 310009, Hangzhou, China
Full list of author information is available at the end of the article

various roles of astrocytes and astrocytes-derived molecules in plasticity and reconstruction and explore the possibility of using astrocytes to optimize their therapeutic benefit while attenuating the harmful effects of them.

## Overview of TBI and astrocyte

### Traumatic brain injury

Traumatic brain injury is a prevalent disease, with a global annual burden of approximately $US400 billion [2, 3]. According to statistics by the World Health Organization, TBI affiliated mortalities and disability will surpass that of many diseases as from the year 2020 [19]. However, there are currently no effective therapies for TBI [6, 7]. And the main form of clinical treatment is restricted to surgical interventions and supportive managements, including hyperbaric oxygen, task-oriented functional electrical stimulation, non-invasive brain stimulation, and behavioral therapy [6, 20]. One of the main challenges of treating TBI is the heterogeneity of its pathologic and pathogenic mechanisms. Consequently, an in-depth elucidation of the underlying pathophysiological mechanisms is required to provide new therapeutic targets.

### The pathophysiology of TBI

Traumatic brain injury is characterized by instant damage to mechanical force and delayed damage to the subsequent pathophysiological processes [21]. The mechanical force directly leads to neuronal or diffuse axonal damage and vascular disruption, followed by secondary injury mediated by extensive neuroinflammation, dysfunction of the BBB, oxidative stress, and apoptosis [22–26]. While the immediate primary injury is considered untreatable, the delayed secondary injury gives a window for intervention and has, therefore, attracted a lot of attention [27].

Following the initial injury, local environment changes and damaged cells release intracellular components, triggering the activation and recruitment of resident glial cells in the brain as well as the production of various cytokines, chemokines, and excitotoxins; then the peripheral immune cells are recruited into the brain with further release of signaling factors to induce a robust sterile immune reaction [28–30]. A broad range of literature data has reported the up-regulated expression of cytokines including interleukin (IL)-1β, tumor necrosis factor (TNF)-α, transforming growth factor-β (TGF-β), interferon γ (IFNγ), IL-6, IL-10 and IL-12 as well as the chemokines such as chemokine (C-C motif) ligand (CCL)2, CCL3, CCL4, chemokine (C-X-C motif) ligand (CXCL)1, CXCL2, CXXL4, CXCL8/IL-8 and CXCL10 in the early stages post-TBI, which boost the sterile inflammation [28, 31]. These lead to additional attraction of peripheral cells, continuous activation of resident glial cells, and aggravated neuronal damage [28, 32]. Disruption of the BBB integrity and the neurovascular unit (Fig. 1) can occur as a result of the initial injury or arise secondarily to the extensive neuroinflammation, astrocytic dysfunction, and metabolic disturbances. These damages result in vascular leakage, brain edema, cerebral hemorrhage, and hypoxia [27, 29, 33–35]. Neuronal apoptosis also significantly contributes to secondary injury [36, 37]. In addition to apoptosis, necroptosis, a recently identified programmed cell death bearing resemblance to both apoptosis and necrosis, has also been demonstrated to play an indispensable role in secondary neuronal cell death and neuroinflammation post-TBI [38, 39]. Mechanically, upon pathogenic stimuli following TBI, TNF-α-induced receptor-interacting protein 1 activation contributes to the formation of the so-called necrosome, a complex necessary for necroptosis [40, 41]. And after necroptosis, inflammatory factors released from damaged cells flow into the extracellular space, boosting the neuroinflammation [41–43]. All these primary or secondary pathologic mechanisms contribute to cell death, tissue loss, structural and metabolic abnormalities, and an ultimate neurological dysfunction in the patients [15, 44]. And whether neural structure and function can be restored determines the final outcome of the TBI patients [36].

### Astrocyte reaction after TBI onset

Among brain resident glial cells such as astrocytes (astroglia), oligodendrocytes and microglia, astrocytes are the most abundant [45]. Astrocytes are characterized by the presence of glial fibrillary acidic protein (GFAP), a unique structural protein [45]. Under normal physiological conditions, astrocytes are involved in the homeostasis and blood flow control of the CNS [12]. Astrocytes structurally support neurons and separate the CNS from the meninges, blood vessels, and perivascular spaces by the creation of a functional barrier named glia limitans, which is formed via the interaction of astrocytic foot processes with the parenchymal basement membrane [46]. In addition, astrocytes provide functional support for neurons, including the recycling of the neurotransmitter glutamate, the most potent neurotoxin in the brain, via glutamate transporters (Fig. 2), the glutamate-glutamine shuttle system, and cystine–glutamate antiporter system [47–49]. Astrocytes play a role in the release of neurotrophic factors and gliotransmitters such as glutamate, ATP, γ-aminobutyrate (GABA), and D-serine [1, 15, 50]; the synthesis of glutamine, cholesterol, superoxide dismutases, glutathione, ascorbate and thrombospondin (TSP)-1 and 2 [9, 51, 52]. Astrocytes are also involved in the regulation of energy metabolism by the conversion of glucose into lactate

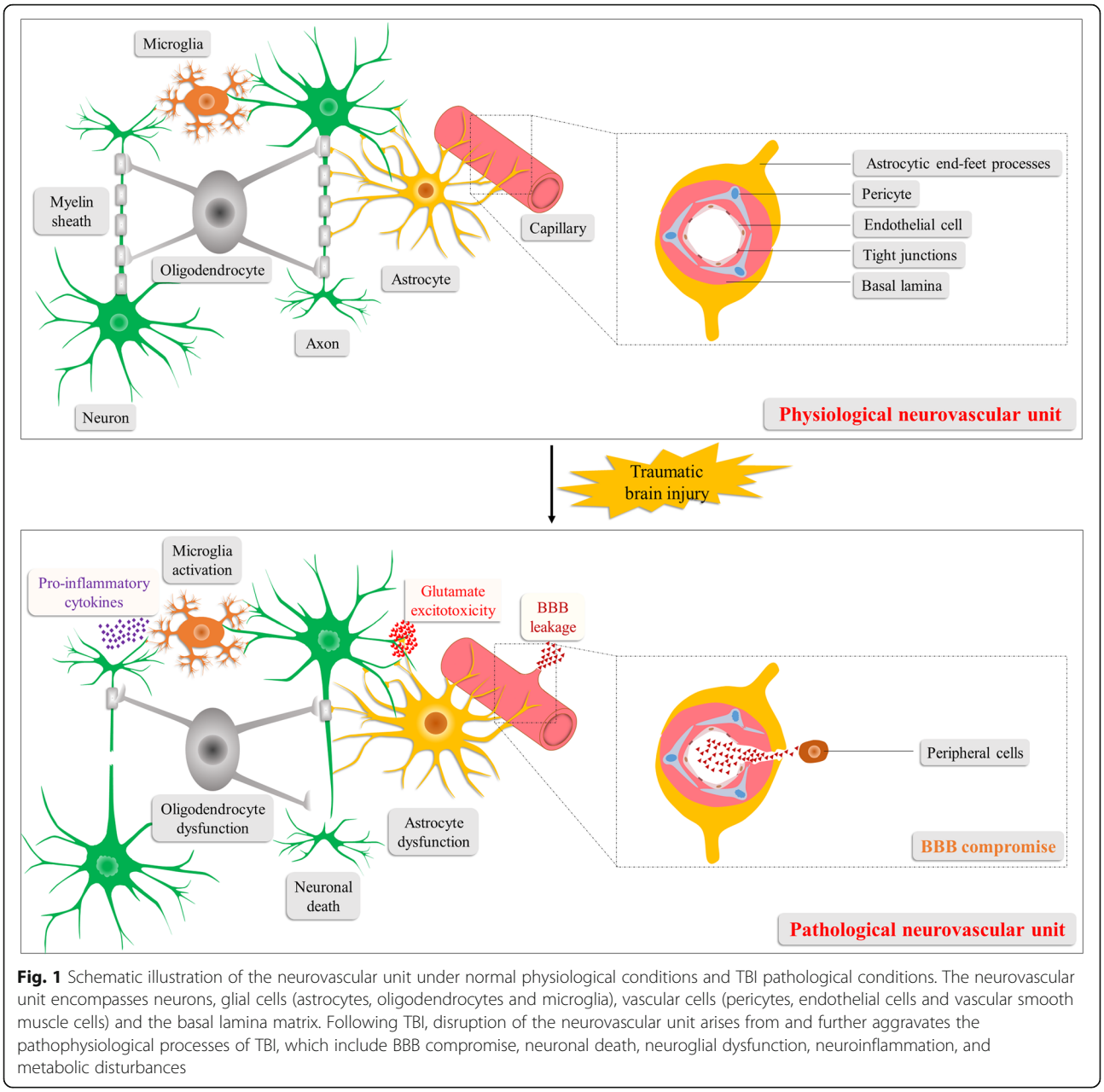


**Fig. 1** Schematic illustration of the neurovascular unit under normal physiological conditions and TBI pathological conditions. The neurovascular unit encompasses neurons, glial cells (astrocytes, oligodendrocytes and microglia), vascular cells (pericytes, endothelial cells and vascular smooth muscle cells) and the basal lamina matrix. Following TBI, disruption of the neurovascular unit arises from and further aggravates the pathophysiological processes of TBI, which include BBB compromise, neuronal death, neuroglial dysfunction, neuroinflammation, and metabolic disturbances

[53–55] and the regulation of neuronal activation and water homeostasis through extracellular ion concentrations [56–59]. Given the multifunctional roles of astrocytes in the CNS, they can affect neuronal activity, modulate plasticity, and participate in CNS regeneration after brain injury [60–64].

Microglia are cells of myeloid origin and are considered "the CNS professional macrophages", which express a large repertoire of pattern-recognition receptors and are often the first cells responding to any inflammatory events [29, 65]. Importantly, more and more lines of evidence suggests that astrocytes also express a series of receptors related to inflammatory and immune processes, including Toll-like receptors, purinergic receptors, mannose receptors, scavenger receptors, nucleotide-binding oligomerization domain proteins, double-stranded RNA dependent protein kinase, and components of the complement system, through which they sense a wide range of endogenous and exogenous signals and respond dynamically to sterile injuries and infectious non-self [29, 65–67]. Therefore, danger signals post-TBI can trigger inflammasomes and innate immune response via their interaction with the receptors on the innate immune neuroglia. Mechanically, when the local

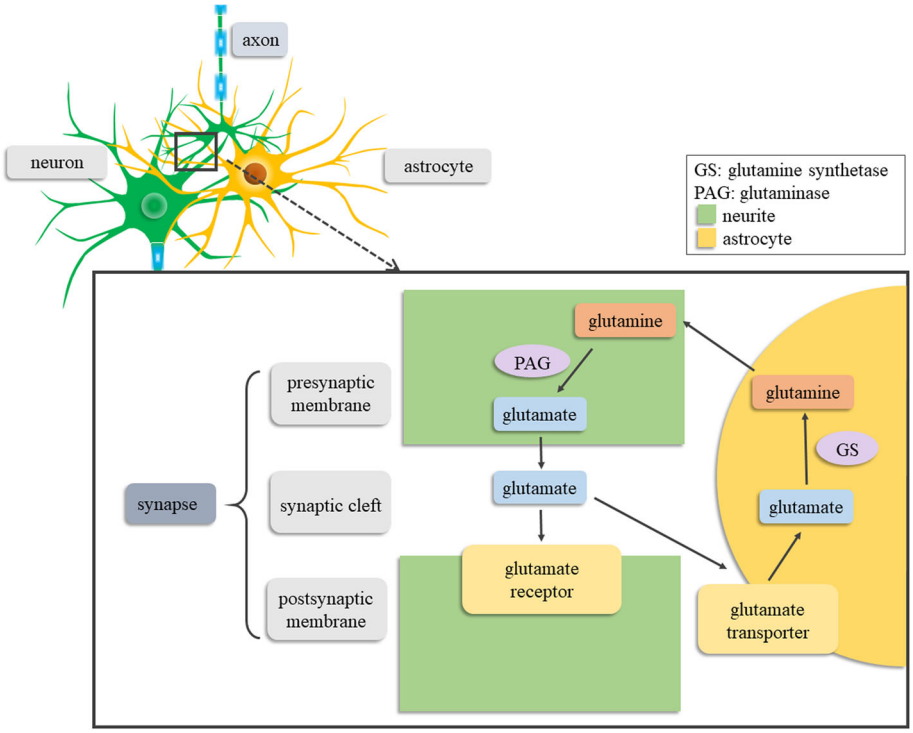


**Fig. 2** Schematic illustration of the glutamate-glutamine cycle in astrocytes. Astrocytes play a crucial role in the glutamate cycle of glutamate-glutamine. After the presynaptic membrane releases neurotransmitter glutamate, astrocytes can take in glutamate from the synaptic cleft through the glutamate receptor and synthesize glutamine with the catalysis of glutamine synthetase. And the glutamine can cross the cell membrane into the cytoplasm of presynaptic membrane and be deaminated by glutaminase to produce glutamate

biochemical environment changes following the onset of TBI, danger signals induce the structural and functional alterations of astrocytes, including hypertrophy and increased expression of the intermediate filaments (nestin, vimentin, and GFAP), resulting in astrocyte activation (reactive astrogliosis) [15, 68]. Other cells such as brain-resident microglia are also activated [31]. Both astrocytes and microglia react within 24 hours and peak around day 3-7, however, microglia rapidly decline to control levels approximately 21 days after the lesion while astrocytes exhibit a long-lasting proliferative response, at least, 28 days after TBI [69–71]. The activation and proliferation of glial cells, in turn, have utility in releasing signaling factors and triggering a robust sterile immune reaction that consists of brain-resident as well as peripherally recruited inflammatory cells. This reaction is initiated to exert neuroprotective effects and promote wound healing, but may become maladaptive over time [29, 72].

As the inflammatory response progresses, local astroglial progenitors around the injured tissue form the glial scar that isolates the damaged area, contains the spread of inflammatory cells, provides a favorable environment for surviving neurons, and maintains the integrity of the BBB [46, 68, 73–75]. Nonetheless, the glial scar is considered the main hindrance to axonal regeneration and recovery of neuronal connectivity [76, 77]. This shows one of the Janus-like effects of astrocytes. Controversy also remains as to whether reactive astrogliosis is beneficial for the maintenance of BBB integrity after TBI [21, 78], since astrocytes can largely affect BBB integrity and water homeostasis [79] as detailed below: (1) the BBB is sheathed by perivascular astrocyte foot processes [80]; (2) the glymphatic system is formed by astrocytes [81]; (3) the perivascular aquaporin-4 (AQP4) is densely and exclusively expressed in astrocyte end-feet [82]; (4) the permeability of the BBB can be affected by astrocyte-derived factors [78]; and (5) the concentration of extracellular ions is controlled by astrocytes [9]. These “irrational” phenomena can be caused by an overreaction and dysfunction of reactive astrocytes after brain injury, or due to the release of neurodeleterious molecules [78]. Astrocytes, therefore, hold both neuroprotective and neurodeleterious effects following TBI, making it a double-edged sword for neurorestoration [83–85]. This also indicates that we cannot simply suppress or promote reactive astrogliosis, but should selectively stimulate the beneficial effects and ameliorate the deleterious ones in the astrocyte-targeting therapy [78].

## Dual roles of astrocytes in plasticity and reconstruction after TBI

As previously mentioned, all the primary and secondary pathologic mechanisms underlying TBI contribute to cell death, tissue loss, structural and metabolic abnormality, and ultimately lead to neurological dysfunction of TBI patients [15, 44]. And the ability to restore neural structure and function determine the outcome of the patients [36, 86]. Thus, promoting the astrocytes/astrogliosis-induced neuroprotective effects/molecules or attenuating the neurodeleterious ones in terms of neuronal regeneration and tissue reconstruction may represent a promising therapeutic target for TBI. Below, we will describe the astrocytes and a range of astrocyte-derived molecules, as well as their roles in neurogenesis, synaptogenesis, angiogenesis, blood-brain barrier repair, and glial scar formation after neurotrauma.

### Neurogenesis

Emerging evidence has indicated that astrocytes play a vital role in neurogenesis, which is attributed to the regulation of the microenvironment of neurogenic niche [87, 88].

#### *The neurogenesis-promoting effects of astrocytes*

Some studies suggested a beneficial effect of astrocytes in neurogenesis, both through the instruction of neuronal fate commitment and the promotion of proliferation of adult neural stem cells [88]. In addition, the neurogenesis-promoting effect of astrocytes has regional characteristics: hippocampal-derived astrocytes retain this potential, whereas astrocytes from the adult spinal cord do not [88]. Currently, some potential mechanisms concerning astrocytes-induced neurogenesis have been proposed. Astrocytes produce the neurotrophic and mitogenic protein S100β *in vivo*. Intraventricularly administration of S100β enhances neurogenesis within the hippocampus and improves cognitive function recovery following TBI. These improvements are mediated by the facilitation of neuronal differentiation, proliferation, and survival of hippocampal progenitor cells [89, 90]. Heme oxygenase induced by astrocytes after TBI catalyzes heme to carbon monoxide (CO), ferrous iron, and biliverdin. Notably, low concentrations (lower than 250 ppm possibly) of CO exert promotive effects on neurogenesis, as well as synaptic plasticity and angiogenesis [91]. Moreover, previous studies reported that mature astrocytes might regress to an immature phenotype and show stem cell characteristics [92].

Besides stimulating stem cell genesis, astrocytes also contribute to the prolonged survival of newborn neurons [93]. Neurotrophic factors secreted by astrocytes are closely involved in neuronal support and survival, and intraperitoneal administration of a formulation composed of co-ultramicronized palmitoylethanolamide and luteolin was found to promote this process [94, 95]. Additionally, pituitary adenylate cyclase-activating peptide expressed by astrocytes plays a significant role in the support and survival of new neurons post-TBI [93]. Both the enhanced neurogenesis and long-lasting survival of newborn neurons result in a better neurological recovery.

#### *The neurogenesis-suppressing effects of astrocytes*

However, under certain pathological conditions, such as severe TBI with devastating excitotoxicity and inflammatory response, the microenvironment of neurogenic niche may lose its homeostasis [21, 96]. Correspondingly, some studies proposed that knockout/knockdown of molecules produced by astrocytes or suppression of astrocyte-related signaling enhances neurogenesis. Mice devoid of GFAP and vimentin are found to be developmentally normal with increased hippocampal neurogenesis and axonal regeneration post-TBI, despite that GFAP is essential for astrocyte activation and acute cellular stress handling [97–100]. This disparity may be due to the mechanism that differentiation of uncommitted neural progenitor cells is skewed towards neuronal lineage under the null of *GFAP* gene condition, and inhibition of Sirt1 expression may strengthen this inclination [101]. The effects and mechanisms of several GFAP suppressors have also been evaluated in experimental TBI [45].

Garber *et al.* revealed that astrocytes impaired neuronal progenitor cell homeostasis via the up-regulated expression of IL-1, thus hindering hippocampal neurogenesis in West Nile virus neuroinvasive disease, which could be reversed by IL-1R1 antagonist [83]. Up-regulated IL-1β is also found to aggravate excitotoxicity and seizures post-TBI, although the latter can develop independently from the neurotoxic effects [102, 103]. Interestingly, Barkho *et al.* suggested that IL-1β and IL-6 could promote neuronal differentiation of neural stem/progenitor cells at relatively low concentrations and thus they proposed a concentration-depending effect of astrocyte-derived pro-inflammatory cytokines. They also indicated that three other astrocyte-derived molecules: insulin-like growth factor (IGF) binding protein 6 and decorin, which inhibit IGF and TGF-β respectively, and opioid receptor agonist enkephalin, could inhibit neurogenesis [104].

### Synaptogenesis

Astrocytes also play a crucial role in synaptic plasticity, remodeling, and regeneration post-TBI [105, 106]. As mentioned earlier, astrocytes are involved in the biochemical synthesis, metabolism, and secretion of many molecules. Some of these molecules, such as TSP-1 and

TSP-2, promote synaptogenesis, while molecules, including trophic factors and cholesterol, preserve synapse maturation and maintenance [106–108]. Reversely, these mechanisms (and others) are also potentially critical for eliciting pathological responses during and after TBI [87, 109].

#### *The synaptogenesis-promoting effects of astrocytes*

Several studies have reported the beneficial role of astrocytes in synaptogenesis, which is reflected in its involvement in synaptic formation, metabolic support, and neurotransmitter release [9, 110]. For instance, astrocytes regulate the expression and localization of agrin, one of matrix metalloproteinase (MMP)-3 substrates, which induces reactive synaptogenesis and neurological recovery [111]. And astrocytes support ovarian steroids estradiol-enhanced neurite outgrowth, although this can be antagonized by activated microglial-induced progesterone [112]. Remarkably, astrocytic signal transducer and activator of transcription-3 (STAT3) is capable to regulate the process formation and re-expression of TSP-1 of perineuronal astrocytes [18]. Furthermore, STAT3 supports neuronal integrity and mediates anti-inflammatory reactions [18, 113, 114]. The augmentation of STAT3 discloses a neuroprotective effect, whereas the conditional ablation of STAT3 has the opposite effect [113, 114]. Nevertheless, Christopherson *et al.* demonstrated that TSP-induced excitatory synapses are post-synaptically silent, which owes to the lack of functional α-amino-3-hydroxy-5-methyl-4-isoxazole propionic acid (AMPA) receptors [115]. Similarly, Kucukdereli *et al.* demonstrated that hevin, another matricellular protein secreted by astrocytes, could induce the same type of synapse as TSP [116]. On the contrary, the homologous sequence protein, secreted protein acidic and rich in cysteine (SPARC) inhibits hevin-induced synapse formation [116–118]. Other astrocyte-derived molecules such as glypicans [119], TGF-β [120, 121], and brain-derived neurotrophic factor [122] can induce excitatory synapse formation, while γ-protocadherin can induce the formation of either excitatory or inhibitory synapse via a contact-dependent mechanism [123].

#### *The synaptogenesis-suppressing effects of astrocytes*

Following the breakdown of the BBB, an influx of serum elements, and the inflammatory cytokines, including IL-1, TGF-β trigger the formation of a glial scar to cope with injury. Nonetheless, the glial scar is considered the main hindrance to axonal regeneration and neuronal connectivity recovery, due to the production of growth-inhibitory components and the formation of physical and chemical barriers that hinder axon elongation [30, 76, 77, 124]. Among the inhibitory components, chondroitin sulfate proteoglycans (CSPGs), one of the ECM molecules produced by astrocytes, are of prime importance as they are predominantly responsible for the non-permissive characteristic of glial scar and have been extensively studied [125–128]. The major brain CSPGs include lecticans (neurocan, brevican, versican, and aggrecan), phosphacans, and transmembrane NG2; they surround and affect the perineuronal nets (PNNs), which are comprised of rich ECM and cell adhesion proteins and have been found to stabilize synapses [129, 130]. The class IIa/Leukocyte common antigen-related (LAR) family [131] and the NOGO receptors NgR1 and NgR3 [132] have been identified as CSPG receptors and convey subsequent axonal growth inhibition. However, heparan sulfate proteoglycans (HSPGs), another ligand for the LAR family receptors promotes axon extension [133]. This role of HSPGs may result from the switch of axonal endings between states of growth and inactivity via the oligomerization status of PTPσ (a member of the LAR family) [76]. Therefore, agents targeting these receptors or that mimic HSPG binding may mitigate the inhibitory environment of glial scar and augment neuronal regeneration, thus suggesting multiple candidates of therapeutic application for TBI [134, 135]. For instance, the hepatocyte growth factor, which exhibits pleiotropic functions in the CNS has been shown to suppress the expression of CSPGs after brain injury, as well as block the secretion of TGF-β1 and β2 and the subsequent induction of the glial scar [124]. Another ECM component, tenascin-C, was also shown to inhibit axon outgrowth and therefore represents a target for intervention [136, 137].

Matrix metalloproteinases cleave ECM and are involved in the modulation of synaptogenesis. However, the definite role of MMPs in neurological recovery post-TBI remains elusive, since it depends on where and when it is activated [138]. After severe TBI, astrocytes induce the expression of MMP-3 in a higher and more persistent pattern, resulting in maladaptive synaptogenesis and poor recovery of neural function, while MMP inhibitor FN-439 is shown to attenuate the activity of MMP-3 and then facilitate functional recovery [139]. Moreover, persistent expression of another MMP, *a d*isintegrin *a*nd *m*etalloproteinase-10 (ADAM-10), parallels the attenuation of the N-cadherin level, which is critical to synapse stability, and consequently contributing to reduced functional recovery; whereas inhibition of MMP shifts the expression of ADAM-10 and N-cadherin towards an adaptive pattern and facilitates the synapse formation [17].

### Synaptic plasticity

In addition to the number of synapses, synaptic plasticity is also necessary for learning and memory formation. Synaptic plasticity can be influenced by activation and

localization of glutamate receptor, synaptic strength, intracellular calcium levels, neurotrophic factors, and cytokines following TBI [140–142]. Considering the involvement of astrocytes in the pathophysiological processes including supporting neuronal metabolism, secreting different molecules that induce the formation of excitatory synaptic structure and function, and releasing gliotransmitters that affect the balance of neural network as well as synaptic potentiation or depression, astrocyte may be a promising target for modulating synaptic plasticity [87]. Following TBI, the general role of astrocytes in synaptic plasticity again remains obscure. For instance, the sphingosine 1-phosphate (S1P) receptor 1 antagonist siponimod preserves neural plasticity via attenuating activation of astrocytes, microglia, and other inflammatory cells [143]. On the contrary, minocycline influences neuronal plasticity and improves neurological recovery by increasing the astrogliosis following experimental stroke [144].

#### *The synaptic stability-promoting effects of astrocytes*

The previously mentioned neurogenesis-promoting CO also facilitates synaptic plasticity [91]. Besides, the synaptogenic factor TSP-1 can also suppress MMP-9-induced cleavage of extracellular matrix molecules and synaptic instability [145, 146]. AQP4, which is the main water channel of astrocytes and exclusively expressed on astrocytes, plays a critical role in synaptic plasticity and memory encoding [147]. Moreover, AQP4 is also highly correlated with the balance of water, the function of glymphatic pathway and the integrity of the BBB while the role of AQP4 may, however, depend on the stage of TBI progression [147, 148]. The study by Zhang *et al.* revealed that lack of AQP4 could lead to the accumulation and removal of excess water in the brain during acute and late stages of TBI, respectively [149], making AQP4-targeting therapy a great challenge.

Although the glial scar is regarded as the main impediment to axonal regeneration and neuronal connectivity recovery, it initially acts as a barrier isolating the damaged area, containing the spread of inflammatory cells, providing a favorable environment for surviving neurons and maintaining the BBB [30, 76, 150, 151]. Moreover, despite the detrimental roles mentioned above, CSPGs may help restrict inflammation by shifting monocytes towards resolving phenotype and enhancing the expression of anti-inflammatory cytokines, such as IL-10, as well as help stabilize the ionic microenvironment by limiting diffusion of cations, such as potassium, calcium, and sodium [152, 153]. Furthermore, CSPGs [154, 155] and TNF-α [156–158] have been demonstrated to alter the level or mobility of AMPA receptors in a beneficial manner, which are critical in synaptic plasticity. Consistent with these findings, several studies have reported that most of the ECM molecules produced by astrocytes elicit both restrictive and permissive effects on axonal sprouting post-lesion [79]. Indeed, studies demonstrated that ablation of astrogliosis in transgenic mice disrupted scar formation, which in turn exacerbated the spread and persistence of inflammation response, vasogenic edema, neuronal loss, demyelination, and functional recovery [159–162]. Furthermore, blocking scar formation in STAT3 deletion mice has similar effects of inducing extensive lesions and increasing neuronal loss and locomotor deficits after CNS injury, while enhancing scar formation in protein suppressor of cytokine signaling 3 deletion mice has the opposite effects [113, 114]. These findings strongly suggest that astrogliosis and glial scar formation may be neuroprotective against brain damage under particular circumstances, highlighting a dichotomous role again.

#### *The synaptic stability-suppressing effects of astrocytes*

Astrocytes play a crucial role in regulating excitatory chemical transmission via glutamate transporters (Fig. 2), glutamate-glutamine shuttle system, and cystine–glutamate antiporter system. However, the impairment of astrocytic glutamate uptake and GABA release lead to glutamate excitotoxicity as well as ion and water imbalance post-TBI [1, 9]. Glutamate is the primary excitatory neurotransmitter and the most potent neurotoxin once concentrated in the extracellular space of CNS. Notably, the homeostasis of glutamate is closely associated with synaptic plasticity [47–49]. Ephrin-A3, a member of the ephrin family, is expressed in astrocytes and is involved in the regulation of glial glutamate transporters. Ephrin-A3 is required for maintenance of long-term potentiation via its interaction with the A-type Eph receptor, namely EphA4, and thus influences synaptic plasticity. Once Ephrin-A3 is over-expressed following TBI, it decreases glutamate transporters and increases glutamate excitotoxicity, hence prolonging neuronal depolarization and focal dendritic swelling [163–165]. Therefore, inhibition of Ephrin-A3 represents a potential therapeutic strategy. Besides, the glutamate receptor antagonist MK-801 has also been shown to enhance synaptic integrity and improve cognitive outcomes [138, 139].

Traumatic brain injury constitutes one of the most common causes of acquired epilepsy [166]. Epileptogenesis can be induced by several pathological processes, including glial scar, ECM remodeling, axonal plasticity alteration, excitation/inhibition imbalance, cell death, and neuronal heterotopia [167]. Once the structural integrity of PNNs is compromised by astrocyte-derived ECM molecules, dysfunctional PNNs around the fast-spiking inhibitory interneurons might underlie excitation/inhibition imbalance and lead to the development of post-traumatic epilepsies [168]. The involvement of

hyperphysiologic TNF-α in post-traumatic epileptogenesis has also been revealed [169, 170]. In addition to its influences on glutamatergic transmission and synaptic plasticity, TNF-α also has an important role in the initial activation of microglia and astrocytes and the disruption of the BBB; and the biologic TNF antagonist etanercept was shown to improve the outcomes of experimental TBI [171]. Furthermore, astrogliotic upregulation of enzyme adenosine kinase also contributes to epileptogenesis [172]. Notably, TBI is also an important risk factor for the development of many neurodegenerative diseases such as Alzheimer's disease, chronic traumatic encephalopathy, amyotrophic lateral sclerosis, and etcetera; the deposition and accumulation of amyloid-beta and tau are considered as part of the pathological mechanisms [173–176].

### BBB repair

Although TBI-induced astrogliosis and glial scar seem to promote the BBB repair [30], astrocytic dysfunction is one of the main pathological mechanisms giving rise to the BBB disruption post-TBI [27, 29, 33]. The dual roles of reactive astrogliosis owe to the distinct functions of various astrocyte-derived molecules in BBB integrity [78] (**Table 1**). Furthermore, these astrocyte-derived factors also regulate cell adhesion molecules on the endothelial cells, thereby controlling the leukocyte infiltration influx to the CNS, and participate in one or more pathophysiological processes including angiogenesis, neurogenesis, and neuroplasticity [78].

#### *The BBB integrity-promoting effects of astrocytes*

The integrity of the BBB is determined by the endothelial tight junctions and the basal lamina. While endothelial tight junctions are formed by proteins such as claudin, occludin and zonula occluden (ZO), the basal lamina forms the basement membrane of ECM and includes laminin, collagen, and fibronectin [177, 178]. Astrocyte-derived factors including angiopoietin-1 (ANG-1) [179–181], sonic hedgehog (SHH) [182–185], glial-derived neurotrophic factor (GDNF) [186–188], retinoic acid (RA) [189–191], and IGF-1 [192, 193] have been demonstrated to promote recovery of the BBB by protecting endothelial cells and/or enhancing tight junction reassembly, via signaling mediated by their receptors, tie-2, patched-1, GDNF receptor alpha-1 and alpha-2, nuclear RA receptor, and IGF-1 receptor, respectively [78, 79] (Table. 1). Besides, the astrocyte-secreted apolipoprotein E (APOE) isoforms APOE2, APOE3, and APOE4, are also closely involved in the regulation of BBB integrity [194]. Notably, APOE exerts its regulation in an isoform-dependent manner [195]. Despite that APOE3 protects against BBB disruption via the suppression of a cyclophilin A (CypA)-nuclear factor-κB (NFκB)-MMP-9 pathway, APOE4 activates the pathway and results in neuronal dysfunction and degeneration [196]. Overall, APOE tends to maintain BBB integrity and promote neurological recovery. While APOE-deficiency provokes BBB dysfunction, exogenously administered APOE or its mimetic peptides preserve BBB integrity in experimental studies [197–203].

#### *The BBB integrity-suppressing effects of astrocytes*

Despite that some astrocyte-derived factors maintain the BBB function, some astrocyte-derived factors damage the BBB by inducing endothelial cell apoptosis or decreasing the expression of endothelial tight junction-related proteins, which include vascular endothelial growth factor (VEGF) [204–207], glutamate [208–210], endothelins (ETs) [21, 211, 212], MMP [208, 213, 214], and nitric oxide (NO) [215, 216] (Table 1). As zinc-endopeptidases, MMPs can directly degrade endothelial tight junction-related proteins and ECM molecules, which promotes angiogenesis whereas simultaneously increases BBB permeability [78, 217, 218]. And it is through the signaling pathway activating or suppressing MMPs that many other factors such as APOE, NO, and ETs get to affect the BBB integrity [201, 212, 215]. Although both NO and glutamate can decrease endothelial tight junction-related proteins, NO may have inconsistent effects on apoptosis through different pathways [219]. Furthermore, glutamate also exacerbates vascular permeability via the activation of glutamate receptors [220], and cytokines such as TNF-α are strictly related to BBB disruption [171, 211, 221].

The study by Prager *et al.* indicates that S1P binds to and activates five G protein-coupled receptors. Among these receptors, S1P receptor 1 (S1PR1) primarily preserves BBB integrity while the S1P receptor 2 damages integrity [222] and correspondingly, agents activating S1PR1 such as artesunate and isoflurane have been demonstrated to preserve the BBB integrity [223, 224]. However, several antagonists which suppress the activation of S1PR1 have also been found to preserve the BBB integrity [143, 222]. Remarkably, the S1PR1 antagonist fingolimod (FTY720) can also possibly induce S1P1 activation [225]. These observations suggest that S1PR1 plays a dual role in BBB permeability, depending on the ligand, which is in line with the assumption proposed by Schuhmann *et al.* [226].

## Usage of astrocyte and astrocyte-derived molecules as therapeutic targets

As a result, all of the described neuroprotective and neurodeleterious molecules, as well as their upstream and downstream factors, represent potential therapeutic targets (Fig. 3 and Table 1). However, both astrocytes and astrocyte-derived molecules can only act as targets for particular subtypes, specific damage regions, and certain

**Table 1** Dual roles of astrocyte-derived factors in the BBB integrity after TBI

| Astrocyte-derived factors | Characters | Receptors | Role in BBB post-TBI | Mechanisms | Related agents | Other functions | References |
|---|---|---|---|---|---|---|---|
| ANG-1 | Glycoprotein | Tie-2 | Protect | Promote endothelial cells, vascular remodeling, and stability; increase TJ-related proteins | Exogenous ANG-1 or ANG-1 mimetic peptides | Promote angiogenesis; suppress VEGF-induce expression of cell adhesion molecules and leukocyte infiltration | 179-181 |
| SHH | Glycoprotein | Patched-1 | Protect | Attenuate endothelial cells apoptosis; increase TJ-related proteins | Exogenous SHH | Promote angiogenesis; promote normal pattern formation and cellular differentiation in the developing CNS; suppress cell adhesion molecules expression and leukocyte infiltration | 182-185 |
| GDNF | Neurotrophic factor | GDNF receptor α-1 and -2 | Protect | Increase TJ-related proteins | Exogenous GDNF | Promote the normal postnatal development of BBB, neuronal survival and angiogenesis; axon guidance and synapse formation; control endothelial functions; | 186-188 |
| RA | Active metabolite synthesized from retinol by retinaldehyde dehydrogenase | Nuclear RA receptors | Protect | Increase TJ-related proteins and vascular endothelial cadherin | Exogenous RA | Promote growth and development in the CNS; regulate synaptic plasticity; suppress the expression of cell adhesion molecules | 189-191 |
| IGF-1 | A member of insulin gene family | IGF-1 receptors | Protect | Attenuate endothelial cells apoptosis | Exogenous IGF-1 | Promote neurogenesis; reduce cell death; support injury repair; regulate synaptic neuroplasticity | 78, 192, 193 |
| APOE | A member of the apolipoprotein family | \ | Protect* | Suppress the activity of MMP-9; increase TJ-related proteins | APOE-mimetic peptide COG1410 | Support lipid transport and injury repair | 194-203 |
| VEGF | An angiogenetic factor | VEGFR-1 and VEGFR-2 | Damage | Decrease TJ-related proteins | SU5416 (VEGFR-2 inhibitor); cavtratin (a selective inhibitor of VEGF-A) | Promote endothelial proliferation and differentiation for angiogenesis; induce cell adhesion molecules expression and leukocyte infiltration | 204-207 |
| MMP | Zinc-endopeptidases | \ | Damage | Enhance endothelial cell apoptosis; degrade TJ-related proteins and ECM molecules | Ro32–3555 (a broad spectrum MMP inhibitor) | Promote angiogenesis; regulate expression of cell adhesion molecules and subsequent leukocyte infiltration | 208, 213, 214 |
| NO | A potent vasodilator synthesized from L-arginine by NO synthase | \ | Damage | Enhance MMPs activation; decrease TJ-related proteins; induce apoptosis through cGMP monophosphate-independent pathways, suppress apoptosis through cGMP pathway | Nomega-Nitro-L-arginine methyl ester (a non-specific NOS inhibitor) | Regulate blood flow for neuronal activity; exacerbate inflammatory reaction | 78, 215, 216 |
| Glutamate | A major excitatory transmitter and | NMDA receptor and the AMPA receptor | Damage | Induce excessive vascular permeability via activation of NMDA receptors; decrease TJ-related proteins | MK-801 (non-competitive NMDA receptor antagonist); CGS-19755 (competitive NMDA receptor antagonist); NBQX, DNQX (competitive AMPA receptor antagonists)** | Regulate synaptic plasticity and formation; induce vasodilatation; regulate neuronal survival | 208-210 |

**Table 1** Dual roles of astrocyte-derived factors in the BBB integrity after TBI *(Continued)*

| Astrocyte-derived factors | Characters | Receptors | Role in BBB post-TBI | Mechanisms | Related agents | Other functions | References |
|---|---|---|---|---|---|---|---|
| ETs | Potent endogenous vasoconstrictors | Endothelin receptor type A/B | Damage | Exacerbate BBB inflammation; enhance MMPs activation; degrade TJ-related proteins | S-0139 (selective ETA receptor antagonist); BQ788 (selective ETB receptor antagonist) | Induce expression of cell adhension molecules; regulate endothelial function | 21, 211, 212 |
| S1P | A biologically active lipid | S1PR 1-5 | Dual | Regulate VEGF activation and TJ-related proteins | Siponimod, fingolimod, TASP0277308 (antagonists of S1PR 1); artesunate, isoflurane (agonists of S1PR 1)† | Regulate synaptic plasticity | 143, 222-226 |

*APOE exerts its regulation of BBB integrity in an isoform-dependent manner, APOE4 activates the activity of MMP-9 and accelerates the BBB permeability[195, 196]
**Some studies suggested that blockade of AMPA receptor did not promote glutamate-mediated BBB breakdown[210]
†Both the antagonists which suppress the activation of S1PR 1 and agonists which activate S1PR 1 have been demonstrated to preserve the BBB integrity[143, 222-226]

*Abbreviations*: *ANG-1* angiopoietin-1, *TJ* tight junction, *VEGF* vascular endothelial growth factor, *BBB* blood-brain barrier, *TBI* traumatic brain injury, *SHH* sonic hedgehog, *GDNF* glial-derived neurotrophic factor, *RA* retinoic acid, *IGF-1* insulin-like growth factor-1, *APOE* apolipoprotein E, *MMP* matrix metalloproteinases, *ECM* extracellular matrix, *NO* nitric oxide, *cGMP* cyclic guanosine, *NMDA* N-methyl-D-aspartate, *ETs* endothelins, *S1P* sphingosine 1-phosphate, *AMPA* α-amino-3-hydroxy-5-methyl-4-isoxazolepropionic acid, *S1PR* S1P receptor

stages of TBI. Therefore, therapeutic strategies must focus on the enhancement of neuroprotective effects and blockage of the neurodeleterious effects of the different factors under specific conditions.

Besides targeting astrocyte-derived molecules, stimulating the function of astrocyte-related receptors is also promising for the restoration of neuronal plasticity and reconstruction. Some astrocyte-derived molecules such as S1P and ETs also act as ligands of astrocytic receptors, and the probable therapeutic drugs are shown in the Table 1. Other receptors such as Toll-like receptors [127], purinergic receptor [227], glutamate receptor [228], hormone receptor [10, 229], and cannabinoid receptor [230] have also attracted widespread attention. Although we previously mentioned that MK-801, one of the glutamate receptor antagonists, had been shown to enhance synaptic integrity and improve cognitive outcome in the experimental study; but regrettably, clinical trials concerning the glutamate receptor antagonists have been widely carried out but failed to provide a statistically significant benefit for TBI patients [231]. According to Ikonomidou *et al.,* the failure could be attributed to the attenuation of synaptic transmission, which impedes neuronal survival [228].

Modulating the maladaptive microenvironment post-TBI is also a considerable therapeutic strategy [140–142]. Relevantly, agents for reducing the glutamate excitotoxicity by enhancing glutamate transporters such as parawexin 1 and certain β-lactam antibiotics could be of therapeutic benefit [232, 233]. Other potential therapeutic mediators include agents for the restoration of ionic and water balance by targeting $Na^+/H^+$ transporters, $Na^+/K^+/2Cl^-$ cotransporters, or $Na^+/Ca2^+$ exchangers such as fluorenyl drugs [234, 235] and agents that promote neuronal survival and function such as recombinant neurotrophins or peptidomimetics [9]. Agents that alter the lesion environment by modulating inflammatory responses such as minocycline and etanercept have also been proposed as potential candidates for neuroprotection [144, 171].

We have previously reviewed the advance of stem cell treatment for TBI, which has not reached a general success in clinic application [86]. Given the vital roles of astrocyte-secreted factors in the neurogenesis and neural differentiation, a combination of stem cell treatment and astrocytic functions may present a novel therapeutic strategy. Besides, non-coding RNAs also hold therapeutic potential as astrocytes express various non-coding RNAs, which in turn control astrocytic functions [236–238]. And hypertonic saline has been found to elicit neuroprotection by regulating the expression of non-coding RNAs [239].

## Conclusion and perspectives

In this article, we describe for the first time the detailed dual roles of astrocytes in the field of neuronal plasticity and reconstruction including neurogenesis, synaptogenesis, angiogenesis, BBB repair, glial scar formation after TBI, and attempt to classify astrocyte-derived factors by neuroprotection and neurotoxicity to make the targeted therapy more relevant and meaningful. However, not only astrocytes have a dual role, but some factors derived from astrocytes also have double-sided properties, which may due to the distinct microenvironment and molecular mechanisms underlying the different subtypes, different damage zone, and different stages of neurotrauma. For example, mild TBI and severe TBI will induce different physiological and pathological mechanisms as well as different astrocytic reaction; hippocampus-derived astrocytes and spinal cord-derived astrocytes boost different effects on neurogenesis; the acute and the late stages post-TBI elicit different roles of AQP4. Therefore, simply suppressing or promoting

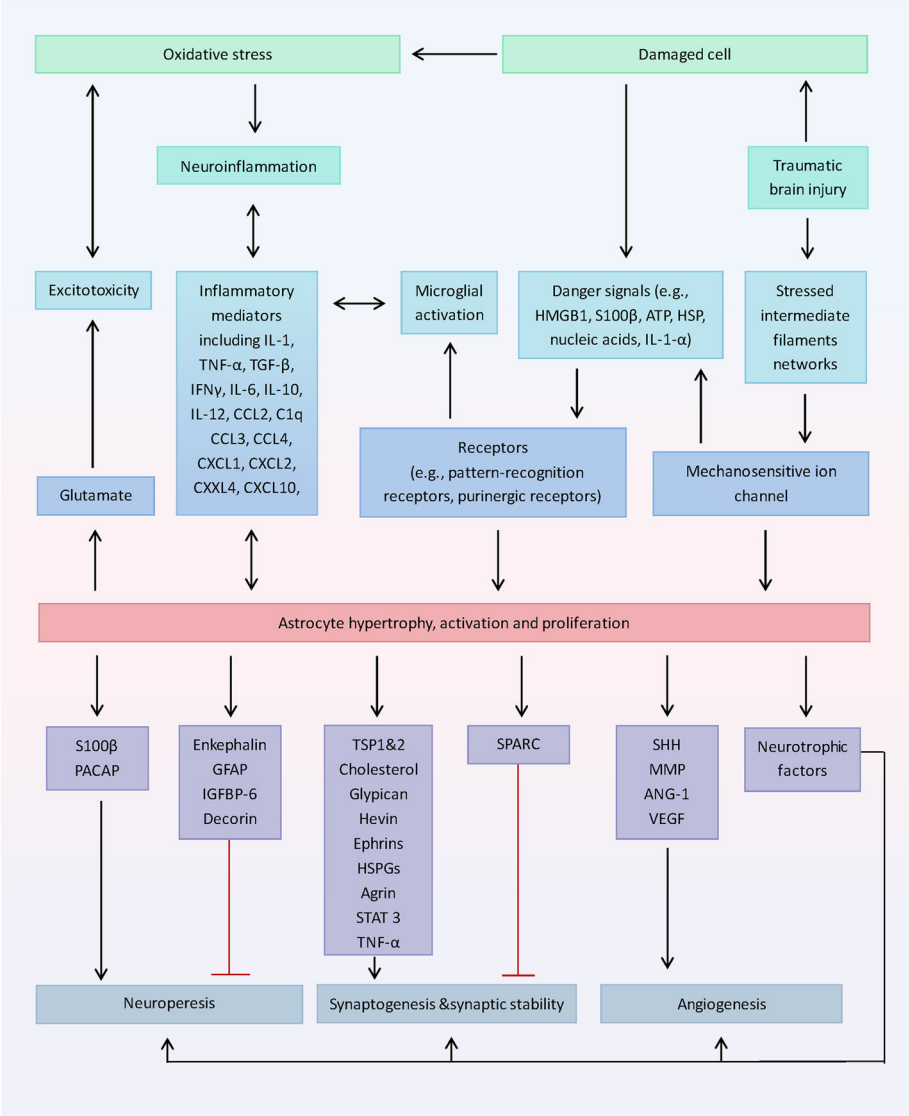


**Fig. 3** Potential therapeutic targets regarding astrocyte-derived molecules following TBI. Following TBI, damaged cells release danger signals. And stressed intermediate filaments networks within astrocytes activate ion influx through the mechanosensitive ion channel, resulting in the further release of danger signals. These signals serve to activate neuroglia and induce a robust sterile immune reaction and other secondary TBI pathogenesis. Reactive astrocytes secrete a wide range of factors that affect neurogenesis, synaptogenesis and synaptic stability, and angiogenesis, which may represent the therapeutic targets. Modulating the maladaptive microenvironment caused by neuroinflammation, excitotoxicity and oxidative stress post-TBI is also a considerable therapeutic strategy. ANG-1, angiopoietin-1; CCL, chemokine (C-C motif) ligand; CXCL, chemokine (C-X-C motif) ligand; GFAP, glial fibrillary acidic protein; HMGB1, high mobility group protein B1; HSP, heat shock proteins; HSPGs, heparan sulfate proteoglycans; IFN, interferon; IGFBP-6, insulin-like growth factor binding protein 6; IL, interleukin; MMP, matrix metalloprotein; PACAP, pituitary adenylate cyclase-activating peptide; SHH, sonic hedgehog; SPARC, secreted protein acidic and rich in cysteine; STAT3, signal transducer and activator of transcription-3; TBI, traumatic brain injury; TGF-β, transforming growth factor-β; TNF, tumor necrosis factor; TSP, thrombospondin; VEGF, vascular endothelial growth factor

reactive astrogliosis does not have a satisfying curative effect, whereas selectively stimulating the beneficial astrocyte-derived molecules while attenuating the deleterious ones based on the spatiotemporal-environment represents a promising astrocyte-targeting therapeutic strategy. As far, there are a number of related animal experiments that provide some novel therapeutic targets for the pharmacotherapy of TBI, but related clinical trials are rare and the existing ones have failed to show promise for long-term prognosis. Future research should focus more strictly on distinguishing the various functions of astrocyte-derived molecules in a clear subtype, region, and stage of TBI. In addition, more clinical trials concerning astrocyte-targeting therapy are warranted.

**Abbreviations**
ADAM-10: a distintegrin and metalloproteinase-10; AMPA: α-amino-3-hydroxy-5-methyl-4-isoxazolepropionic acid; ANG-1: Angiopoietin-1; APOE: Apolipoprotein E; AQP4: Aquaporin-4; BBB: Blood-brain barrier; CCL: Chemokine (C-C motif) ligand; cGMP: Cyclic guanosine; CNS: Central nervous system; CO: Carbon monoxide; CSPGs: Chondroitin sulfate proteoglycans; CXCL: Chemokine (C-X-C motif) ligand; CypA: Cyclophilin A; ECM: Extracellular matrix; ETs: Endothelins; GDNF: Glial-derived neurotrophic factor; GFAP: Glial fibrillary acidic protein; HSPGs: Heparan sulfate proteoglycans; IFN: Interferon; IGF-1: Insulin-like growth factor-1; IL: Interleukin; MMP: Matrix metalloprotein; NFκB: Nuclear factor-κB; NMDA: N-methyl-D-aspartate; NO: Nitric oxide; PNNs: Perineuronal nets; RA: Retinoic acid; S1P: Sphingosine 1-phosphate; S1PR: S1P receptor; SHH: Sonic hedgehog; SPARC: Secreted protein acidic and rich in cysteine; STAT3: Signal transducer and activator of transcription-3; TBI: Traumatic brain injury; TGF-β: Transforming growth factor-β; TJ: Tight junction; TNF: Tumor necrosis factor; TSP: Thrombospondin; VEGF: Vascular endothelial growth factor; ZO: Zonula occluden

**Authors' contributions**
All the authors participated in analyzing and discussing the literature, commenting on and approving the manuscript. AWS supervised the research, led the discussion, wrote and revised the manuscript. All authors read and approved the final manuscript.

**Funding**
This work was funded by China Postdoctoral Science Foundation (2017M612010) and National Natural Science Foundation of China (81701144).

**Availability of data and materials**
Not applicable.

**Ethics approval and consent to participate**
Not applicable.

**Consent for publication**
Not applicable.

**Competing interests**
The authors declare that they have no competing interests.

**Author details**
[1]Department of Surgical Oncology, The Second Affiliated Hospital, Zhejiang University School of Medicine, No. 88, Jiefang Road, Zhejiang 310009, Hangzhou, China. [2]Department of Neurosurgery, The Second Affiliated Hospital, School of Medicine, Zhejiang University, Province, Zhejiang 310009, Hangzhou, China. [3]State Key Laboratory for Diagnosis and Treatment of Infectious Diseases, Collaborative Innovation Center for Diagnosis and Treatment of Infectious Diseases, The First Affiliated Hospital, College of Medicine, Zhejiang University, Zhejiang, Hangzhou, China.

Received: 19 December 2019 Accepted: 6 March 2020
Published online: 15 April 2020

**References**
1. Kardos J, et al. The nature of early astroglial protection-Fast activation and signaling. Prog Neurobiol. 2017;153:86–99.
2. GBD 2016 Traumatic Brain Injury and Spinal Cord Injury Collaborators. Global, regional, and national burden of traumatic brain injury and spinal cord injury, 1990-2016: a systematic analysis for the Global Burden of Disease Study 2016. Lancet Neurol. 2019;18(1):56–87.
3. Maas AIR, et al. Traumatic brain injury: integrated approaches to improve prevention, clinical care, and research. Lancet Neurol. 2017;16(12):987–1048.
4. An C, et al. Severity-Dependent Long-Term Spatial Learning-Memory Impairment in a Mouse Model of Traumatic Brain Injury. Transl Stroke Res. 2016;7(6):512–20.
5. Cooper DJ, et al. Effect of Early Sustained Prophylactic Hypothermia on Neurologic Outcomes Among Patients With Severe Traumatic Brain Injury: The POLAR Randomized Clinical Trial. JAMA. 2018;320(21):2211–20.
6. Dang B, et al. Rehabilitation Treatment and Progress of Traumatic Brain Injury Dysfunction. Neural Plast. 2017;2017:1582182.
7. Roozenbeek B, Maas AI, Menon DK. Changing patterns in the epidemiology of traumatic brain injury. Nat Rev Neurol. 2013;9(4):231–6.
8. Khaksari M, Soltani Z, Shahrokhi N. Effects of Female Sex Steroids Administration on Pathophysiologic Mechanisms in Traumatic Brain Injury. Transl Stroke Res. 2018;9(4):393–416.
9. Colangelo AM, et al. Targeting reactive astrogliosis by novel biotechnological strategies. Biotechnol Adv. 2012;30(1):261–71.
10. Arbo BD, Bennetti F, Ribeiro MF. Astrocytes as a target for neuroprotection: Modulation by progesterone and dehydroepiandrosterone. Prog Neurobiol. 2016;144:27–47.
11. Shields J, et al. Therapeutic targeting of astrocytes after traumatic brain injury. Transl Stroke Res. 2011;2(4):633–42.
12. Sofroniew MV, Vinters HV. Astrocytes: biology and pathology. Acta Neuropathol. 2010;119(1):7–35.
13. Pu H, et al. Repetitive and Prolonged Omega-3 Fatty Acid Treatment After Traumatic Brain Injury Enhances Long-Term Tissue Restoration and Cognitive Recovery. Cell Transplant. 2017;26(4):555–69.
14. Wu Y, et al. Implantation of Brain-Derived Extracellular Matrix Enhances Neurological Recovery after Traumatic Brain Injury. Cell Transplant. 2017; 26(7):1224–34.
15. Perez EJ, et al. Enhanced astrocytic d-serine underlies synaptic damage after traumatic brain injury. J Clin Invest. 2017;127(8):3114–25.
16. Furman JL, et al. Blockade of Astrocytic Calcineurin/NFAT Signaling Helps to Normalize Hippocampal Synaptic Function and Plasticity in a Rat Model of Traumatic Brain Injury. J Neurosci. 2016;36(5):1502–15.
17. Warren KM, Reeves TM, Phillips LL. MT5-MMP, ADAM-10, and N-cadherin act in concert to facilitate synapse reorganization after traumatic brain injury. J Neurotrauma. 2012;29(10):1922–40.
18. Tyzack GE, et al. Astrocyte response to motor neuron injury promotes structural synaptic plasticity via STAT3-regulated TSP-1 expression. Nat Commun. 2014;5:4294.
19. de la Tremblaye PB, et al. Elucidating opportunities and pitfalls in the treatment of experimental traumatic brain injury to optimize and facilitate clinical translation. Neurosci Biobehav Rev. 2018;85:160–75.
20. Lee SW, et al. The role of microglial inflammasome activation in pyroptotic cell death following penetrating traumatic brain injury. J Neuroinflammation. 2019;16(1):27.
21. Hostenbach S, et al. The pathophysiological role of astrocytic endothelin-1. Prog Neurobiol. 2016;144:88–102.
22. Ichkova A, et al. Vascular impairment as a pathological mechanism underlying long-lasting cognitive dysfunction after pediatric traumatic brain injury. Neurochem Int. 2017;111:93–102.
23. Hayes JP, et al. Mild traumatic brain injury is associated with reduced cortical thickness in those at risk for Alzheimer's disease. Brain. 2017;140(3):813–25.
24. Lin C, et al. Melatonin attenuates traumatic brain injury-induced inflammation: a possible role for mitophagy. J Pineal Res. 2016;61(2): 177–86.
25. Menge T, et al. Mesenchymal stem cells regulate blood-brain barrier integrity through TIMP3 release after traumatic brain injury. Sci Transl Med. 2012;4(161):161ra150.
26. Wu H, et al. Melatonin attenuates neuronal apoptosis through up-regulation of K(+) -Cl(-) cotransporter KCC2 expression following traumatic brain injury in rats. J Pineal Res. 2016;61(2):241–50.
27. Shlosberg D, et al. Blood-brain barrier breakdown as a therapeutic target in traumatic brain injury. Nat Rev Neurol. 2010;6(7):393–403.
28. Gyoneva S, Ransohoff RM. Inflammatory reaction after traumatic brain injury: therapeutic potential of targeting cell-cell communication by chemokines. Trends Pharmacol Sci. 2015;36(7):471–80.
29. Corps KN, Roth TL, McGavern DB. Inflammation and neuroprotection in traumatic brain injury. JAMA Neurol. 2015;72(3):355–62.
30. Sharma K, Zhang G, Li S. In: So K-F, Xu X-M, editors. Chapter 11 - Astrogliosis and Axonal Regeneration. Neural Regeneration. Oxford: Academic Press; 2015. p. 181–96.
31. Jassam YN, et al. Neuroimmunology of Traumatic Brain Injury: Time for a Paradigm Shift. Neuron. 2017;95(6):1246–65.
32. Kumar A, et al. Microglial-derived microparticles mediate neuroinflammation after traumatic brain injury. J Neuroinflammation. 2017;14(1):47.
33. Johnson VE, et al. Mechanical disruption of the blood-brain barrier following experimental concussion. Acta Neuropathol. 2018;135(5):711–26.

34. Badaut J, Bix GJ. Vascular neural network phenotypic transformation after traumatic injury: potential role in long-term sequelae. Transl Stroke Res. 2014;5(3):394–406.
35. Cai W, et al. Pericytes in Brain Injury and Repair After Ischemic Stroke. Transl Stroke Res. 2017;8(2):107–21.
36. Villapol S, et al. Neurorestoration after traumatic brain injury through angiotensin II receptor blockage. Brain. 2015;138(Pt 11):3299–315.
37. Wennersten A, Holmin S, Mathiesen T. Characterization of Bax and Bcl-2 in apoptosis after experimental traumatic brain injury in the rat. Acta Neuropathol. 2003;105(3):281–8.
38. Nirmala JG, Lopus M. Cell death mechanisms in eukaryotes. Cell Biol Toxicol. 2019.
39. Chen T, et al. Arc silence aggravates traumatic neuronal injury via mGluR1-mediated ER stress and necroptosis. Cell Death Dis. 2020;11(1):4.
40. Degterev A, Ofengeim D, Yuan J. Targeting RIPK1 for the treatment of human diseases. Proc Natl Acad Sci U S A. 2019;116(20):9714–22.
41. Bao Z, et al. Silencing of A20 Aggravates Neuronal Death and Inflammation After Traumatic Brain Injury: A Potential Trigger of Necroptosis. Front Mol Neurosci. 2019;12:222.
42. Royce GH, Brown-Borg HM, Deepa SS. The potential role of necroptosis in inflammaging and aging. Geroscience. 2019;41(6):795–811.
43. Chen J, et al. Molecular Insights into the Mechanism of Necroptosis: The Necrosome As a Potential Therapeutic Target. Cells. 2019:8(12).
44. Zhang X, et al. Bench-to-bedside review: Apoptosis/programmed cell death triggered by traumatic brain injury. Crit Care. 2005;9(1):66–75.
45. Yang Z, Wang KK. Glial fibrillary acidic protein: from intermediate filament assembly and gliosis to neurobiomarker. Trends Neurosci. 2015;38(6):364–74.
46. Sofroniew MV. Astrocyte barriers to neurotoxic inflammation. Nat Rev Neurosci. 2015;16(5):249–63.
47. Rothstein JD, et al. Knockout of glutamate transporters reveals a major role for astroglial transport in excitotoxicity and clearance of glutamate. Neuron. 1996;16(3):675–86.
48. Anderson CM, Swanson RA. Astrocyte glutamate transport: review of properties, regulation, and physiological functions. Glia. 2000;32(1):1–14.
49. Zou J, et al. Glutamine synthetase down-regulation reduces astrocyte protection against glutamate excitotoxicity to neurons. Neurochem Int. 2010;56(4):577–84.
50. Ye ZC, et al. Functional hemichannels in astrocytes: a novel mechanism of glutamate release. J Neurosci. 2003;23(9):3588–96.
51. Slemmer JE, et al. Antioxidants and free radical scavengers for the treatment of stroke, traumatic brain injury and aging. Curr Med Chem. 2008; 15(4):404–14.
52. Dringen R, Gutterer JM, Hirrlinger J. Glutathione metabolism in brain metabolic interaction between astrocytes and neurons in the defense against reactive oxygen species. Eur J Biochem. 2000;267(16):4912–6.
53. Magistretti PJ, Pellerin L. Cellular mechanisms of brain energy metabolism and their relevance to functional brain imaging. Philos Trans R Soc Lond B Biol Sci. 1999;354(1387):1155–63.
54. Danbolt NC. Glutamate uptake. Prog Neurobiol. 2001;65(1):1–105.
55. Magistretti PJ. Neuron-glia metabolic coupling and plasticity. J Exp Biol. 2006;209(Pt 12):2304–11.
56. Jayakumar AR, Norenberg MD. The Na–K–Cl Co-transporter in astrocyte swelling. Metab Brain Dis. 2010;25(1):31–8.
57. LANG F, et al. Functional Significance of Cell Volume Regulatory Mechanisms. Physiol Rev. 1998;78(1):247–306.
58. Walz W. Role of astrocytes in the clearance of excess extracellular potassium. Neurochem Int. 2000;36(4-5):291–300.
59. Kofuji P, Newman EA. Potassium buffering in the central nervous system. Neuroscience. 2004;129(4):1045–56.
60. Zhai X, et al. Astrocytes Regulate Angiogenesis Through the Jagged1-Mediated Notch1 Pathway After Status Epilepticus. Mol Neurobiol. 2016; 53(9):5893–901.
61. Baldwin KT, Eroglu C. Molecular mechanisms of astrocyte-induced synaptogenesis. Curr Opin Neurobiol. 2017;45:113–20.
62. Muthukumar AK, Stork T, Freeman MR. Activity-dependent regulation of astrocyte GAT levels during synaptogenesis. Nat Neurosci. 2014;17(10):1340–50.
63. Stogsdill JA, et al. Astrocytic neuroligins control astrocyte morphogenesis and synaptogenesis. Nature. 2017;551(7679):192–7.
64. Robinson C, Apgar C, Shapiro LA. Astrocyte Hypertrophy Contributes to Aberrant Neurogenesis after Traumatic Brain Injury. Neural Plast. 2016;2016:1347987.
65. Farina C, Aloisi F, Meinl E. Astrocytes are active players in cerebral innate immunity. Trends Immunol. 2007;28(3):138–45.
66. Shastri A, Bonifati DM, Kishore U. Innate immunity and neuroinflammation. Mediators Inflamm. 2013;2013:342931.
67. Ransohoff RM, Brown MA. Innate immunity in the central nervous system. J Clin Invest. 2012;122(4):1164–71.
68. Sofroniew MV. Molecular dissection of reactive astrogliosis and glial scar formation. Trends Neurosci. 2009;32(12):638–47.
69. Fujita T, et al. Cellular dynamics of macrophages and microglial cells in reaction to stab wounds in rat cerebral cortex. Acta Neurochir (Wien). 1998; 140(3):275–9.
70. Di Giovanni S, et al. Cell cycle inhibition provides neuroprotection and reduces glial proliferation and scar formation after traumatic brain injury. Proc Natl Acad Sci U S A. 2005;102(23):8333–8.
71. Susarla BT, et al. Temporal patterns of cortical proliferation of glial cell populations after traumatic brain injury in mice. ASN Neuro. 2014;6(3):159–70.
72. Murakami K, et al. Subarachnoid Hemorrhage Induces Gliosis and Increased Expression of the Pro-inflammatory Cytokine High Mobility Group Box 1 Protein. Transl Stroke Res. 2011;2(1):72–9.
73. Peng L, Parpura V, Verkhratsky A. EDITORIAL Neuroglia as a Central Element of Neurological Diseases: An Underappreciated Target for Therapeutic Intervention. Curr Neuropharmacol. 2014;12(4):303–7.
74. Karimi-Abdolrezaee S, Billakanti R. Reactive astrogliosis after spinal cord injury-beneficial and detrimental effects. Mol Neurobiol. 2012;46(2):251–64.
75. Burda JE, Sofroniew MV. Reactive Gliosis and the Multicellular Response to CNS Damage and Disease. Neuron. 2014;81(2):229–48.
76. Cregg JM, et al. Functional regeneration beyond the glial scar. Exp Neurol. 2014;253:197–207.
77. Voskuhl RR, et al. Reactive astrocytes form scar-like perivascular barriers to leukocytes during adaptive immune inflammation of the CNS. J Neurosci. 2009;29(37):11511–22.
78. Michinaga S, Koyama Y. Dual Roles of Astrocyte-Derived Factors in Regulation of Blood-Brain Barrier Function after Brain Damage. Int J Mol Sci. 2019:20(3).
79. Burda JE, Bernstein AM, Sofroniew MV. Astrocyte roles in traumatic brain injury. Exp Neurol. 2016;275(Pt 3):305–15.
80. Sweeney MD, Sagare AP, Zlokovic BV. Blood-brain barrier breakdown in Alzheimer disease and other neurodegenerative disorders. Nat Rev Neurol. 2018;14(3):133–50.
81. Jessen NA, et al. The Glymphatic System: A Beginner's Guide. Neurochem Res. 2015;40(12):2583–99.
82. Louveau A, et al. Understanding the functions and relationships of the glymphatic system and meningeal lymphatics. J Clin Invest. 2017;127(9):3210–9.
83. Garber C, et al. Astrocytes decrease adult neurogenesis during virus-induced memory dysfunction via IL-1. Nat Immunol. 2018;19(2):151–61.
84. Tsai HH, et al. Regional astrocyte allocation regulates CNS synaptogenesis and repair. Science. 2012;337(6092):358–62.
85. Vignoli B, et al. Peri-Synaptic Glia Recycles Brain-Derived Neurotrophic Factor for LTP Stabilization and Memory Retention. Neuron. 2016;92(4): 873–87.
86. Zhou Y, et al. Advance of Stem Cell Treatment for Traumatic Brain Injury. Front Cell Neurosci. 2019;13:301.
87. Papa M, et al. Astrocyte-neuron interplay in maladaptive plasticity. Neurosci Biobehav Rev. 2014;42:35–54.
88. Song H, Stevens CF, Gage FH. Astroglia induce neurogenesis from adult neural stem cells. Nature. 2002;417(6884):39–44.
89. Kleindienst A, et al. Enhanced hippocampal neurogenesis by intraventricular S100B infusion is associated with improved cognitive recovery after traumatic brain injury. J Neurotrauma. 2005;22(6):645–55.
90. Hinkle DA, et al. GFAP and S100beta expression in the cortex and hippocampus in response to mild cortical contusion. J Neurotrauma. 1997; 14(10):729–38.
91. Choi YK. Role of Carbon Monoxide in Neurovascular Repair Processing. Biomol Ther (Seoul). 2018;26(2):93–100.
92. Seri B, et al. Astrocytes give rise to new neurons in the adult mammalian hippocampus. J Neurosci. 2001;21(18):7153–60.
93. van Landeghem FK, et al. Cellular localization of pituitary adenylate cyclase-activating peptide (PACAP) following traumatic brain injury in humans. Acta Neuropathol. 2007;113(6):683–93.
94. Crupi R, et al. Co-Ultramicronized Palmitoylethanolamide/Luteolin Promotes Neuronal Regeneration after Spinal Cord Injury. Front Pharmacol. 2016;7(47).
95. Gao X, Chen J. Conditional knockout of brain-derived neurotrophic factor in the hippocampus increases death of adult-born immature neurons following traumatic brain injury. J Neurotrauma. 2009;26(8):1325–35.

96. Amorini AM, et al. Severity of experimental traumatic brain injury modulates changes in concentrations of cerebral free amino acids. J Cell Mol Med. 2017;21(3):530–42.
97. Wilhelmsson U, et al. The role of GFAP and vimentin in learning and memory. Biol Chem. 2019;400(9):1147–56.
98. Wilhelmsson U, et al. Absence of glial fibrillary acidic protein and vimentin prevents hypertrophy of astrocytic processes and improves post-traumatic regeneration. J Neurosci. 2004;24(21):5016–21.
99. de Pablo Y, et al. Intermediate filaments are important for astrocyte response to oxidative stress induced by oxygen-glucose deprivation and reperfusion. Histochem Cell Biol. 2013;140(1):81–91.
100. Wang X, Messing A, David S. Axonal and Nonneuronal Cell Responses to Spinal Cord Injury in Mice Lacking Glial Fibrillary Acidic Protein. Exp Neurol. 1997;148(2):568–76.
101. Prozorovski T, et al. Sirt1 contributes critically to the redox-dependent fate of neural progenitors. Nat Cell Biol. 2008;10(4):385–94.
102. Viviani B, et al. Interleukin-1beta enhances NMDA receptor-mediated intracellular calcium increase through activation of the Src family of kinases. J Neurosci. 2003;23(25):8692–700.
103. Vezzani A, Baram TZ. New roles for interleukin-1 Beta in the mechanisms of epilepsy. Epilepsy Curr. 2007;7(2):45–50.
104. Barkho BZ, et al. Identification of astrocyte-expressed factors that modulate neural stem/progenitor cell differentiation. Stem Cells Dev. 2006;15(3):407–21.
105. Ullian EM, et al. Control of synapse number by glia. Science. 2001;291(5504):657–61.
106. Pfrieger FW, Barres BA. New views on synapse-glia interactions. Curr Opin Neurobiol. 1996;6(5):615–21.
107. Nieweg K, Schaller H, Pfrieger FW. Marked differences in cholesterol synthesis between neurons and glial cells from postnatal rats. J Neurochem. 2009;109(1):125–34.
108. Pfrieger FW. Roles of glial cells in synapse development. Cell Mol Life Sci. 2009;66(13):2037–47.
109. Buss A, et al. Growth-modulating molecules are associated with invading Schwann cells and not astrocytes in human traumatic spinal cord injury. Brain. 2007;130(Pt 4):940–53.
110. Ullian EM, Christopherson KS, Barres BA. Role for glia in synaptogenesis. Glia. 2004;47(3):209–16.
111. Falo MC, Reeves TM, Phillips LL. Agrin expression during synaptogenesis induced by traumatic brain injury. J Neurotrauma. 2008;25(7):769–83.
112. Bali N, et al. Progesterone antagonism of neurite outgrowth depends on microglial activation via Pgrmc1/S2R. Endocrinology. 2013;154(7):2468–80.
113. Herrmann JE, et al. STAT3 is a critical regulator of astrogliosis and scar formation after spinal cord injury. J Neurosci. 2008;28(28):7231–43.
114. Okada S, et al. Conditional ablation of Stat3 or Socs3 discloses a dual role for reactive astrocytes after spinal cord injury. Nat Med. 2006;**12**(7):829–34.
115. Christopherson KS, et al. Thrombospondins are astrocyte-secreted proteins that promote CNS synaptogenesis. Cell. 2005;120(3):421–33.
116. Kucukdereli H, et al. Control of excitatory CNS synaptogenesis by astrocyte-secreted proteins Hevin and SPARC. Proc Natl Acad Sci. 2011;108(32):E440–9.
117. Albrecht D, et al. SPARC prevents maturation of cholinergic presynaptic terminals. Mol Cell Neurosci. 2012;49(3):364–74.
118. Jones EV, et al. Astrocytes control glutamate receptor levels at developing synapses through SPARC-beta-integrin interactions. J Neurosci. 2011;31(11):4154–65.
119. Allen NJ, et al. Astrocyte glypicans 4 and 6 promote formation of excitatory synapses via GluA1 AMPA receptors. Nature. 2012;486:410.
120. Fuentes-Medel Y, et al. Integration of a Retrograde Signal during Synapse Formation by Glia-Secreted TGF-β Ligand. Current Biology. 2012;22(19):1831–8.
121. Diniz LP, et al. Astrocyte-induced synaptogenesis is mediated by transforming growth factor beta signaling through modulation of D-serine levels in cerebral cortex neurons. J Biol Chem. 2012;287(49):41432–45.
122. Gómez-Casati ME, et al. Nonneuronal cells regulate synapse formation in the vestibular sensory epithelium via erbB-dependent BDNF expression. Proc Natl Acad Sci. 2010;107(39):17005–10.
123. Garrett AM, Weiner JA. Control of CNS synapse development by {gamma}-protocadherin-mediated astrocyte-neuron contact. J Neurosci. 2009;29(38):11723–31.
124. Jeong SR, et al. Hepatocyte growth factor reduces astrocytic scar formation and promotes axonal growth beyond glial scars after spinal cord injury. Exp Neurol. 2012;233(1):312–22.
125. Yi JH, et al. Alterations in sulfated chondroitin glycosaminoglycans following controlled cortical impact injury in mice. J Comp Neurol. 2012;520(15):3295–313.
126. Buss A, et al. Gradual loss of myelin and formation of an astrocytic scar during Wallerian degeneration in the human spinal cord. Brain. 2004;127(Pt 1):34–44.
127. Li L, et al. Toll-like receptor 9 antagonism modulates astrocyte function and preserves proximal axons following spinal cord injury. Brain Behav Immun. 2019;80:328–43.
128. Bradbury EJ, et al. Chondroitinase ABC promotes functional recovery after spinal cord injury. Nature. 2002;416(6881):636–40.
129. Wang D, Fawcett J. The perineuronal net and the control of CNS plasticity. Cell Tissue Res. 2012;349(1):147–60.
130. Sorg BA, et al. Casting a Wide Net: Role of Perineuronal Nets in Neural Plasticity. J Neurosci. 2016;36(45):11459–68.
131. Shen Y, et al. PTPsigma is a receptor for chondroitin sulfate proteoglycan, an inhibitor of neural regeneration. Science. 2009;326(5952):592–6.
132. Dickendesher TL, et al. NgR1 and NgR3 are receptors for chondroitin sulfate proteoglycans. Nat Neurosci. 2012;15(5):703–12.
133. Coles CH, et al. Proteoglycan-specific molecular switch for RPTPsigma clustering and neuronal extension. Science. 2011;332(6028):484–8.
134. Brown JM, et al. A sulfated carbohydrate epitope inhibits axon regeneration after injury. Proc Natl Acad Sci U S A. 2012;109(13):4768–73.
135. Carulli D, et al. Animals lacking link protein have attenuated perineuronal nets and persistent plasticity. Brain. 2010;133(Pt 8):2331–47.
136. Treloar HB, et al. Tenascin-C is an inhibitory boundary molecule in the developing olfactory bulb. J Neurosci. 2009;29(30):9405–16.
137. Deller T, et al. Up-regulation of astrocyte-derived tenascin-C correlates with neurite outgrowth in the rat dentate gyrus after unilateral entorhinal cortex lesion. Neuroscience. 1997;81(3):829–46.
138. Kim HJ, et al. Elevation of hippocampal MMP-3 expression and activity during trauma-induced synaptogenesis. Exp Neurol. 2005;192(1):60–72.
139. Falo MC, et al. Matrix metalloproteinase-3 expression profile differentiates adaptive and maladaptive synaptic plasticity induced by traumatic brain injury. J Neurosci Res. 2006;84(4):768–81.
140. Albensi BC. Models of brain injury and alterations in synaptic plasticity. J Neurosci Res. 2001;65(4):279–83.
141. Allen NJ. Role of glia in developmental synapse formation. Curr Opin Neurobiol. 2013;23(6):1027–33.
142. Clarke LE, Barres BA. Emerging roles of astrocytes in neural circuit development. Nat Rev Neurosci. 2013;14(5):311–21.
143. Cuzzocrea S, et al. Sphingosine 1-Phosphate Receptor Subtype 1 as a Therapeutic Target for Brain Trauma. J Neurotrauma. 2018;35(13):1452–66.
144. Yew WP, et al. Early treatment with minocycline following stroke in rats improves functional recovery and differentially modifies responses of peri-infarct microglia and astrocytes. J Neuroinflammation. 2019;16(1):6.
145. Rodriguez-Manzaneque JC, et al. Thrombospondin-1 suppresses spontaneous tumor growth and inhibits activation of matrix metalloproteinase-9 and mobilization of vascular endothelial growth factor. Proc Natl Acad Sci U S A. 2001;98(22):12485–90.
146. Pan H, et al. The absence of Nrf2 enhances NF-kappaB-dependent inflammation following scratch injury in mouse primary cultured astrocytes. Mediators Inflamm. 2012;2012:217580.
147. Hubbard JA, Szu JI, Binder DK. The role of aquaporin-4 in synaptic plasticity, memory and disease. Brain Res Bull. 2018;136:118–29.
148. Ashkar S, et al. Eta-1 (osteopontin): an early component of type-1 (cell-mediated) immunity. Science. 2000;287(5454):860–4.
149. Zhang C, Chen J, Lu H. Expression of aquaporin-4 and pathological characteristics of brain injury in a rat model of traumatic brain injury. Mol Med Rep. 2015;12(5):7351–7.
150. Giulian D, et al. Interleukin-1 injected into mammalian brain stimulates astrogliosis and neovascularization. J Neurosci. 1988;**8**(7):2485–90.
151. Asher RA, et al. Neurocan is upregulated in injured brain and in cytokine-treated astrocytes. J Neurosci. 2000;20(7):2427–38.
152. Kwok JC, et al. Extracellular matrix and perineuronal nets in CNS repair. Dev Neurobiol. 2011;71(11):1073–89.
153. Fawcett JW, Oohashi T, Pizzorusso T. The roles of perineuronal nets and the perinodal extracellular matrix in neuronal function. Nat Rev Neurosci. 2019;20(8):451–65.
154. Frischknecht R, et al. Brain extracellular matrix affects AMPA receptor lateral mobility and short-term synaptic plasticity. Nat Neurosci. 2009;12(7):897–904.

155. Pyka M, et al. Chondroitin sulfate proteoglycans regulate astrocyte-dependent synaptogenesis and modulate synaptic activity in primary embryonic hippocampal neurons. Eur J Neurosci. 2011;33(12):2187–202.
156. Beattie EC, et al. Control of synaptic strength by glial TNFalpha. Science. 2002;295(5563):2282–5.
157. Stellwagen D, Malenka RC. Synaptic scaling mediated by glial TNF-alpha. Nature. 2006;440(7087):1054–9.
158. Steinmetz CC, Turrigiano GG. Tumor necrosis factor-alpha signaling maintains the ability of cortical synapses to express synaptic scaling. J Neurosci. 2010;30(44):14685–90.
159. Sofroniew MV. Reactive astrocytes in neural repair and protection. Neuroscientist. 2005;11(5):400–7.
160. Bush TG, et al. Leukocyte infiltration, neuronal degeneration, and neurite outgrowth after ablation of scar-forming, reactive astrocytes in adult transgenic mice. Neuron. 1999;23(2):297–308.
161. Faulkner JR, et al. Reactive astrocytes protect tissue and preserve function after spinal cord injury. J Neurosci. 2004;24(9):2143–55.
162. Myer DJ, et al. Essential protective roles of reactive astrocytes in traumatic brain injury. Brain. 2006;129(Pt 10):2761–72.
163. Murai KK, Pasquale EB. Eph receptors and ephrins in neuron-astrocyte communication at synapses. Glia. 2011;59(11):1567–78.
164. Filosa A, et al. Neuron-glia communication via EphA4/ephrin-A3 modulates LTP through glial glutamate transport. Nat Neurosci. 2009;12(10):1285–92.
165. Gupta RK, Prasad S. Early down regulation of the glial Kir4.1 and GLT-1 expression in pericontusional cortex of the old male mice subjected to traumatic brain injury. Biogerontology. 2013;14(5):531–41.
166. Klein P, et al. Commonalities in epileptogenic processes from different acute brain insults: Do they translate? Epilepsia. 2018;59(1):37–66.
167. Buritica E, et al. Changes in calcium-binding protein expression in human cortical contusion tissue. J Neurotrauma. 2009;26(12):2145–55.
168. Kim SY, et al. A potential role for glia-derived extracellular matrix remodeling in postinjury epilepsy. J Neurosci Res. 2016;94(9):794–803.
169. Volman V, Bazhenov M, Sejnowski TJ. Divide and conquer: functional segregation of synaptic inputs by astrocytic microdomains could alleviate paroxysmal activity following brain trauma. PLoS Comput Biol. 2013;9(1):e1002856.
170. Akassoglou K, et al. Astrocyte-specific but not neuron-specific transmembrane TNF triggers inflammation and degeneration in the central nervous system of transgenic mice. J Immunol. 1997;158(1):438–45.
171. Tuttolomondo A, Pecoraro R, Pinto A. Studies of selective TNF inhibitors in the treatment of brain injury from stroke and trauma: a review of the evidence to date. Drug Des Devel Ther. 2014;8:2221–38.
172. Boison D. The adenosine kinase hypothesis of epileptogenesis. Prog Neurobiol. 2008;84(3):249–62.
173. Bloom GS. *Amyloid-β and tau: the trigger and bullet in Alzheimer disease pathogenesis*. JAMA Neurol. 2014;71(4):505–8.
174. McKee AC, et al. The spectrum of disease in chronic traumatic encephalopathy. Brain. 2013;136(Pt 1):43–64.
175. Chen H, et al. Head injury and amyotrophic lateral sclerosis. Am J Epidemiol. 2007;166(7):810–6.
176. McKee AC, et al. Chronic traumatic encephalopathy in athletes: progressive tauopathy after repetitive head injury. J Neuropathol Exp Neurol. 2009;68(7):709–35.
177. Luissint AC, et al. Tight junctions at the blood brain barrier: physiological architecture and disease-associated dysregulation. Fluids Barriers CNS. 2012;9(1):23.
178. Burek, M., et al., Hypoxia-Induced MicroRNA-212/132 Alter Blood-Brain Barrier Integrity Through Inhibition of Tight Junction-Associated Proteins in Human and Mouse Brain Microvascular Endothelial Cells. Transl Stroke Res, 2019.
179. Brickler TR, et al. Angiopoietin/Tie2 Axis Regulates the Age-at-Injury Cerebrovascular Response to Traumatic Brain Injury. J Neurosci. 2018;38(45):9618–34.
180. Gurnik S, et al. Angiopoietin-2-induced blood-brain barrier compromise and increased stroke size are rescued by VE-PTP-dependent restoration of Tie2 signaling. Acta Neuropathol. 2016;131(5):753–73.
181. Zhao J, et al. Angiopoietin-1 protects the endothelial cells against advanced glycation end product injury by strengthening cell junctions and inhibiting cell apoptosis. J Cell Physiol. 2015;230(8):1895–905.
182. Alvarez JI, Katayama T, Prat A. Glial influence on the blood brain barrier. Glia. 2013;61(12):1939–58.
183. Alvarez JI, et al. The Hedgehog pathway promotes blood-brain barrier integrity and CNS immune quiescence. Science. 2011;334(6063):1727–31.
184. Brilha S, et al. Matrix metalloproteinase-9 activity and a downregulated Hedgehog pathway impair blood-brain barrier function in an in vitro model of CNS tuberculosis. Sci Rep. 2017;7(1):16031.
185. Xia YP, et al. Recombinant human sonic hedgehog protein regulates the expression of ZO-1 and occludin by activating angiopoietin-1 in stroke damage. PLoS One. 2013;8(7):e68891.
186. Igarashi Y, et al. Expression of receptors for glial cell line-derived neurotrophic factor (GDNF) and neurturin in the inner blood-retinal barrier of rats. Cell Struct Funct. 2000;25(4):237–41.
187. Shimizu F, et al. Pericyte-derived glial cell line-derived neurotrophic factor increase the expression of claudin-5 in the blood-brain barrier and the blood-nerve barrier. Neurochem Res. 2012;37(2):401–9.
188. Xiao W, et al. GDNF is involved in the barrier-inducing effect of enteric glial cells on intestinal epithelial cells under acute ischemia reperfusion stimulation. Mol Neurobiol. 2014;50(2):274–89.
189. Mizee MR, et al. Astrocyte-derived retinoic acid: a novel regulator of blood-brain barrier function in multiple sclerosis. Acta Neuropathol. 2014;128(5):691–703.
190. Kong L, et al. Retinoic acid ameliorates blood-brain barrier disruption following ischemic stroke in rats. Pharmacol Res. 2015;99:125–36.
191. Gille J, et al. Retinoic acid inhibits the regulated expression of vascular cell adhesion molecule-1 by cultured dermal microvascular endothelial cells. J Clin Invest. 1997;99(3):492–500.
192. Bake S, et al. Insulin-Like Growth Factor (IGF)-I Modulates Endothelial Blood-Brain Barrier Function in Ischemic Middle-Aged Female Rats. Endocrinology. 2016;157(1):61–9.
193. Bake S, et al. Insulin-like Growth Factor (IGF)-1 treatment stabilizes the microvascular cytoskeleton under ischemic conditions. Exp Neurol. 2019;311:162–72.
194. Mahley RW, Weisgraber KH, Huang Y. Apolipoprotein E: structure determines function, from atherosclerosis to Alzheimer's disease to AIDS. J Lipid Res. 2009;50(Suppl):S183–8.
195. Nishitsuji K, et al. Apolipoprotein E regulates the integrity of tight junctions in an isoform-dependent manner in an in vitro blood-brain barrier model. J Biol Chem. 2011;286(20):17536–42.
196. Bell RD, et al. Apolipoprotein E controls cerebrovascular integrity via cyclophilin A. Nature. 2012;485(7399):512–6.
197. Cao F, et al. Apolipoprotein E-Mimetic COG1410 Reduces Acute Vasogenic Edema following Traumatic Brain Injury. J Neurotrauma. 2016;33(2):175–82.
198. Teng Z, et al. ApoE Influences the Blood-Brain Barrier Through the NF-kappaB/MMP-9 Pathway After Traumatic Brain Injury. Sci Rep. 2017;7(1):6649.
199. Methia N, et al. ApoE deficiency compromises the blood brain barrier especially after injury. Mol Med. 2001;7(12):810–5.
200. Hafezi-Moghadam A, Thomas KL, Wagner DD. ApoE deficiency leads to a progressive age-dependent blood-brain barrier leakage. Am J Physiol Cell Physiol. 2007;292(4):C1256–62.
201. Zheng M, et al. ApoE-deficient promotes blood-brain barrier disruption in experimental autoimmune encephalomyelitis via alteration of MMP-9. J Mol Neurosci. 2014;54(2):282–90.
202. Pang J, et al. Inhibition of Blood-Brain Barrier Disruption by an Apolipoprotein E-Mimetic Peptide Ameliorates Early Brain Injury in Experimental Subarachnoid Hemorrhage. Transl Stroke Res. 2017;8(3):257–72.
203. Pang J, et al. Apolipoprotein E Exerts a Whole-Brain Protective Property by Promoting M1? Microglia Quiescence After Experimental Subarachnoid Hemorrhage in Mice. Transl Stroke Res. 2018;9(6):654–68.
204. Jiang S, et al. Vascular endothelial growth factors enhance the permeability of the mouse blood-brain barrier. PLoS One. 2014;9(2):e86407.
205. Wu L, et al. Vascular endothelial growth factor aggravates cerebral ischemia and reperfusion-induced blood-brain-barrier disruption through regulating LOC102640519/HOXC13/ZO-1 signaling. Exp Cell Res. 2018;369(2):275–83.
206. Argaw AT, et al. Astrocyte-derived VEGF-A drives blood-brain barrier disruption in CNS inflammatory disease. J Clin Invest. 2012;122(7):2454–68.
207. Kim E, et al. Inhibition of VEGF Signaling Reduces Diabetes-Exacerbated Brain Swelling, but Not Infarct Size, in Large Cerebral Infarction in Mice. Transl Stroke Res. 2018;9(5):540–8.
208. Yang Y, et al. Matrix metalloproteinase-mediated disruption of tight junction proteins in cerebral vessels is reversed by synthetic matrix metalloproteinase inhibitor in focal ischemia in rat. J Cereb Blood Flow Metab. 2007;27(4):697–709.

209. Liu X, et al. Effects of blockade of ionotropic glutamate receptors on blood-brain barrier disruption in focal cerebral ischemia. Neurol Sci. 2010;31(6):699–703.
210. Andras IE, et al. The NMDA and AMPA/KA receptors are involved in glutamate-induced alterations of occludin expression and phosphorylation in brain endothelial cells. J Cereb Blood Flow Metab. 2007;27(8):1431–43.
211. Kim JE, Ryu HJ, Kang TC. Status epilepticus induces vasogenic edema via tumor necrosis factor-alpha/ endothelin-1-mediated two different pathways. PLoS One. 2013;8(9):e74458.
212. Kim JY, et al. ETB receptor-mediated MMP-9 activation induces vasogenic edema via ZO-1 protein degradation following status epilepticus. Neuroscience. 2015;304:355–67.
213. Min H, et al. TLR2-induced astrocyte MMP9 activation compromises the blood brain barrier and exacerbates intracerebral hemorrhage in animal models. Mol Brain. 2015;8:23.
214. Zhang S, et al. Autophagy- and MMP-2/9-mediated Reduction and Redistribution of ZO-1 Contribute to Hyperglycemia-increased Blood-Brain Barrier Permeability During Early Reperfusion in Stroke. Neuroscience. 2018;377:126–37.
215. Gu Y, et al. Caveolin-1 regulates nitric oxide-mediated matrix metalloproteinases activity and blood-brain barrier permeability in focal cerebral ischemia and reperfusion injury. J Neurochem. 2012;120(1):147–56.
216. Jiang Z, et al. Role of nitric oxide synthases in early blood-brain barrier disruption following transient focal cerebral ischemia. PLoS One. 2014;9(3):e93134.
217. Chen H, et al. Baicalin Attenuates Blood-Brain Barrier Disruption and Hemorrhagic Transformation and Improves Neurological Outcome in Ischemic Stroke Rats with Delayed t-PA Treatment: Involvement of ONOO(-)-MMP-9 Pathway. Transl Stroke Res. 2018;9(5):515–29.
218. Sang H, et al. Early Increased Bradykinin 1 Receptor Contributes to Hemorrhagic Transformation After Ischemic Stroke in Type 1 Diabetic Rats. Transl Stroke Res. 2017;8(6):597–611.
219. Shen YH, Wang XL, Wilcken DE. Nitric oxide induces and inhibits apoptosis through different pathways. FEBS Lett. 1998;433(1-2):125–31.
220. Vazana U, et al. Glutamate-Mediated Blood-Brain Barrier Opening: Implications for Neuroprotection and Drug Delivery. J Neurosci. 2016;36(29):7727–39.
221. Shohami E, et al. Cytokine production in the brain following closed head injury: dexanabinol (HU-211) is a novel TNF-alpha inhibitor and an effective neuroprotectant. J Neuroimmunol. 1997;72(2):169–77.
222. Prager B, Spampinato SF, Ransohoff RM. Sphingosine 1-phosphate signaling at the blood-brain barrier. Trends Mol Med. 2015;21(6):354–63.
223. Zuo S, et al. Artesunate Protected Blood-Brain Barrier via Sphingosine 1 Phosphate Receptor 1/Phosphatidylinositol 3 Kinase Pathway After Subarachnoid Hemorrhage in Rats. Mol Neurobiol. 2017;54(2):1213–28.
224. Sun N, et al. Critical Role of the Sphingolipid Pathway in Stroke: a Review of Current Utility and Potential Therapeutic Targets. Transl Stroke Res. 2016;7(5):420–38.
225. Hasegawa Y, et al. Role of the sphingosine metabolism pathway on neurons against experimental cerebral ischemia in rats. Transl Stroke Res. 2013;4(5):524–32.
226. Schuhmann MK, et al. Fingolimod (FTY720-P) Does Not Stabilize the Blood-Brain Barrier under Inflammatory Conditions in an in Vitro Model. Int J Mol Sci. 2015;16(12):29454–66.
227. Choo AM, et al. Antagonism of purinergic signalling improves recovery from traumatic brain injury. Brain. 2013;136(Pt 1):65–80.
228. Ikonomidou C, Turski L. Why did NMDA receptor antagonists fail clinical trials for stroke and traumatic brain injury? Lancet Neurol. 2002;1(6):383–6.
229. Barreto G, et al. Selective estrogen receptor modulators decrease reactive astrogliosis in the injured brain: effects of aging and prolonged depletion of ovarian hormones. Endocrinology. 2009;150(11):5010–5.
230. Katz PS, et al. Endocannabinoid degradation inhibition improves neurobehavioral function, blood-brain barrier integrity, and neuroinflammation following mild traumatic brain injury. J Neurotrauma. 2015;32(5):297–306.
231. Morris GF, et al. Failure of the competitive N-methyl-D-aspartate antagonist Selfotel (CGS 19755) in the treatment of severe head injury: results of two phase III clinical trials.The Selfotel Investigators. J Neurosurg. 1999;91(5):737–43.
232. Rothstein JD, et al. Beta-lactam antibiotics offer neuroprotection by increasing glutamate transporter expression. Nature. 2005;433(7021):73–7.
233. Fontana AC, et al. Enhancing glutamate transport: mechanism of action of Parawixin1, a neuroprotective compound from Parawixia bistriata spider venom. Mol Pharmacol. 2007;72(5):1228–37.
234. Barron KD, et al. Ultrastructural features of a brain injury model in cat. I. Vascular and neuroglial changes and the prevention of astroglial swelling by a fluorenyl (aryloxy) alkanoic acid derivative (L-644,711). Acta Neuropathol. 1988;75(3):295–307.
235. Kimelberg HK, et al. Brain anti-cytoxic edema agents. Prog Clin Biol Res. 1990;361:363–85.
236. Bhalala OG, et al. MicroRNA-21 regulates astrocytic response following spinal cord injury. J Neurosci. 2012;32(50):17935–47.
237. Pan YB, Sun ZL, Feng DF. The Role of MicroRNA in Traumatic Brain Injury. Neuroscience. 2017;367:189–99.
238. Hong P, Jiang M, Li H. Functional requirement of dicer1 and miR-17-5p in reactive astrocyte proliferation after spinal cord injury in the mouse. Glia. 2014;62(12):2044–60.
239. Yang X, et al. Hypertonic saline maintains coagulofibrinolytic homeostasis following moderatetosevere traumatic brain injury by regulating monocyte phenotype via expression of lncRNAs. Mol Med Rep. 2019;19(2):1083–91.

## Publisher's Note

communications biology

ARTICLE

https://doi.org/10.1038/s42003-021-02808-5 OPEN

# Traumatic brain injury to primary visual cortex produces long-lasting circuit dysfunction

Jan C. Frankowski[1,3], Andrzej T. Foik[2,3], Alexa Tierno[1], Jiana R. Machhor[1], David C. Lyon[1] & Robert F. Hunt[1✉]

Primary sensory areas of the mammalian neocortex have a remarkable degree of plasticity, allowing neural circuits to adapt to dynamic environments. However, little is known about the effects of traumatic brain injury on visual circuit function. Here we used anatomy and in vivo electrophysiological recordings in adult mice to quantify neuron responses to visual stimuli two weeks and three months after mild controlled cortical impact injury to primary visual cortex (V1). We found that, although V1 remained largely intact in brain-injured mice, there was ~35% reduction in the number of neurons that affected inhibitory cells more broadly than excitatory neurons. V1 neurons showed dramatically reduced activity, impaired responses to visual stimuli and weaker size selectivity and orientation tuning in vivo. Our results show a single, mild contusion injury produces profound and long-lasting impairments in the way V1 neurons encode visual input. These findings provide initial insight into cortical circuit dysfunction following central visual system neurotrauma.



[1] Department of Anatomy & Neurobiology, University of California, Irvine, CA 92697, USA. [2] Ophthalmic Biology Group, International Centre for Translational Eye Research, Institute of Physical Chemistry, Polish Academy of Sciences, Warsaw, Poland. [3] These authors contributed equally: Jan C. Frankowski, Andrzej T. Foik. ✉email: robert.hunt@uci.edu

Posterior impact injuries to the occipital cortex are extremely common in human. Traumatic brain injury (TBI) can lead to long-lasting visual impairments, such as visual acuity and field loss, binocular dysfunction, and spatial perceptual deficits[1–3], and as many as 75% of military Service members live with permanent visual dysfunction or cortical blindness resulting from a TBI[3]. Restrictive lesions applied to the visual cortex have been shown to trigger cortical plasticity and functional disturbances[4–6]. However, TBI involves mechanical brain damage and a wide range of cortical network abnormalities including cell death, inflammation, and synaptic circuit remodeling[7]. There is essentially nothing known about how visual circuit function is affected by TBI.

Following TBI in human, histological studies have documented a reduction in the number of neurons in the hippocampus[8] and neocortex[9]. In nonhuman animal models, TBI produces region- and subtype-specific reductions of neurons in various brain areas[10–21], dramatic circuit rewiring ([22–31]), and a loss of inhibition that does not recover with time[20,21,27,32–39]. However, nearly all of the information about neocortical responses to TBI comes from studies evaluating somatosensory, motor, or frontal cortex. Each of these areas receives numerous intra- and inter-hemispheric inputs from throughout the topographic map[40–42], whereas callosal connectivity of the visual cortex is limited to the vertical meridian representation along the V1 border[43,44]. Therefore, a deeper understanding of functional disturbances in the brain-injured visual cortex is important, because it has the potential to provide a rational basis for the development of circuit-level therapies for visual cortex injury.

To produce central visual system TBI in adult mice, we applied a focal controlled cortical impact (CCI) injury to the primary visual cortex (V1). We show that although mild contusion injury did not produce a sizable lesion, there was a subtype- and layer-specific loss of neurons in the brain-injured V1. Then, using in vivo electrophysiological recordings of visually evoked responses, we found that mild contusion injury chronically impairs the response of V1 neurons to a variety of visual stimuli. These findings suggest there are profound long-lasting impairments in visual circuit function that result from a single, mild contusive injury to the central visual system. As an initial characterization of central visual system neurotrauma, our results also lay the foundation for future mechanistic investigations of altered cortical network activity and preclinical studies to restore circuit function in the traumatically injured visual cortex.

## Results

**Occipital CCI produces a mild contusion in V1**. To evaluate the effect of a single, mild contusion injury to the central visual system, we delivered mild CCI injury centered over the rostral end of V1 in young-adult mice at P60 (Supplementary Fig. 1). We selected CCI as a model, because the injury is highly reproducible from animal to animal, reliably recapitulates structural and functional deficits of TBI and focal contusion injuries are among the most common posterior impact injuries observed in human[1–3]. In all CCI-injured animals ($N = 7$ mice), the lesion consisted of mild tissue compression that was restricted to superficial layers of the cortex at the injury epicenter (Supplementary Fig. 2).

To define the lesion location, we examined glial responses in V1 following mild CCI injury (Fig. 1a). To do this, we performed an immunostaining analysis at 0.5 months and 3 months after injury for glial fibrillary acidic protein (GFAP), a marker of astrocytes, and ionizing calcium-binding adaptor molecule 1 (IBA1), a marker of activated microglia. In brain-injured animals, the impact site could be clearly identified by a dense pattern of GFAP and IBA1 staining in V1 ipsilateral to the injury. A significant increase in GFAP expression was found in V1 surrounding the injury at 0.5 months, as compared to uninjured controls, sham animals that received a craniotomy but no injury and contralateral tissue sections (Supplementary Fig. 3), and it remained significantly elevated 3 months post-CCI (Fig. 1b). IBA1 immunostaining was also significantly increased ipsilateral to the injury, but only at 0.5 months after injury (Fig. 1c). Uninjured and sham controls did not have an identifiable cortical lesion in any animal.

At 0.5 months post-CCI, a time point when lesion volume is considered to be largely stable[15,45], there was no significant difference in cortical volume between uninjured control and brain-injured littermates (TBI: 96 ± 3%, sham: 102 ± 2%, compared to 99 ± 1% in uninjured control; $P = 0.15$; one-way ANOVA; $N = 4$–6 mice per group; Fig. 1d). However, when we evaluated the thickness of cortical tissue remaining in the contused portion of the visual cortex, we found a 14% decrease in cortical thickness in brain-injured animals at the injury epicenter, as compared to controls (uninjured: 883 ± 25 µm, sham: 966 ± 58 µm, TBI: 760 ± 32 µm, $P = 0.048$; two-way rmANOVA; $N = 3$–4 mice per group; Fig. 1e). This difference was only observed at the injury epicenter (0 µm); no difference in cortical thickness was observed in tissue sections 300 and 600 µm caudal to the epicenter. We found a similar degree of mild tissue loss at 90d post-CCI (Fig. 1f, g). Thus, CCI produced a mild focal injury with minimal structural damage to V1.

**Neuron loss after V1 injury**. Next, we quantified neuron density in V1 using GAD67-GFP reporter mice that label nearly all GABAergic neurons[46]. Sections were immunostained for GFP to identify inhibitory interneurons and NEUN to identify putative excitatory neurons (i.e., NEUN-positive/GAD67-GFP-negative) (Fig. 2). At 0.5 months after TBI, we found a ~35% reduction in NEUN + /GAD67-GFP- cell density in V1 ipsilateral to the injury (Fig. 2a, b; Supplementary Data 1). The reduction in excitatory neurons was most profound at the injury epicenter (45% reduction after TBI) and rapidly decreased with distance away from the impact site (Fig. 2c). We also observed ~35% decrease in the overall density of GAD67-GFP+cells in V1 ipsilateral to the injury ($P = 1.07E-06$, TBI versus uninjured control, two-way ANOVA; Fig. 2d; Supplementary Data 1). However, unlike excitatory neurons, GFP + interneuron density was reduced by ~35% at each distance from the impact site (Fig. 2e). No change in cell density was observed in the contralateral hemisphere. These findings suggest mild contusion to the visual cortex produces substantial neuron loss in V1, and the loss of inhibitory neurons is more widespread than excitatory neurons.

To determine if post-traumatic neuron loss was layer-specific, we quantified neuron density in cortical layers I, II/III, IV, and V/VI of brain-injured and uninjured control littermates (Fig. 3; Supplementary Data 2). For this analysis, we fitted a random intercept mixed model for each cell type to account for the distance from the injury, layer, and treatment condition. We found that excitatory cell loss extended throughout the cortical column ipsilateral to the injury, with significant reductions in NEUN+/ GAD67-GFP- cells in cortical layers II/III, IV, and V/VI (Fig. 3b, f, j); no significant differences were found in layer I where excitatory neurons are rarely found. In contrast, GFP + inhibitory neuron density was most profoundly affected in superficial layers, with significant reductions in GAD67-GFP + neurons in layers I-IV (Fig. 3c, g, k). However, no change in inhibitory neuron density was observed in layers V/VI. Despite these cell-type specific changes in cell density, the ratio of excitatory to inhibitory neurons did not change in any layer of V1 (Fig. 3d, h, l). We conclude that there are subtype- and layer-

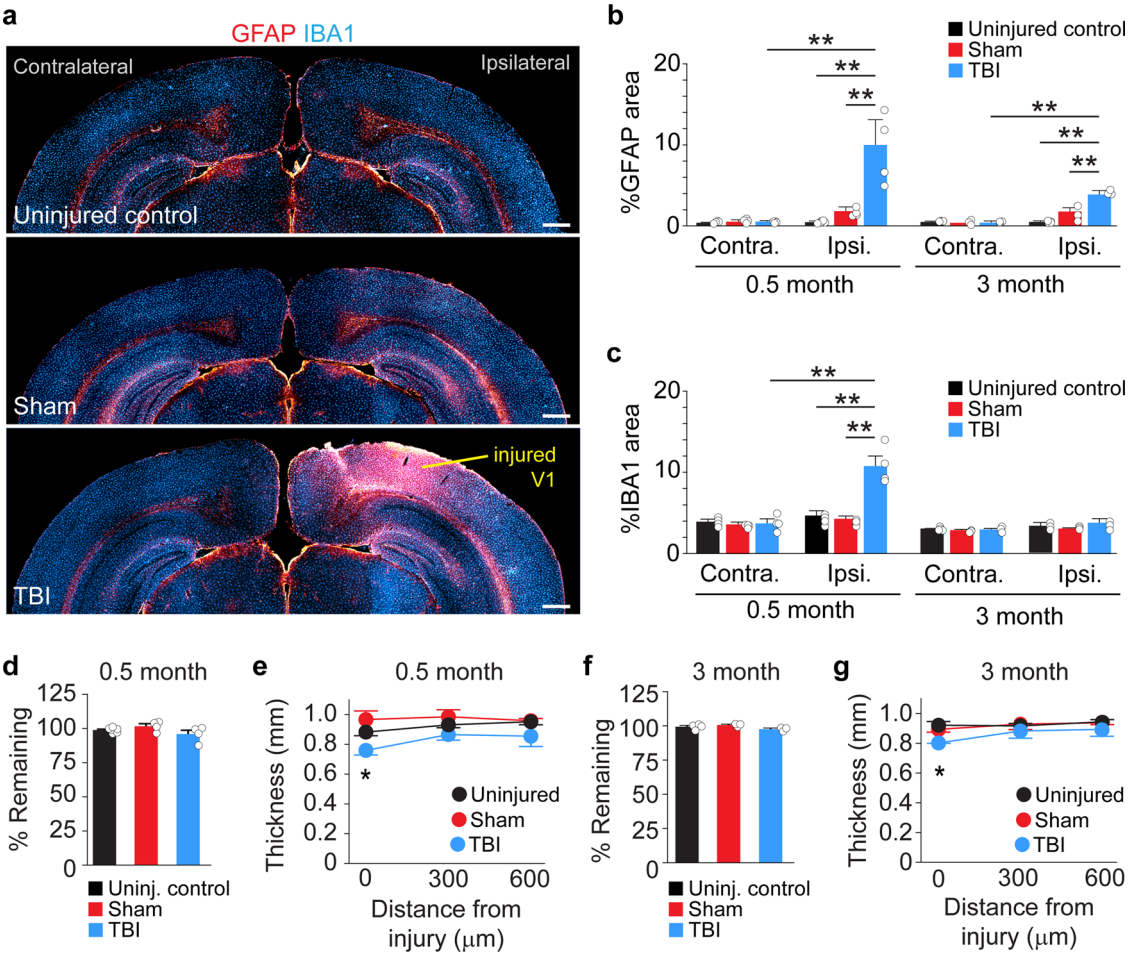


**Fig. 1 Visual cortex TBI produces a mild cortical lesion. a** Coronal sections of GFAP (red) and IBA1 (blue) labeling in a control animal and 0.5 months after sham or CCI injury. **b** Quantification of GFAP expression in V1 at 0.5 and 3 months postinjury. $^{**}P = 2.9E\text{-}07$, ipsilateral control versus ipsilateral TBI; $^{**}P = 1.3E\text{-}05$, ipsilateral sham versus ipsilateral TBI; $^{**}P = 1.3E\text{-}06$, ipsilateral TBI versus contralateral TBI at 0.5 months; $^{**}P = 1.3E\text{-}06$, ipsilateral control versus ipsilateral TBI; $^{**}P = 8.7E\text{-}05$, ipsilateral sham versus ipsilateral TBI; $^{**}P = 6.0E\text{-}06$, ipsilateral TBI versus contralateral TBI at 3 months two-way ANOVA with Tukey's post hoc test, $N = 3$–6 mice per group. **c** Quantification of IBA1 expression in V1 at 0.5 and 3 months postinjury. $^{**}P = 2.4E\text{-}08$, ipsilateral control versus ipsilateral TBI, $^{**}P = 2.9E\text{-}08$, ipsilateral sham versus ipsilateral TBI, $^{**}P = 2.3E\text{-}08$, ipsilateral TBI versus contralateral TBI at 0.5 months; two-way ANOVA with Tukey's post hoc test, $N = 3$–6 mice per group. **d** Quantification of cortical tissue volume in control, sham, and CCI-injured mice 0.5 months post-CCI. **e** Average thickness of cortex with distance from the injury 0.5 months post-CCI. $^{*}P = 0.048$, Control versus TBI, two-way repeated-measures ANOVA with Tukey's post hoc test, $N = 4$–6 mice per group. **f** Quantification of cortical tissue volume in control, sham, and CCI-injured mice 3 months post-CCI. **g** Average cortex thickness with distance from the injury 3 months post-CCI. $^{*}P = 0.023$, Uninjured versus TBI, two-way repeated-measures ANOVA with Tukey's post hoc test, $N = 3$–4 mice per group. Scale bars, 500 μm; error bars, SEM.

specific differences in the degree and extent of neuron loss after visual cortex injury.

We next asked whether the loss of neurons at the injury site persisted long term. At 3 months after injury, NEUN+/GAD67-GFP- cell density remained reduced by 32% ipsilateral to the injury (Fig. 4a, b; Supplementary Data 3). GAD67-GFP+ interneuron density was also reduced 3 months post-CCI by 32% (Fig. 4a, c; Supplementary Data 3). These data reproduce our observations at 0.5 months and are consistent with a chronic loss of excitatory and inhibitory neurons after mild contusion injury to the visual cortex.

**Early and long-term disruption of visually evoked responses after TBI**. To evaluate the in vivo functional state of the visual cortex following TBI, we measured visually evoked potentials (VEPs) and single-unit responses to a range of stimuli across a wide extent of injured V1 at 0.5 and 3 months after injury (Figs. 5–7). First, we recorded VEPs in response to brief flashes of light. These local field potential responses represent the electrical response of a population of V1 neurons to light stimuli. Representative examples of flash-evoked responses are shown in individual animals (Fig. 5a), along with group averages (Fig. 5b). Compared to uninjured controls, evoked VEP amplitudes were significantly reduced by more than 80% in brain-injured mice (control: 277 ± 39 μV, 0.5 months after TBI: 24 ± 4 μV, 3 months after TBI: 53 ± 7 μV; $P = 9.95E\text{-}09$, Kruskal–Wallis H test; Fig. 5c), and response latencies rose to more than 60% longer (control: 88 ± 6 ms, 0.5 months after TBI: 146 ± 17 ms, 3 months after TBI: 100 ± 6 ms; $P = 0.02$, Kruskal–Wallis H test; Fig. 5d). Of note, response latencies between light flash and maximal response were longer only at 0.5 months after injury and were similar to controls at 3 months. At both time points, we found that wave profiles in the injured brain lacked a negative wave component normally present in deeper cortical layers (Supplementary Fig. 4).

Single-neuron responses to the same flashes of light were also measured (Fig. 6a; Supplementary Fig. 5). Average response profiles showed moderate to negligible activity at both 0.5 and

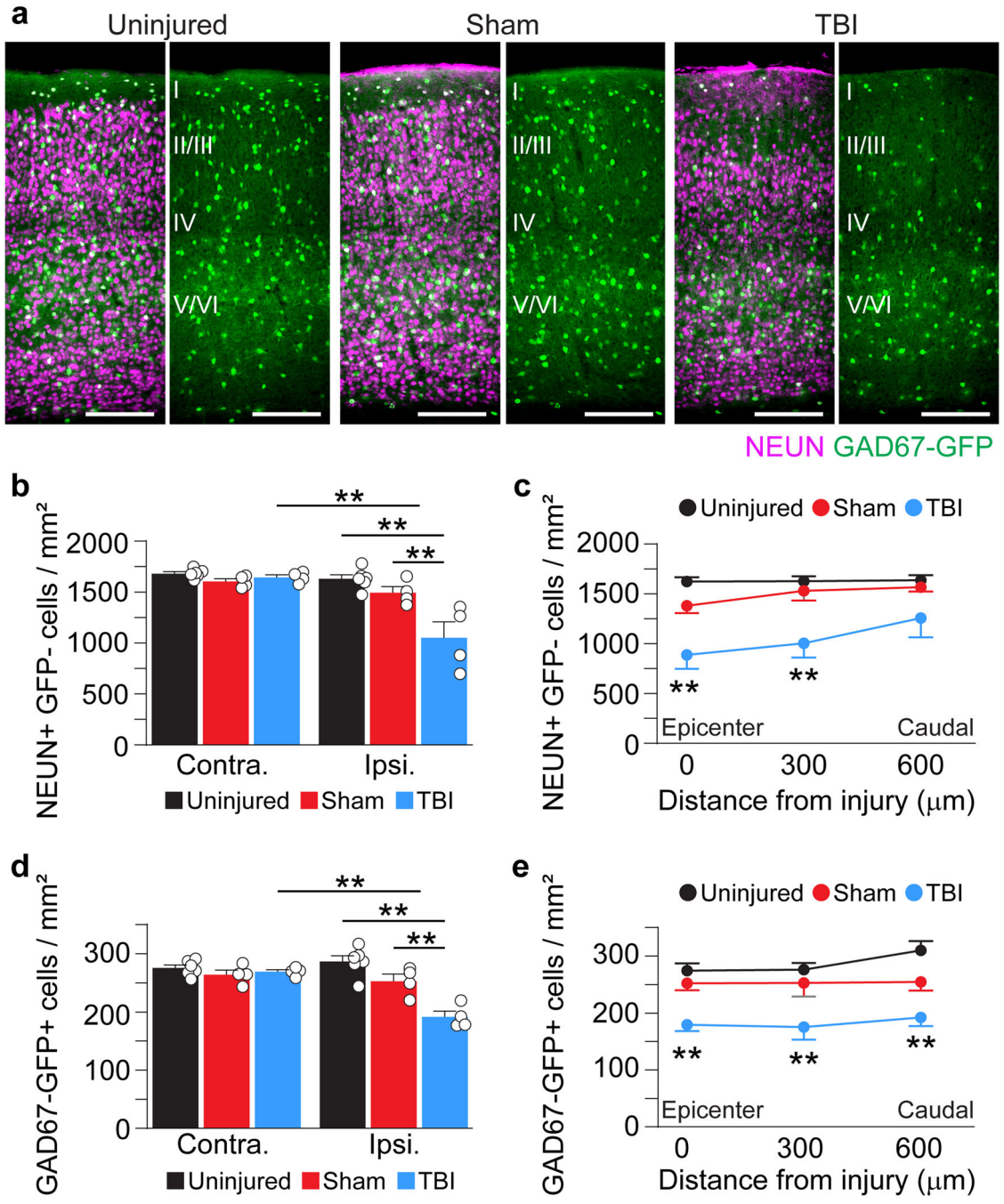


**Fig. 2 Neuron loss in V1 0.5 months after TBI. a** Coronal images of control, sham, and CCI-injured V1 labeled for NEUN (magenta) and GAD67-GFP (green). **b** Quantification of NEUN+/GFP- cell density in uninjured control, sham, and brain-injured mice 0.5 months after CCI. $^{**}P = 1.79E-05$, ipsilateral control versus ipsilateral TBI, $^{**}P = 1.77E-03$, ipsilateral sham versus ipsilateral TBI, $^{**}P = 4.56E-05$, ipsilateral TBI versus contralateral TBI; two-way ANOVA with Tukey's post hoc test, $N = 4$–6 mice per group. **c** NEUN+/GFP- cell density at 0–600 μm from the injury epicenter. $^{**}P = 7.86E-05$, control versus TBI (0 μm), $^{**}P = 1.01E-03$, control versus TBI (300 μm); two-way repeated-measures ANOVA with Tukey's post hoc test; N = 4–6 mice per group. **d** Quantification of GAD67-GFP+ cell density in uninjured control, sham, and brain-injured mice 0.5 months after CCI. $^{**}P = 1.07E-06$, ipsilateral control versus ipsilateral TBI, $^{**}P = 1.58E-03$, ipsilateral sham versus ipsilateral TBI, $^{**}P = 9.25E-05$, ipsilateral TBI versus contralateral TBI, two-way ANOVA with Tukey's post hoc test, $n = 4$–6 per group. **e** GAD67-GFP+ cell density at 0–600 μm from the injury epicenter. $^{**}P = 3.53E-03$, control versus TBI (0 μm), $^{**}P = 1.66E-03$, control versus TBI (300 μm), $^{**}P = 1.74E-04$, control versus TBI (600 μm); two-way repeated-measures ANOVA with Tukey's post hoc test; $N = 4$–6 mice per group. Scale bars, 500 μm; error bars, SEM. See Supplementary Data 1 for statistical analyses.

3 months, respectively, compared to the high average spike rate in control mice (Fig. 6b). After TBI, less than half of the isolated neurons were visually responsive (32% at 0.5 months; 49% at 3 months), compared to 90% of control V1 cells (Chi-square = 56.3, df = 2, $P = 5.94E-13$; Fig. 6c). Similarly, average peak firing rates were significantly lower in brain-injured V1 (control: 42.7 ± 5.7 spikes/s, compared to 5.2 ± 0.4 spikes/s 0.5 months after TBI and 9.9 ± 1.7 spikes/s 3 months after TBI; $P = 3.6E-20$, Kruskal–Wallis H test; Fig. 6d). Prior to stimulation, background activity was highest for the uninjured control group (7.6 ± 2.8 spikes/s) and included one outlier with a baseline firing rate over 150 spikes/second; whereas background activity for cells

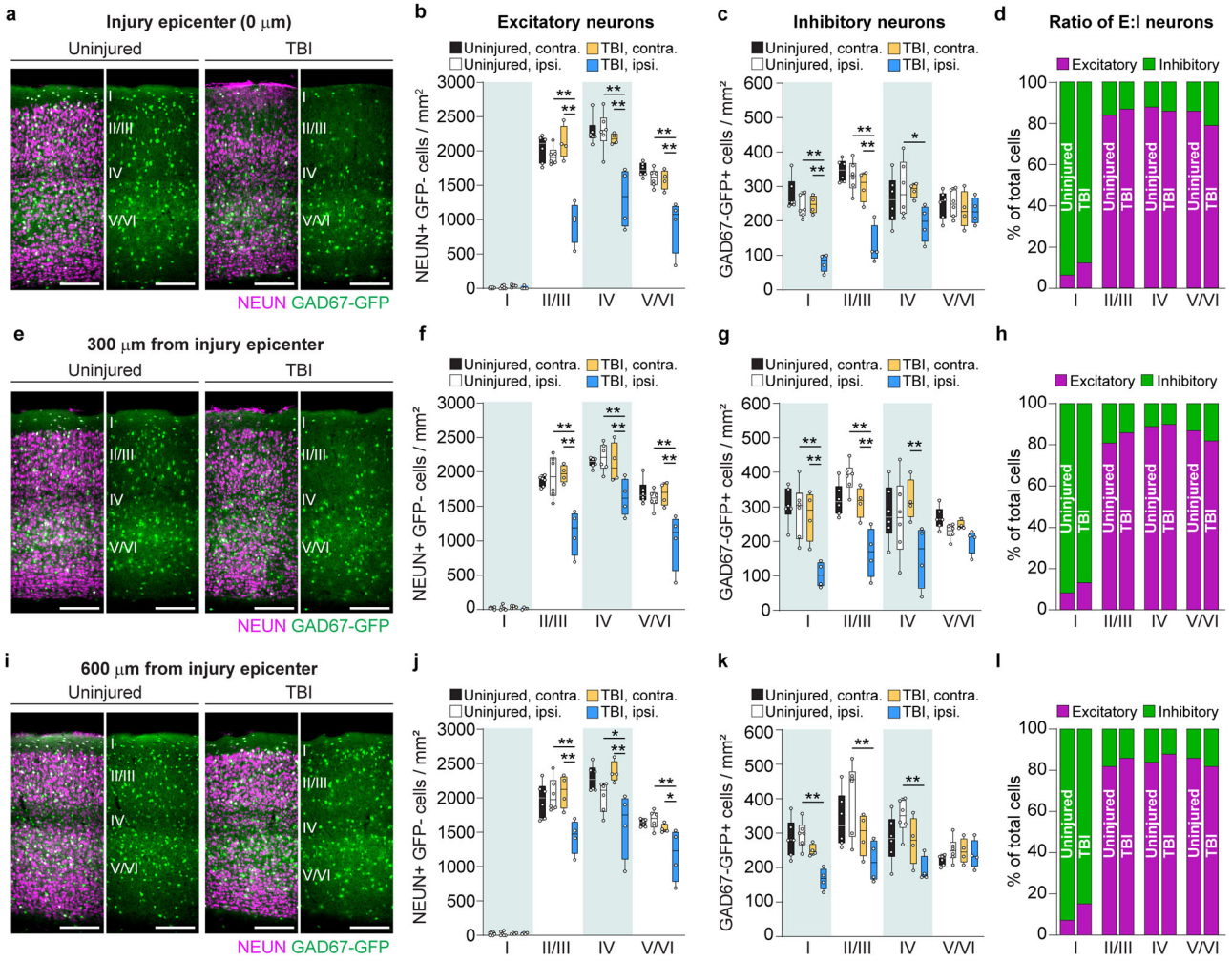


**Fig. 3 V1 injury produces subtype- and layer-specific loss of neurons. a, e, i** Coronal images of control and CCI-injured V1 labeled for NEUN (magenta) and GAD67-GFP (green) at 0 (**a**), 300 (**e**), and 600 μm (**i**) from the injury. **b, f, j** Quantification of NEUN+/GFP- cell density in layers I, II/III, IV, and V/VI. $N = 4$–6 mice per group. **c, g, k** Quantification of GAD67-GFP cell density in layers I, II/III, IV, and V/VI. $N = 4$–6 mice per group. **d, h, l** Analysis of the proportion of excitatory to inhibitory neuron density at the injury site (Chi-square = 2.17, df = 3, P = 0.54; **d**), 300 μm (Chi-square = 1.32, df = 3, $P = 0.72$; **h**), or 600 μm caudal to the epicenter (Chi-square = 2.68, df = 3, $P = 0.44$; **l**). Scale bars, 500 μm. Box and whisker plots show median, 25th and 75th percentiles, and the whisker bars represent maximum and minimum values. $^{**}P < 0.01$, $^{*}P < 0.05$; random intercept mixed model with Tukey-Kramer post hoc test. See Supplementary Data 2 for statistical analyses.

0.5 months (2.7 ± 2.5 spikes/s) and 3 months (1.6 ± 2.2 spikes/s) after TBI was significantly lower than in uninjured controls ($P = 3.59$E-20, Kruskal–Wallis H test; Fig. 6e). Together, these findings suggest there is damage to the local V1 neuron population that lasts for several months after TBI.

To evaluate the functional profile of injured V1 in more detail, we next measured single-neuron responses to a range of fundamental visual stimuli, including orientation, size, spatial frequency, and temporal frequency in vivo (Fig. 7; Supplementary Fig. 6). For these analyses, only visually responsive cells were included (see criteria in Methods). Brain-injured mice showed weaker tuning and selectivity to all four types of stimulus parameters compared to uninjured controls (Fig. 7) and had a substantial percentage of cells that were nonresponsive to one or more stimulus conditions (Supplementary Fig. 6). For the cell population, these differences were significant for orientation (Fig. 7b), size (Fig. 7d), and spatial frequency (Fig. 7f), but not temporal frequency (Fig. 7h). The difference was quite striking for orientation and size tuning, both of which are strongly mediated through local cortical inhibition[47–49]. For orientation, the tuning width, measured as the half-width at half-height (HWHH) of the preferred direction (90° in the example cells) was nearly twice as sharp in the control example (23.7°) compared to 0.5 months after injury (45.0°), and more than 50% broader 3 months after injury (36.3°; Fig. 7a). These differences were also seen for the population (control: 30.9° ± 1.9°, 0.5 months after TBI: 43.1° ± 4.0°; 3 months after TBI: 42.6° ± 2.8°; $P = 0.0013$, Kruskal–Wallis H test; Fig. 7b). Broader tuning after TBI is consistent with orientation tuning mediated more through intact thalamocortical feed-forward mechanisms and impairments in cortical inhibition[48,49]. Similarly, the larger size preference in TBI compared to control neuron examples (73° and 60° at 0.5 and 3 months post-TBI vs. 35° in uninjured controls; Fig. 7c) and populations (control: 41.5 ± 2.1°, compared to 79.3 ± 3.4° at 0.5 months and 52.1 ± 3.1° at 3 months postinjury; $P = 1.16$E-13, Kruskal–Wallis H test; Fig. 7d) is also consistent with a loss of cortical inhibition[47]. This is because stimulus size is normally kept small through a process of lateral suppression mediated by long-range intrinsic excitatory V1 neurons synapsing onto local inhibitory neurons[47,50]. We note that the 3 months postinjury group had a statistically smaller preferred size than the 0.5-month group ($P = 2.04$E-05, Kruskal–Wallis H test; Fig. 7d). This could be a sign of recovery, however, a larger

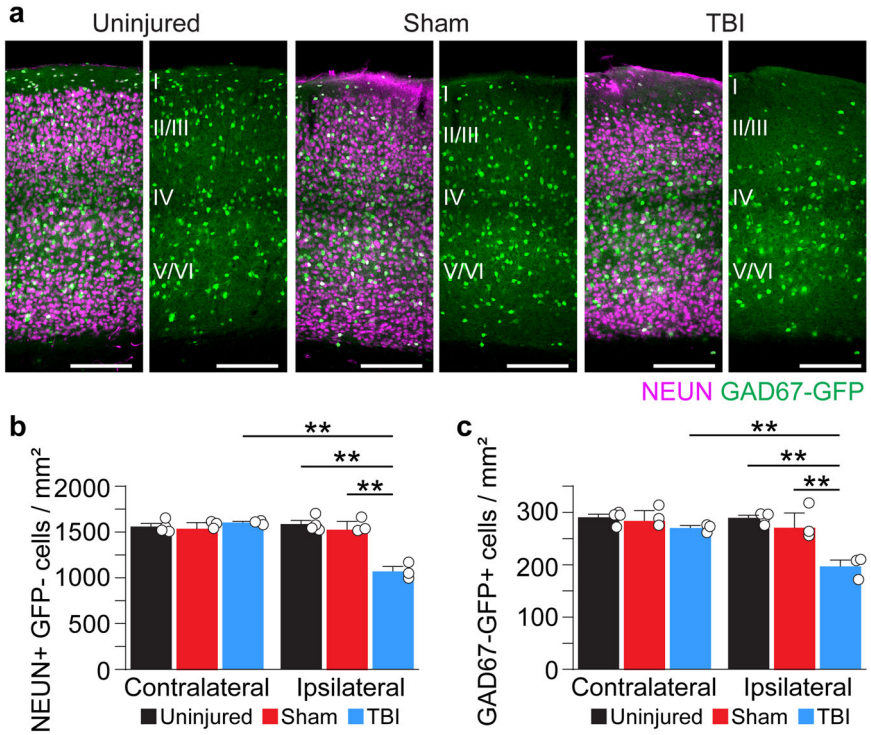


**Fig. 4 Chronic neuron loss in V1 after TBI. a** Coronal images of control, sham and CCI-injured V1 labeled for NEUN (magenta) and GAD67-GFP (green) 3 months after TBI. **b** Quantification of NEUN+/GFP- cell density in control, sham, and brain-injured mice 3 months after CCI. $^{**}P = 1.33E-06$, ipsilateral control versus ipsilateral TBI, $^{**}P = 4.23E-06$, ipsilateral sham versus ipsilateral TBI, $^{**}P = 1.99E-06$, ipsilateral TBI versus contralateral TBI; two-way ANOVA with Tukey's post hoc test, $N = 3$–4 mice per group. **c** Quantification of GAD67-GFP+ cell density in control, sham, and brain-injured mice 90 d after CCI. $^{**}P = 1.60E-04$, ipsilateral control versus ipsilateral TBI, $^{**}P = 1.02E-03$, ipsilateral sham versus ipsilateral TBI, $^{**}P = 2.96E-03$, ipsilateral TBI versus contralateral TBI; two-way ANOVA with Tukey's post hoc test, $N = 3$–4 mice per group. Scale bar, 500 μm; error bars, SEM. See Supplementary Data 3 for statistical analyses.

percentage of 3-month animal cells did not even respond to the size stimuli (Supplementary Fig. 6c).

## Discussion

Patients with TBI can show long-lasting deficits in visual system function, such as visual acuity and field loss, binocular dysfunction, and spatial perceptual deficits[1]. Here, we delivered a mild focal contusion injury directly to V1 to model occipital contusion injuries, which occur almost exclusively after a direct blow to the back of the head[2,51]. Although V1 was relatively well-preserved, compared to traditional approaches that produce substantial tissue damage[13,16,18], we found neuron loss at the injury site that extended into deep cortical layers. Interestingly, the degree of neuron loss was different in excitatory versus inhibitory systems. Excitatory neurons were lost throughout all layers of brain-injured V1, but the greatest degree of cell loss was contained at the injury site. In contrast, inhibitory neurons were uniformly lost by ~35% across all sections examined, but cell loss was restricted to superficial layers I-IV of V1. These observations are different from TBI to the hippocampus, where hilar interneurons are widely considered to be the most vulnerable to injury despite being the deepest layer from the site of impact[13,17,20]. The cellular mechanism for these cell-type-specific responses to injury is unknown. In vivo recordings revealed a massive reduction in VEP amplitudes, consistent with damage to the local V1 neuron population, and dramatically altered single-neuron tuning to visual stimuli, including changes in orientation and size, which have been shown to be modulated by cortical interneurons[52]. These findings are consistent with human studies showing visual field dysfunction can occur in individuals with no measurable lesion[53].

Structural and functional damage following V1 injury appear to be permanent. This is different from damage to other sensory areas. For example, in the whisker barrel cortex, previous in vivo electrophysiology studies have shown there is an initial hypoactivity of neuronal responses 24 h after TBI that recovers within 12 weeks after injury, despite persistent structural changes[28,29]. In the current study, we evaluated the effect of V1 TBI on all GABAergic neurons, but specific subtypes may be more or less vulnerable to injury, as has been seen in other brain areas[13]. Further studies evaluating synaptic plasticity and neuronal connectivity in brain-injured V1 will ultimately be required to determine potential candidate mechanisms underlying the permanent disruption of V1 neuron tuning after TBI.

Individuals with TBI can develop visual impairments independent from other injury-induced motor or cognitive deficits[54–57]. Increases in light intensity evoke inhibitory synaptic activity to prevent changes in luminance intensity from disrupting cortical circuit function[58] and inability to modulate cortical gain has been proposed as a potential mechanism of injury-related photosensitivity[54,57]. Here we show that basic visual processes in V1 are altered to reflect a loss of cortically mediated inhibition. We found significantly broader orientation tuning widths consistent with reduced local inhibitory neuron activity[52]. Instead, in brain-injured animals, V1 orientation tuning resembles the broader widths mediated through feed-forward mechanisms from the thalamus[48,49], which are likely more intact. Similarly, increased spatial summation indicated by larger stimulus size preference in TBI is consistent with the loss of local inhibitory neurons mediating surround suppression[59] and likely reflects preservation of feed-forward mediated mechanisms[47].

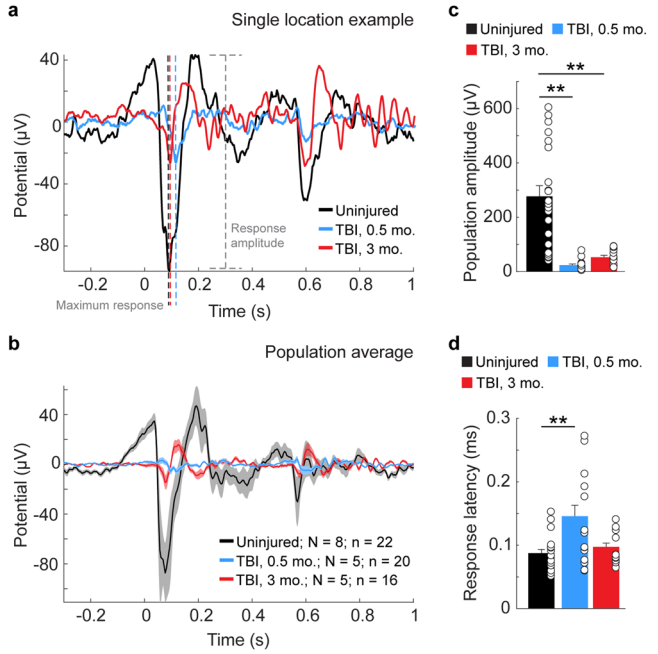


**Fig. 5 TBI disrupts V1 responses to visual stimuli. a** Representative example of VEPs in layer 5 of an uninjured control animal (black trace) and animals 0.5 months (blue trace) and 3 months after CCI (red trace). The maximum response for each trace is indicated by dotted black, blue and red lines. Response amplitude for the control condition is indicated by the dotted gray line. **b** Average evoked potentials from recording sites in uninjured control (black) and 0.5 months (blue) and 3 months (red) after TBI. *N* = number of animals; *n* = number of recording locations. Shading indicates S.E.M. **c** Quantification of average evoked amplitude. $^{**}P = 6.23E\text{-}09$, control versus 0.5 months after TBI; $^{**}P = 1.88E\text{-}03$, control versus 3 months after TBI; Kruskal–Wallis H with Dunn's post hoc. **d** Quantification of average response latency. $^{**}P = 0.02$, control versus 0.5 months after TBI, Kruskal–Wallis H with Dunn's post hoc. Individual data points represent the value for each of the recording locations. N, animals; n, recording location; error bars, SEM.

In V1, GABAergic inhibition is essential for a wide range of basic V1 functions, such as tuning a neuron's preference for stimulus contrast, size, and orientation[52,60,61], as well as higher-order processing, such as contrast perception[62]. During development, cortical inhibition modulates critical periods, a transient time of enhanced sensitivity to sensory experience. This has been most extensively studied in juvenile V1, in which obstructing vision through one eye results in cortical blindness to this eye, even after normal vision is restored[63]. Cortical inhibition is required for opening the developmental critical period in the visual cortex[64] and inactivating interneurons can prolong the critical period[65] or impair cortical plasticity[66]. Even in adulthood, after binocular vision is well established, manipulating inhibition through pharmacology[61,67] or interneuron transplantation[68,69] can have dramatic effects on cortical plasticity in response to monocular visual deprivation. Given our recent success using interneuron transplantation to treat post-traumatic memory problems and epilepsy[70,71], future studies evaluating the effect of manipulating excitatory versus inhibitory activity in brain-injured V1 may reveal new avenues for circuit-based therapy.

## Methods

**Animals**. Mice were maintained in standard housing conditions on a 12 h light/dark cycle with food and water provided *ad libitum*. All protocols and procedures were approved by and followed the guidelines of the University Laboratory Animal Resources at the University of California, Irvine and adhered to National Institutes of Health Guidelines for the Care and Use of Laboratory Animals. For electrophysiology experiments, we used C57Bl/6 J mice (Jackson Laboratories, cat no. 000664), and for anatomy experiments, we used a hemizygous glutamic acid decarboxylase—enhanced green fluorescence protein (GAD67-GFP) knock-in line[46] maintained on a CD-1 background for > 10 generations.

**Experimental design**. Male and female mice were randomly allocated to experimental groups prior to TBI. Brain injury was performed at P60, and experiments were performed 0.5 or 3 months after TBI. Brain injuries were only considered to be successful if the lesion was found to be centered over the rostral end of V1. Three animals were excluded from the immunostaining analysis, because upon histological inspection the lesion was not found to be centered over the rostral end of V1. No additional animals were generated to replace these mice. All other brain-injured mice survived and remained otherwise healthy until the day of experimentation.

**Controlled cortical impact (CCI)**. Unilateral controlled cortical impact was performed as previously described[13,71], with modifications to the location and depth of injury. Mice were anesthetized with 2% isoflurane until unresponsive to toe-pinch, then placed into a stereotactic frame and maintained on 1% isoflurane. The fur overlying the skull was trimmed and the scalp was scrubbed with betadine before exposing the skull with a midline incision. The skull was rotated 20 degrees counterclockwise along the rostral-caudal axis and the rostral end of the skull was lowered 20 degrees relative to skull-flat. This orientation centered the impactor tip at the rostral end of V1. A ~4-5 mm craniotomy was centered 3 mm lateral to the midline and 3 mm rostral to the lambdoid suture in the right hemisphere. The skull cap was removed leaving the dura intact. A computer-controlled pneumatically driven impactor (TBI-0310, Precision Systems and Instrumentation) with a 3 mm beveled stainless-steel tip was used to deliver a 0.2 mm depth contusive injury perpendicular to the dura at 3.5 m/s velocity and 500 ms of impactor dwell time. The skull cap was not replaced, and the incision was closed with silk sutures. Animals undergoing surgical procedures received buprenorphine hydrochloride (Buprenex, 0.05 mg/kg, delivered i.p.) preoperatively and once daily for 3d. A postoperative health assessment was performed for 5d following surgical procedures.

**Immunostaining**. At 0.5 or 3 months after injury, mice were transcardially perfused with 4% paraformaldehyde (PFA) and free-floating vibratome sections (50 μm) were processed using standard immunostaining procedures[71]. Sections were stained with the following primary antibodies: GFP (1:1000; cat. no. GFP-1020, Aves Labs), NEUN (1:1000; cat. no. MAB377, Millipore), GFAP (1:500, cat. no. MAB3402, Millipore) and IBA1 (1:1000, cat. no. 019-19740, Fujifilm). Secondary antibodies were Alexa 488, 546, 594, and 647 (1:1000; cat. nos. A-11039, A-11005, A-11030 and A-21244, Fisher Scientific). Sections were then mounted on charged slides (Superfrost plus; Fisher Scientific) with Fluoromount-G containing DAPI (Southern Biotech). Images were obtained with a Leica DM6 epifluorescence microscope. Brightness and contrast were adjusted manually using Adobe Photoshop; z-stacks were generated using Leica software.

**Volumetric analysis**. Quantification of cortical lesion volume was performed by measuring the area of cortical tissue remaining in both hemispheres in eight DAPI-labeled coronal sections along ~2400 μm of the rostral-caudal axis spaced 300 μm apart as previously described[13,71]. Borders of the cortical plate were drawn between the dorsal aspect of the corpus callosum and the pial surface using ImageJ. Regions of the cortical subplate (e.g., amygdala) were excluded from analysis. The % of the ipsilateral cortex remaining for each animal was calculated using the following formula:

$$\%\,\text{Cortex Remaining} = \left(\frac{\sum i_n}{\sum c_n}\right) \times 100$$

where $i$ = the area of the ipsilateral cortex and $c$ = the area of the contralateral cortex and $n$ = the section number.

**Cortical thickness measurement**. Average cortical thickness was measured from a series of three DAPI-labeled x10 images of the entire cortical column centered at the injury epicenter and two 300 μm serial sections caudal to the epicenter. The area of tissue between the pial surface and the ventral aspect of layer V/VI was divided by the width of the frame (958.29 μm) to obtain an average cortical thickness value along the width of the frame. For uninjured controls, images were taken in corresponding brain sections at the most central portion of V1 as defined in the 2017 Allen Reference Atlas.

**Cell quantification**. Fluorescently labeled coronal brain sections (50 μm) were imaged using a Leica DM6 fluorescence microscope with an x20 objective and quantification was performed in ImageJ, as previously described[13,71]. For quantification of cell density, three brain sections spaced 300 μm apart were counted, with the rostral-most section at the injury epicenter and the next two additional sections

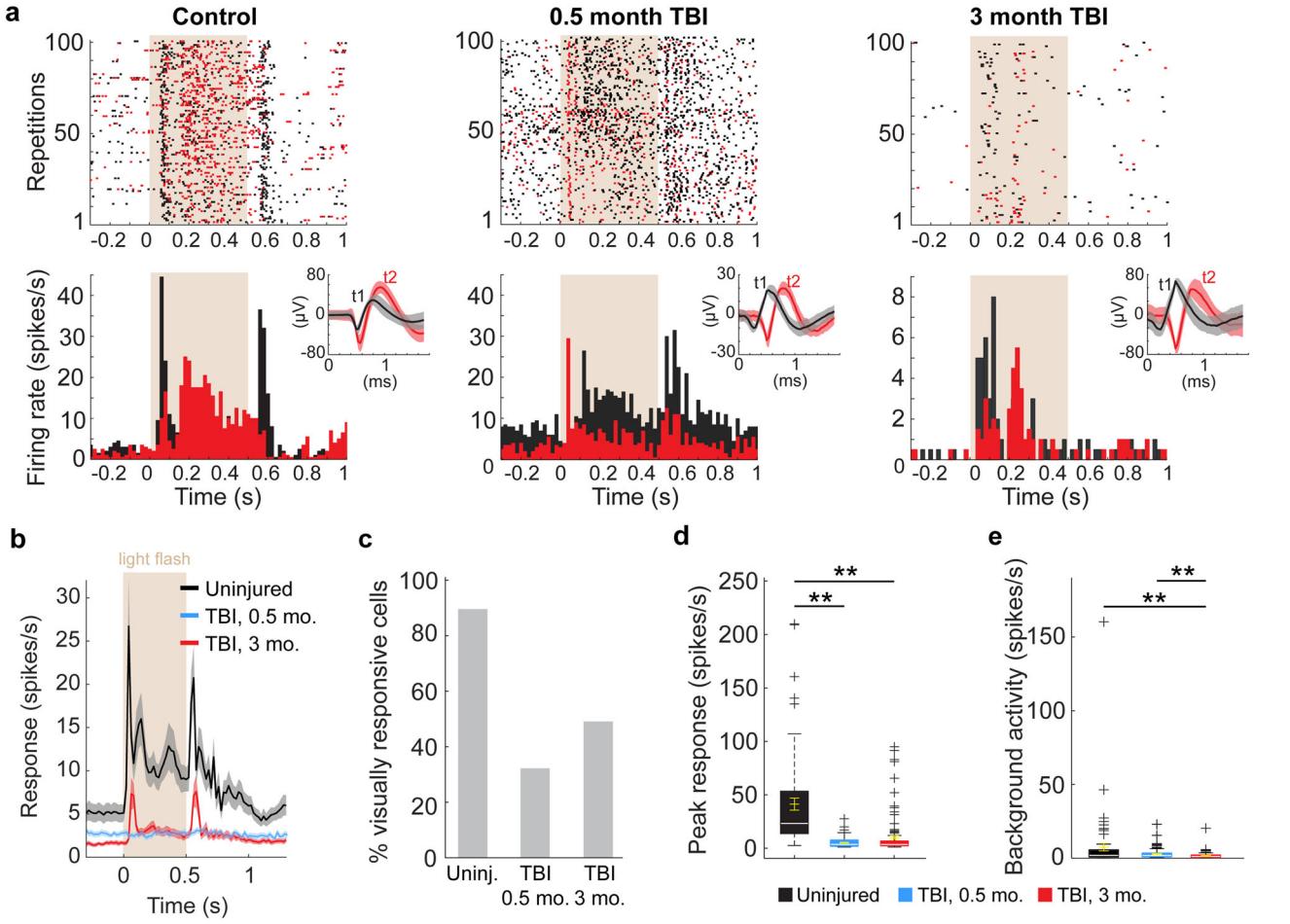


**Fig. 6 Reduced V1 neuron firing following TBI. a** Light-evoked responses of action potential firing for two example neurons (black and red) for each animal group: control (left), 0.5 months (middle) and 3 months after injury (right). The top row shows raster plots to 100 repetitions of the flash stimulus. The bottom row shows the spikes/s averaged over 20 ms bins. In both rows, the 500 ms light stimulus is indicated by beige background shading. Insets in the upper right of the bottom row show raw wave forms isolated by two templates (t1, black and t2, red) based on differences in spike amplitude (uV) and timing (ms). Shading indicates spike variability. **b** Population averages of light-evoked single-unit responses of action potential firing in uninjured controls (black) and CCI-injured mice 0.5 months (blue) and 3 months after injury (red). $n = 67$ cells from 8 controls, 110 cells from 5 mice 0.5 months after TBI, and 115 cells from 5 mice 3 months after TBI. Shading indicates S.E.M. The 500 ms light stimulus is indicated by beige background shading. **c**. Percentage of visually responsive cells. **d** Quantification of peak single-neuron firing rates from each group in response to light stimulus. $^{**}P = 9.56\text{E-}10$, control versus 0.5 months after TBI, $^{**}P = 9.56\text{E-}10$, control versus 3 months after TBI; Kruskal–Wallis H with Dunn's post hoc. **e** Quantification of single-neuron firing rates from each group in the 500 ms prior to the light stimulus. $^{**}P = 2.00\text{E-}03$, control versus 0.5 months after TBI, $^{**}P = 3.02\text{E-}04$, control versus 3 months after TBI; Kruskal–Wallis H with Dunn's post hoc. For box plots, dashed error bars represent the maximum and minimum observations within 1.5 inter-quartile range of the 25th and 75th percentile; values greater than 1.5 inter-quartile range of the 75th percentile are indicated by +.

caudal to the epicenter. For layer analysis, the border of each layer (layers I, II/III, IV, and V/VI) were defined manually by visual inspection of neuron densities in NEUN epifluorescence images, as previously described[72,73]. For quantification of GFAP and IBA1 immunostaining, measurements were analyzed at three different locations and the percentage of the area above fluorescence threshold was applied using ImageJ according to a previous protocol[71]. The same settings were used for all sections.

**Neurophysiology**. Animals were initially anesthetized with 2% isoflurane in a mixture of $N_2O/O_2$ (70%/30%) then placed into a stereotaxic apparatus. A small, custom-made plastic chamber was secured to the exposed skull using dental acrylic. After one day of recovery, re-anesthetized animals were placed in a custom-made hammock, maintained under isoflurane anesthesia (1–2% in $N_2O/O_2$) and multiple single tungsten electrodes were inserted into V1 layers II–VI using the same craniotomy produced during the injury phase. All recording locations were within the CCI damaged region of V1 (defined as being within the craniotomy). Following electrode placement, the chamber was filled with sterile agar and sealed with sterile bone wax. Animals were then sedated with chlorprothixene hydrochloride (1 mg/kg; IM;[74]) and kept under light isoflurane anesthesia (0.2–0.4% in 30% $O_2$) throughout the recording procedure. EEG and EKG were monitored throughout and body temperature was maintained with a heating pad (Harvard Apparatus, Holliston, MA).

Data was acquired using a multi-channel Scout recording system (Ripple, UT, USA). Local field potentials (LFP) from multiple locations at matching cortical depths were band-pass filtered from 0.1 Hz to 250 Hz and stored along with spiking data at 1 kHz sampling rate. LFP signal was aligned to stimulus time stamps and averaged across trials for each recording depth in order to calculate visually evoked potentials (VEP)[75–77]. Single-neuron spike signals were band-pass filtered from 500 Hz to 7 kHz and stored at a 30 kHz sampling frequency. Spikes were sorted online in Trellis (Ripple, UT, USA) while performing visual stimulation. Action potentials were detected based on negative and positive thresholds that were at least twice as large (S/N > 2:1) as the background noise. For each recording location, thresholds were adjusted to maintain a high signal-to-noise ratio. Waveforms were sorted by marking templates based on the clear amplitude difference, positive or negative peak detection, and the slope between negative and positive component (see insets in Fig. 6a), which can be defined as the spike width. Visual stimuli were generated in Matlab (Mathworks, USA) using Psychophysics Toolbox[78–80] and displayed on a gamma-corrected LCD monitor (55 inches, 60 Hz; 1920 ×1080 pixels; 52 cd/m$^2$ mean luminance). Stimulus onset times were corrected for monitor delay using an in-house designed photodiode system[81].

Visual responses were assessed according to previously published methods[76,81,82]. For recordings of visually evoked responses, cells were first tested with 100 repetitions of a 500 ms bright flash stimulus (105 cd/m$^2$). Receptive fields for visually responsive cells were then located using square-wave drifting gratings,

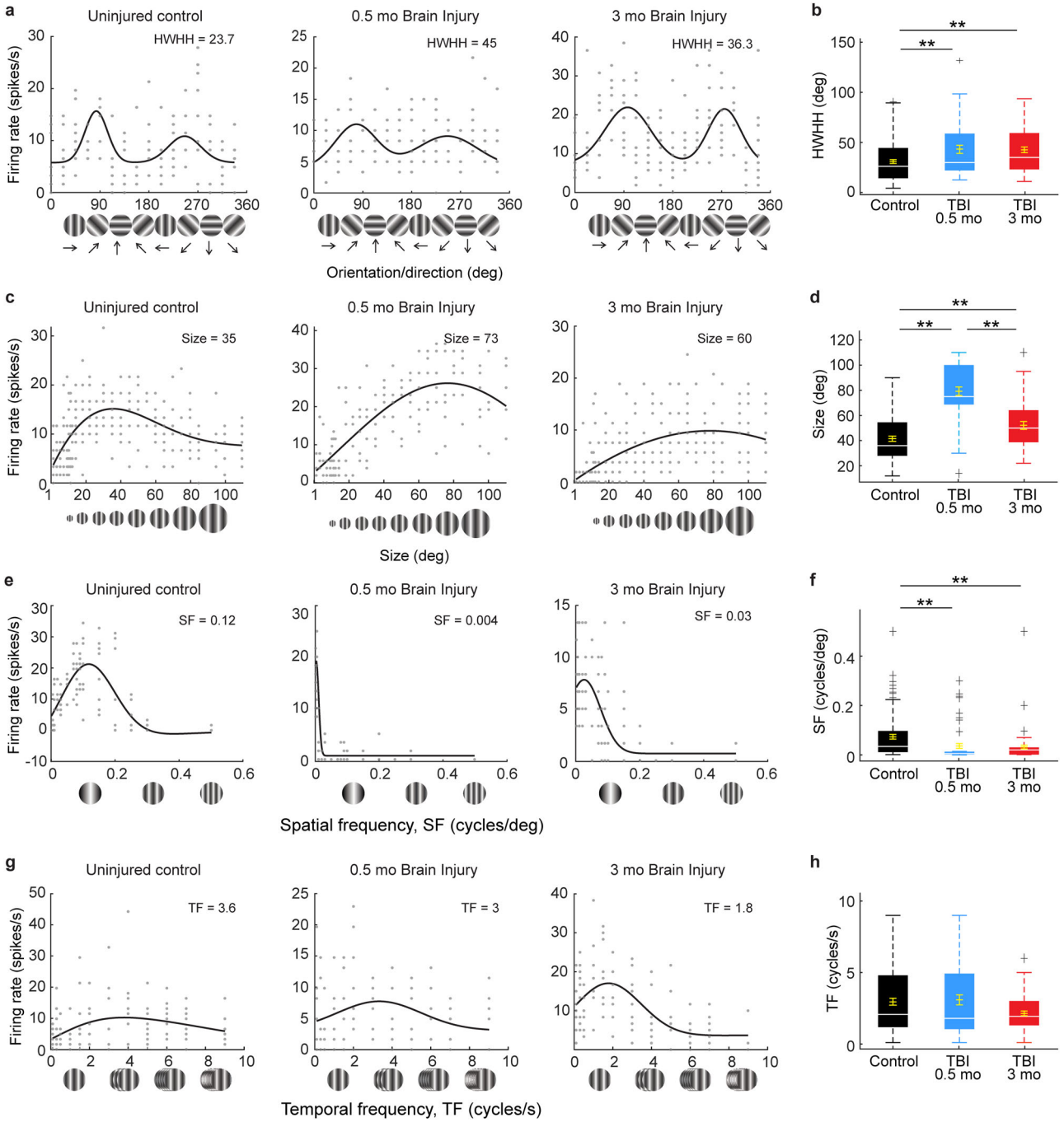


**Fig. 7 TBI disrupts V1 neuron tuning curves in response to drifting gratings. a, b** Orientation tuning curves for single neurons in an uninjured control (black) and CCI-injured mice 0.5 months (blue) and 3 months (red) after injury. To facilitate comparisons across examples orientation preferences have been aligned to 90° and 270°, with 90° representing the preferred direction. Tuning values are given as the half-width at half-height (HWHH) in degrees in each panel (**a**) and the population averages are quantified in (**b**). $^{**}P = 0.03$, control versus 0.5 months after TBI, $^{**}P = 1.99E\text{-}03$, control versus 3 months after TBI; Kruskal–Wallis H with Dunn's post hoc. $n = 109$ cells from 7 uninjured controls, 54 cells from 5 mice 0.5 months after TBI, and 75 cells from 5 mice 3 months after TBI. **c**, **d** Single neuron examples and population average quantification of aperture size (in degrees). $^{**}P = 9.56E\text{-}10$, control versus 0.5 months after TBI, $^{*}P = 0.042$, control versus 3 months after TBI, $^{**}P = 2.04E\text{-}05$, 0.5 versus 3 months after TBI; Kruskal–Wallis H with Dunn's post hoc. $n = 81$ cells for control, 45 cells 0.5 months after TBI and 41 cells 3 months after TBI. **e**, **f** Single neuron examples and quantification of spatial frequency (SF). $^{**}P = 3.80E\text{-}06$, control versus 0.5 months after TBI, $^{**}P = 6.51E\text{-}03$, control versus 3 months after TBI, Kruskal–Wallis H with Dunn's post hoc. $n = 105$ cells for control, 55 cells 0.5 months after TBI, 71 cells 3 months after TBI. **g**, **h** Single neuron examples and quantification of temporal frequency (TF). $P = 0.26$; Kruskal–Wallis H test. Optimal values for each parameter are given in each panel. $n = 95$ cells for control, 59 cells 0.5 months after TBI, and 70 cells 3 months after TBI. Background activity for each cell is indicated by gray dashed lines. For box plots, dashed error bars represent the maximum and minimum observations within 1.5 inter-quartile range of the 25th and 75th percentile; values greater than 1.5 inter-quartile range of the 75th percentile are indicated by +.

after which optimal orientation, direction, and spatial and temporal frequencies were determined using sine-wave gratings. Shown at optimal orientation, spatial frequencies used ranged from 0.001 to 0.5 cycles/°; Temporal frequencies used were from 0.1 to 10 cycles/s. Using optimal parameters, size tuning was assessed with apertures ranging from 1 to 110° at 100% contrast. With optimal size, orientation tuning of the cell was re-assessed using 8 orientations × 2 directions each, stepped by 22.5° increments. Background activity was calculated as average activity from 500 ms before stimulus onset for each repetition. A cell was determined to be visually responsive if the average firing rate was more than 2 standard deviations above background activity and at least 3 spikes/s. Any cell that was nonresponsive to the flash stimulus was not probed using sine-wave gratings. A percentage of flash-responsive cells in the 0.5- and 3-month conditions did not respond to every sine-wave stimulus condition used (Supplemental Fig. 6). Non-responses to sine-wave stimuli were excluded from population analyses because they could not be fit to a curve.

**Local field potential (LFP) analysis**. Amplitude of response was calculated as a difference between the peak of the positive and negative components of the VEP. Response latency was defined as the time from stimulus onset to maximum response. Maximum of the response was defined at the larger of the negative or positive peak. For uninjured control animals, depths corresponding to layer 5 were always used (~500 µm). This is because layer 5 amplitude responses were the highest in control animals (see example in Supplemental Fig. 3a). For TBI animals, the depth with the highest amplitude was used. This is because VEPs were more erratic in TBI animals and not always the most responsive at layer 5 (see examples in Supplemental Fig. 3b, c).

**Single-unit analysis**. Tuning curves were calculated based on the average spike rate centered around the preferred direction (peak response). Optimal visual parameters were chosen as the maximum response value. Orientation tuning was measured in degrees at the half-width at half-height (HWHH; 1.18 × σ) based on fits to Gaussian distributions[47,48,81–84] using:

$$R_{O_s} = baseline + R_p e^{-\frac{(O_s - O_p)^2}{2\sigma^2}} + R_n e^{-\frac{(O_s - O_p + 180)^2}{2\sigma^2}}, \quad (1)$$

where $O_s$ is the stimulus orientation, $R_{Os}$ is the response to different orientations, $O_p$ is the preferred orientation, $R_p$ and $R_n$ are the responses at the preferred and nonpreferred direction, σ is the tuning width, and 'baseline' is the offset of the Gaussian distribution. Gaussian fits were estimated without subtracting spontaneous activity, similar to the procedures of Alitto and Usrey[83].

Size tuning curves were fitted by a difference of Gaussian (DoG) function:

$$R_s = K_e \int_{-s}^{s} e^{\left(-\frac{x}{r_e}\right)^2} dx - K_i \int_{-s}^{s} e^{(-x/r_i)^2} dx + R_0, \quad (2)$$

in which $R_s$ is the response evoked by different aperture sizes. The free parameters, $K_e$ and re, describe the strength and the size of the excitatory space, respectively; Ki and ri represent the strength and the size of the inhibitory space, respectively; and $R_0$ is the spontaneous activity of the cell.

The optimal spatial and temporal frequency was extracted from the data fitted to Gaussian distributions using the following equation:[81,82,85,86]

$$R_{SF/TF} = baseline + R_{pref} e^{-\frac{\left(\frac{SF}{TF} - \frac{SF}{TF_{pref}}\right)^2}{2\sigma^2}}, \quad (3)$$

Where $R_{SF/TF}$ is the estimated response, $R_{pref}$ indicates response at preferred spatial or temporal frequency, SF/TF indicates spatial or temporal frequency, σ is the standard deviation of the Gaussian, and baseline is Gaussian offset.

**Statistics and reproducibility**. Anatomical data analysis was performed in Graphpad Prism 9, Microsoft Excel, and SAS 9.4 software. Experimental groups were averaged across groups (i.e., $N$ = animals) compared by two-way ANOVA with Tukey's post hoc test, or repeated-measures two-way ANOVA followed by Sidak's post hoc test. For layer analysis, data were fitted to a random intercept mixed model followed by Tukey-Kramer post hoc. Cell density was defined as the response variable and distance from the injury, cell layer, group, the interaction of layer by group, and the interaction of distance by layer by the group as explanatory variables. Neurophysiology data analysis was performed in Matlab (Mathworks, USA). Neural responses were averaged across recording locations (i.e., $N$ = animals; $n$ = recording locations) or cells (in single-unit recordings) and groups were compared by Kruskal–Wallis H test followed by multiple comparisons using Dunn's post hoc. All data are expressed as mean ± SEM. Significance was set at $P < 0.05$.

**Reporting Summary**. Further information on research design is available in the Nature Research Reporting Summary linked to this article.

## Data availability

All data that support the findings of this study are available as source data in Supplementary Data 4. All other data are available from the corresponding author upon reasonable request.

## Code availability

Data were collected with previously published custom MatLab script[76] and is available from the corresponding author upon reasonable request.

Received: 8 January 2021; Accepted: 25 October 2021;
Published online: 17 November 2021

## References

1. Armstrong, R. A. Visual problems associated with traumatic brain injury. *Clin. Exp. Optom.* **101**, 716–726 (2018).
2. Sano, K., Nakamura, N., Hirakawa, K., Masuzawa, H. & Hashizume, K. Mechanism and dynamics of closed head injuries (preliminary report). *Neurol. Med Chir. (Tokyo)* **9**, 21–33 (1967).
3. Stelmack, J. A., Frith, T., Van Koevering, D., Rinne, S. & Stelmack, T. R. Visual function in patients followed at a Veterans Affairs polytrauma network site: an electronic medical record review. *Optometry* **80**, 419–424 (2009).
4. Eysel, U. T. & Schweigart, G. Increased receptive field size in the surround of chronic lesions in the adult cat visual cortex. *Cereb. Cortex* **9**, 101–109 (1999).
5. Girard, P., Salin, P. A. & Bullier, J. Visual activity in macaque area V4 depends on area 17 input. *Neuroreport* **2**, 81–84 (1991).
6. Imbrosci, B., Eysel, U. T. & Mittmann, T. Metaplasticity of horizontal connections in the vicinity of focal laser lesions in rat visual cortex. *J. Physiol.* **588**, 4695–4703 (2010).
7. Hunt, R. F., Boychuk, J. A. & Smith, B. N. Neural circuit mechanisms of post-traumatic epilepsy. *Front Cell Neurosci.* **7**, 89 (2013).
8. Swartz, B. E. et al. Hippocampal cell loss in posttraumatic human epilepsy. *Epilepsia* **47**, 1373–1382 (2006).
9. Buriticá, E. et al. Changes in calcium-binding protein expression in human cortical contusion tissue. *J. Neurotrauma* **26**, 2145–2155 (2009).
10. Anderson, K. J., Miller, K. M., Fugaccia, I. & Scheff, S. W. Regional distribution ofFluoro-Jade B staining in the hippocampus following traumatic brain injury. *Exp. Neurol.* **193**, 125–130 (2005).
11. Cantu, D. et al. Traumatic brain injury increases cortical glutamate network activity by compromising GABAergic control. *Cereb. Cortex* **25**, 2306–2320 (2015).
12. Fox, G. B., Fan, L., Levasseur, R. A. & Faden, A. I. Sustained sensory/motor andcognitive deficits with neuronal apoptosis following controlled cortical impactbrain injury in the mouse. *J. Neurotrauma* **15**, 599–614 (1998).
13. Frankowski, J. C., Kim, Y. J. & Hunt, R. F. Selective vulnerability of hippocampal interneurons to graded traumatic brain injury. *Neurobiol. Dis.* **129**, 208–216 (2019).
14. Goodman, J. C., Cherian, L., Bryan Jr, R. M. & Robertson, C. S. Lateral cortical impactinjury in rats. Pathologic effects of varying cortical compression and impactvelocity. *J. Neurotrauma* **11**, 587–597 (1994).
15. Hall, E. D., Gibson, T. R. & Pavel, K. M. Lack of a gender difference in post-traumatic neurodegeneration in the mouse controlled cortical impact injury model. *J. Neurotrauma* **22**, 669–679 (2005).
16. Huusko, N., Römer, C., Ndode-Ekane, X. E., Lukasiuk, K. & Pitkänen, A. Loss of hippocampal interneurons and epileptogenesis: a comparison of two animal models of acquired epilepsy. *Brain Struct. Funct.* **220**, 153–191 (2015).
17. Lowenstein, D. H., Thomas, M. J., Smith, D. H. & McIntosh, T. K. Selective vulnerability of dentate hilar neurons following traumatic brain injury: a potential mechanistic link between head trauma and disorders of the hippocampus. *J. Neurosci.* **12**, 4846–4853 (1992).
18. Nichols, J., Bjorklund, G. R., Newbern, J. & Anderson, T. Parvalbumin fast-spiking interneurons are selectively altered by paediatric traumatic brain injury. *J. Physiol.* **596**, 1277–1293 (2018).
19. Santhakumar, V. et al. Granule cell hyperexcitability in the early post-traumatic rat dentate gyrus: the 'irritable mossy cell' hypothesis. *J. Physiol.* **524**, 117–134 (2000). Pt 1.
20. Toth, Z., Hollrigel, G. S., Gorcs, T. & Soltesz, I. Instantaneous perturbation of dentate interneuronal networks by a pressure wave-transient delivered to the neocortex. *J. Neurosci.* **17**, 8106–8117 (1997).
21. Vascak, M., Jin, X., Jacobs, K. M. & Povlishock, J. T. Mild Traumatic Brain Injury Induces Structural and Functional Disconnection of Local Neocortical Inhibitory Networks via Parvalbumin Interneuron Diffuse Axonal Injury. *Cereb. Cortex* **28**, 1625–1644 (2018).
22. Cajal, S.Ry. Study of traumatic degeneration in the cerebral cortex. in Degeneration and regeneration of the nervous system (ed. May R. M) 656–692 (London, Oxford Univ. Press, 1928).
23. Echlin, F. A. & Battista, A. Epileptiform seizures from chronic isolated cortex. *Arch. Neurol.* **9**, 154–170 (1963).
24. Jin, X., Prince, D. A. & Huguenard, J. R. Enhanced excitatory synaptic connectivity in layer v pyramidal neurons of chronically injured epileptogenic neocortex in rats. *J. Neurosci.* **26**, 4891–4900 (2006).

25. Hunt, R. F., Scheff, S. W. & Smith, B. N. Posttraumatic epilepsy after controlled cortical impact injury in mice. *Exp. Neurol.* **215**, 243–252 (2009).
26. Hunt, R. F., Scheff, S. W. & Smith, B. N. Regionally localized recurrent excitation in the dentate gyrus of a cortical contusion model of posttraumatic epilepsy. *J. Neurophysiol.* **103**, 1490–1500 (2010).
27. Hunt, R. F., Scheff, S. W. & Smith, B. N. Synaptic reorganization of inhibitory hilar interneuron circuitry after traumatic brain injury in mice. *J. Neurosci.* **31**, 6880–6890 (2011).
28. Johnstone, V. P., Shultz, S. R., Yan, E. B., O'Brien, T. J. & Rajan, R. The acute phase of mild traumatic brain injury is characterized by a distance-dependent neuronal hypoactivity. *J. Neurotrauma* **31**, 1881–1895 (2014).
29. Johnstone, V. P. et al. Experimental traumatic brain injury results in long-term recovery of functional responsiveness in sensory cortex but persisting structural changes and sensorimotor, cognitive, and emotional deficits. *J. Neurotrauma* **32**, 1333–1346 (2015).
30. Salin, P., Tseng, G. F., Hoffman, S., Parada, I. & Prince, D. A. Axonal sprouting in layer V pyramidal neurons of chronically injured cerebral cortex. *J. Neurosci.* **15**, 8234–8245 (1995).
31. Scheff, S. W. et al. Synaptogenesis in the hippocampal CA1field following traumatic brain injury. *J. Neurotrauma* **22**, 719–732 (2005).
32. Almeida-Suhett, C. P. et al. Reduced GABAergic inhibition in the basolateral amygdala and the development of anxiety-like behaviors after mild traumatic brain injury. *PLoS One* **9**, e102627 (2014).
33. Almeida-Suhett, C. P. et al. GABAergic interneuronal loss and reduced inhibitory synaptic transmission in the hippocampal CA1 region after mild traumatic brain injury. *Exp. Neurol.* **273**, 11–23 (2015).
34. Butler, C. R., Boychuk, J. A. & Smith, B. N. Differential effects of rapamycin treatment on tonic and phasic GABAergic inhibition in dentate granule cells after focal brain injury in mice. *Exp. Neurol.* **280**, 30–40 (2016).
35. Gupta, A., Elgammal, F. S., Proddutur, A., Shah, S. & Santhakumar, V. Decrease in tonic inhibition contributes to increase in dentate semilunar granule cell excitability after brain injury. *J. Neurosci.* **32**, 2523–2537 (2012).
36. Koenig, J. B., et al. Glycolytic inhibitor 2-deoxyglucose prevents cortical hyperexcitability after traumatic brain injury. *JCI Insight.* 5, e126506 (2019).
37. Li, H. & Prince, D. A. Synaptic activity in chronically injured, epileptogenic sensory-motor neocortex. *J. Neurophysiol.* **88**, 2–12 (2002).
38. Pavlov, I. et al. Progressive loss of phasic, but not tonic, GABAA receptor-mediated inhibition in dentate granule cells in a model of post-traumatic epilepsy in rats. *Neuroscience* **194**, 208–219 (2011).
39. Witgen, B. M. et al. Regional hippocampal alteration associated with cognitive deficit following experimental brain injury: a systems, network and cellular evaluation. *Neuroscience* **133**, 1–15 (2005).
40. Ährlund-Richter, S. et al. A whole-brain atlas of monosynaptic input targeting four different cell types in the medial prefrontal cortex of the mouse. *Nat. Neurosci.* **22**, 657–668 (2019).
41. Hafner, G. et al. Increased Callosal Connectivity in Reeler Mice Revealed by Brain-Wide Input Mapping of VIP Neurons in Barrel Cortex. *Cereb. Cortex* **31**, 1427–1443 (2021).
42. Luo, P., et al. Whole brain mapping of long-range direct input to glutamatergic and GABAergic neurons in motor cortex. *Front. Neuroanat.* **13**, 44 (2019).
43. Lyon, D. C. & Kaas, J. H. Evidence for a modified V3 with dorsal and ventral halves in macaque monkeys. *Neuron* **33**, 453–461 (2002).
44. Wang, Q. & Burkhalter, A. Area map of mouse visual cortex. *J. Comp. Neurol.* **502**, 339–357 (2007).
45. Pleasant, J. M. et al. Rate of neurodegeneration in the mouse controlled cortical impact model is influenced by impactor tip shape: implications for mechanistic and therapeutic studies. *J. Neurotrauma* **28**, 2245–2262 (2011).
46. Tamamaki, N. et al. Green fluorescent protein expression and colocalization with calretinin, parvalbumin, and somatostatin in the GAD67-GFP knock-in mouse. *J. Comp. Neurol.* **467**, 60–79 (2003).
47. Liu, Y. J., Hashemi-Nezhad, M. & Lyon, D. C. Dynamics of extraclassical surround modulation in three types of V1 neurons. *J. Neurophysiol.* **105**, 1306–1317 (2011).
48. Liu, Y. J., Hashemi-Nezhad, M. & Lyon, D. C. Contrast invariance of orientation tuning in cat primary visual cortex neurons depends on stimulus size. *J. Physiol.* **593**, 4485–4498 (2015).
49. Liu, Y. J., Hashemi-Nezhad, M. & Lyon, D. C. Differences in orientation tuning between pinwheel and domain neurons in primary visual cortex depend on contrast and size. *Neurophotonics* **4**, 031209 (2017).
50. Liu, Y. J. et al. Tracing inputs to inhibitory or excitatory neurons of mouse and cat visual cortex with a targeted rabies virus. *Curr. Biol.* **23**, 1746–1755 (2013).
51. Ommaya, A. K., Grubb, R. L. & Naumann, R. A. Coup and contre-coup injury: observations on the mechanics of visible brain injuries in the rhesus monkey. *J. Neurosurg.* **35**, 503–516 (1971).
52. Lee, S. H. et al. Activation of specific interneurons improves V1 feature selectivity and visual perception. *Nature* **488**, 379–383 (2012).
53. Silverman, I. E. et al. SPECT in patients with cortical visual loss. *J. Nucl. Med* **34**, 1447–1451 (1993).
54. Du, T., Ciuffreda, K. J. & Kapoor, N. Elevated dark adaptation thresholds in traumatic brain injury. *Brain Inj.* **19**, 1125–1138 (2005).
55. McKenna, K., Cooke, D. M., Fleming, J., Jefferson, A. & Ogden, S. The incidence of visual perceptual impairment in patients with severe traumatic brain injury. *Brain Inj.* **20**, 507–518 (2006).
56. Padula, W. V., Argyris, S. & Ray, J. Visual evoked potentials (VEP) evaluating treatment for post-trauma vision syndrome (PTVS) in patients with traumatic brain injuries (TBI). *Brain Inj.* **8**, 125–133 (1994).
57. Zihl, J. & Kerkhoff, G. Foveal photopic and scotopic adaptation in patients with brain damage. *Clin. Vis. Sci.* **5**, 185–195 (1990).
58. Tucker, T. R. & Fitzpatrick, D. Luminance-evoked inhibition in primary visual cortex: a transient veto of simultaneous and ongoing response. *J. Neurosci.* **26**, 13537–13547 (2006).
59. Adesnik, H., Bruns, W., Taniguchi, H., Huang, Z. J. & Scanziani, M. A neural circuit for spatial summation in visual cortex. *Nature* **490**, 226–231 (2012).
60. Cardin, J. A., Palmer, L. A. & Contreras, D. Stimulus feature selectivity in excitatory and inhibitory neurons in primary visual cortex. *J. Neurosci.* **27**, 10333–10344 (2007).
61. Sillito, A. M., Salt, T. E. & Kemp, J. A. Modulatory and inhibitory processes in the visual cortex. *Vis. Res* **25**, 375–381 (1985).
62. Cone, J. J., Scantlen, M. D., Histed, M. H. & Maunsell, J. H. R. Different inhibitory interneuron cell classes make distinct contributions to visual contrast perception. *eNeuro* **6**, ENEURO.0337-18 (2019).
63. Wiesel, T. N. Postnatal development of the visual cortex and the influence of environment. *Nature* **299**, 583–591 (1982).
64. Hensch, T. K. et al. Local GABA circuit control of experience-dependent plasticity in developing visual cortex. *Science* **282**, 1504–1508 (1998).
65. Espinosa, J. S. & Stryker, M. P. Development and plasticity of the primary visual cortex. *Neuron* **75**, 230–249 (2012).
66. Fagiolini, M. et al. Specific GABAA circuits for visual cortical plasticity. *Science* **303**, 1681–1683 (2004).
67. Fagiolini, M. & Hensch, T. K. Inhibitory threshold for critical-period activation in primary visual cortex. *Nature* **404**, 183–186 (2000).
68. Davis, M. F. et al. Inhibitory Neuron Transplantation into Adult Visual Cortex Creates a New Critical Period that Rescues Impaired Vision. *Neuron* **86**, 1055–1066 (2015).
69. Larimer, P. et al. Caudal Ganglionic Eminence Precursor Transplants Disperse and Integrate as Lineage-Specific Interneurons but Do Not Induce Cortical Plasticity. *Cell Rep.* **16**, 1391–1404 (2016).
70. Hunt, R. F., Girskis, K. M., Rubenstein, J. L., Alvarez-Buylla, A. & Baraban, S. C. GABA progenitors grafted into the adult epileptic brain control seizures and abnormal behavior. *Nat. Neurosci.* **16**, 693–697. (2013).
71. Zhu, B., Eom, J. & Hunt, R. F. Transplanted interneurons improve memory precisioon after traumatic brain injury. *Nat. Commun.* **10**, 5156 (2019).
72. Stanco, A. et al. NPAS1 represses the generation of specific subtypes of cortical interneurons. *Neuron* **84**, 940–953 (2014).
73. Vogt, D. et al. Lhx6 directly regulates Arx and CXCR7 to determine cortical interneuron fate and laminar position. *Neuron* **82**, 350–364 (2014).
74. Camillo, D. et al. Visual processing by calretinin expressing inhibitory neurons in mouse primary visual cortex. *Sci. Rep.* **8**, 12355 (2018).
75. Foik, A. T. et al. Retinal origin of electrically evoked potentials in response to transcorneal alternating current stimulation in the rat. *Invest Ophthalmol. Vis. Sci.* **56**, 1711–1718 (2015).
76. Suh, S. et al. Treatment of an inherited retinal disease by in vivo base editing in an adult mouse model. *Nat. Biomed. Eng.* **5**, 169–178 (2021).
77. Kordecka, K., Foik, A. T. Wierzbicka, A. & Waleszczyk, W. J. Cortical inactivation does not block response enhancement in the superior colliculus. *Frontiers in Systems Neuroscience* **14**, 4891–4900 (2020).
78. Brainard, D. H. The Psychophysics Toolbox. *Spat. Vis.* **10**, 433–436 (1997).
79. Kleiner, M. et al. What's new in psychtoolbox-3. *Perception* **36**, 1–16 (2007).
80. Pelli, D. G. The VideoToolbox software for visual psychophysics: transforming numbers into movies. *Spat. Vis.* **10**, 437–442 (1997).
81. Foik, A. T. et al. Detailed visual cortical responses generated by retinal sheet transplants in rats with severe retinal degeneration. *J. Neurosci.* **38**, 10709–10724 (2018).
82. Foik, A. T., Scholl, L. R., Lean, G. A. & Lyon, D. C. Visual response characteristics in lateral and medial subdivisions of the rat pulvinar. *Neuroscience* **441**, 117–130 (2020).
83. Alitto, H. J. & Usrey, W. M. Influence of contrast on orientation and temporal frequency tuning in ferret primary visual cortex. *J. Neurophysiol.* **91**, 2797–2808 (2004).
84. Carandini, M. & Ferster, D. Membrane potential and firing rate in cat primary visual cortex. *J. Neurosci.* **20**, 470–484 (2000).
85. DeAngelis, G. C., Ohzawa, I. & Freeman, R. D. Spatiotemporal organization of simple-cell receptive fields in the cat's striate cortex. II. Linearity of temporal and spatial summation. *J. Neurophysiol.* **69**, 1118–1135 (1993).

86. Van den Bergh, G., Zhang, B., Arckens, L. & Chino, Y. M. Receptive-field properties of V1 and V2 neurons in mice and macaque monkeys. *J. Comp. Neurol.* **518**, 2051–2070 (2010).

## Acknowledgements

This work was supported by funding from the National Institutes of Health grants R01–NS096012, R01–EY024890, F31–NS106806, and Department of Defense grant W81XWH-21-1-0884. The International Centre for Translational Eye Research (MAB/2019/12) project is carried out within the International Research Agendas program of the Foundation for Polish Science co-financed by the European Union under the European Regional Development Fund, National Science Center, Poland (2019/34/E/NZ5/00434) for A.T.F. We thank Farideh Dehkordi-Vakil and the UCI Center for Statistical Consulting for assistance with data analysis. We thank members of the Hunt lab for helpful discussions and comments on earlier versions of this manuscript.

## Author contributions

J.C.F contributed to the execution and analysis of experiments, funding and wrote the first draft of the manuscript. A.T.F designed and performed neurophysiology experiments, analyzed data, contributed funding, and edited the manuscript. A.T. performed immunostaining and analysis and edited the manuscript. J.R.M. performed preliminary cell quantifications. D.C.L designed neurophysiology experiments, analyzed data, contributed funding, and edited the manuscript. R.F.H contributed to the concept, design, analysis of experiments, funding, and wrote the manuscript.

## Competing interests

The authors declare no competing interests.

## Additional information

**Supplementary information** The online version contains supplementary material available at https://doi.org/10.1038/s42003-021-02808-5.

**Correspondence** and requests for materials should be addressed to Robert F. Hunt.

**Peer review information** *Communications Biology* thanks Jeffrey (H) Goodman and the other, anonymous, reviewers for their contribution to the peer review of this work. Primary Handling Editor: George Inglis.

**Reprints and permission information** is available at http://www.nature.com/reprints

**Publisher's note** Springer Nature remains neutral with regard to jurisdictional claims in published maps and institutional affiliations.

https://doi.org/10.1093/braincomms/fcab300 BRAIN COMMUNICATIONS 2022: Page 1 of 15

BRAIN COMMUNICATIONS

# Plasticity in the developing brain: neurophysiological basis for lesion-induced motor reorganization

**Mitchell Batschelett,[1,2] Savannah Gibbs,[1] Christen M. Holder,[1,3] Billy Holcombe,[1,3] James W. Wheless[1,3] and Shalini Narayana[1,3,4]**

The plasticity of the developing brain can be observed following injury to the motor cortex and/or corticospinal tracts, the most commonly injured brain area in the pre- or peri-natal period. Factors such as the timing of injury, lesion size and lesion location may affect a single hemisphere's ability to acquire bilateral motor representation. Bilateral motor representation of single hemisphere origin is most likely to occur if brain injury occurs before the age of 2 years; however, the link between injury aetiology, reorganization type and functional outcome is largely understudied. We performed a retrospective review to examine reorganized cortical motor maps identified through transcranial magnetic stimulation in a cohort of 52 patients. Subsequent clinical, anthropometric and demographic information was recorded for each patient. Each patient's primary hand motor cortex centre of gravity, along with the Euclidian distance between reorganized and normally located motor cortices, was also calculated. The patients were classified into broad groups including reorganization type (inter- and intrahemispheric motor reorganization), age at the time of injury (before 2 years and after 2 years) and injury aetiology (developmental disorders and acquired injuries). All measures were analysed to find commonalities between motor reorganization type and injury aetiology, function and centre of gravity distance. There was a significant effect of injury aetiology on type of motor reorganization ($P < 0.01$), with 60.7% of patients with acquired injuries and 15.8% of patients with developmental disorders demonstrating interhemispheric motor reorganization. Within the interhemispheric motor reorganization group, ipsilaterally and contralaterally projecting hand motor cortex centres of gravity overlapped, indicating shared cortical motor representation. Furthermore, the data suggest significantly higher prevalence of bilateral motor representation from a single hemisphere in cases of acquired injuries compared to those of developmental origin. Functional outcome was found to be negatively affected by acquired injuries and interhemispheric motor reorganization relative to their respective counterparts with developmental lesions and intrahemispheric motor reorganization. These results provide novel information regarding motor reorganization in the developing brain via an unprecedented cohort sample size and transcranial magnetic stimulation. Transcranial magnetic stimulation is uniquely suited for use in understanding the principles of motor reorganization, thereby aiding in the development of more efficacious therapeutic techniques to improve functional recovery following motor cortex injury.

1 Neuroscience Institute, Le Bonheur Children's Hospital, Memphis, TN, USA
2 Rhodes College, Memphis, TN, USA
3 Department of Pediatrics, Division of Pediatric Neurology, College of Medicine, University of Tennessee Health Science Center, Memphis, TN, USA
4 Department of Anatomy and Neurobiology, College of Medicine, University of Tennessee Health Science Center, Memphis, TN, USA

Correspondence to: Professor Shalini Narayana, PhD
Department of Pediatrics
Department of Anatomy and Neurobiology
UTHSC College of Medicine

Received May 19, 2021. Revised November 10, 2021. Accepted December 17, 2021. Advance access publication December 21, 2021

Neuroscience Institute
Le Bonheur Children's Hospital
848 Adams Ave, Neurology Clinics
Suite L445B, Memphis, TN 38103, USA
E-mail: snaraya2@uthsc.edu

**Keywords:** motor mapping; transcranial magnetic stimulation; reorganization; cortical dysplasia; peri-natal brain injury

**Abbreviations:** APB = abductor pollicis brevis; CIMT = constraint-induced movement therapy; COG = centre of gravity; IAHR = intrahemispheric reorganization; IEHR = interhemispheric reorganization; MSO = maximum stimulator output; MEP = motor evoked potential; rMT = resting motor threshold; TMS = transcranial magnetic stimulation

**Graphical Abstract**

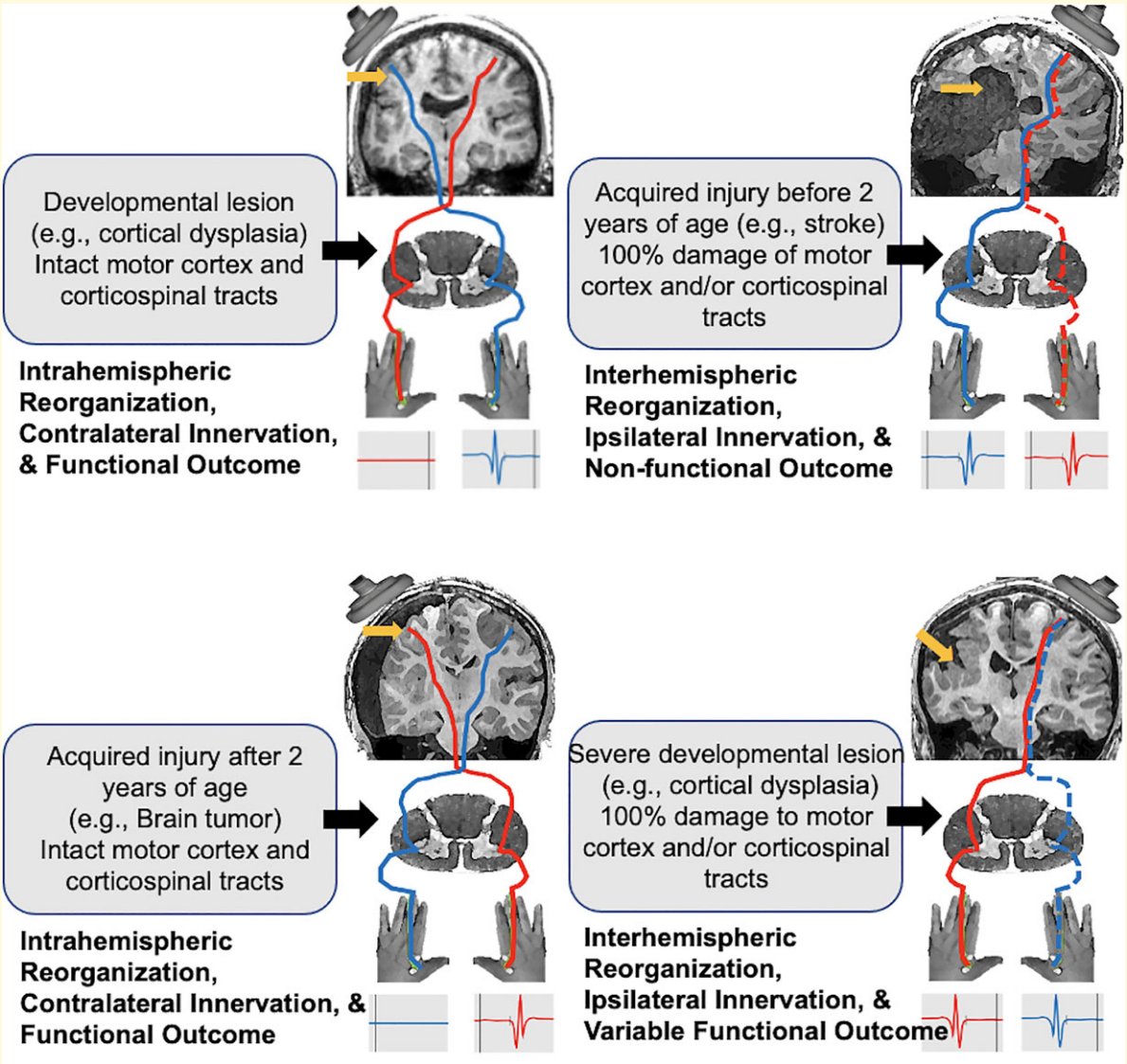


# Introduction

The human brain possesses the intrinsic ability to reorganize and recover function following injury and/or developmental malformations. This reorganizational capability, or plasticity, is observable throughout the human lifespan. For example, many adult stroke patients exhibit post-injury motor cortex plasticity and partial recovery of motor function.[1–3] However, the developing brain displays a greater capacity to recover following injury compared to its adult counterpart.[4–7] Cortical plasticity in the developing brain is readily observed in the case of motor cortex injury, as

the motor cortex and/or corticospinal tract is a common site of brain damage, particularly in the pre- or immediately perinatal period. Therefore, studying motor reorganization in children following injury to the motor cortex and/or corticospinal tract provides an excellent surrogate to understanding basic mechanistic principles of cortical reorganization.

Although the increased plasticity of the developing brain is well documented,[8,9] the exact mechanistic principles that underlie cortical motor reorganization are largely understudied. In humans, it has been shown that the developing brain includes fast and direct ipsilateral corticospinal projections from both hemispheres until ~24 months of postnatal development,[10–14] which disappear following full, unaltered corticospinal maturation. Longitudinal and cross-sectional neurophysiological studies of typically developing infants and children are likewise consistent with the withdrawal of uncrossed corticospinal axons over the first 24 postnatal months, such that ipsilateral motor evoked potentials (MEPs), like those elicited by transcranial magnetic stimulation (TMS), are less frequent, smaller, later in onset and have higher thresholds compared to contralateral muscle responses at 2 years of age.[11,15]

Injury to the motor cortex in young children alters the normal development of the motor cortex and/or corticospinal tract. Generally, two mechanisms of cortical reorganization have been postulated: (i) interhemispheric reorganization (IEHR), where the function is transferred to contralateral homologues and (ii) intrahemispheric reorganization (IAHR), where function is taken over by residual tissue and nearby cortex in the lesioned hemisphere.[10,16] It is thought that in the case of IEHR, the direct ipsilateral corticospinal projections of the unaffected hemisphere fail to regress, but rather persist, subsequently shifting the lesioned hemisphere's motor control to homologous ipsilateral motor areas.[12,13,17,18] The exact factors that govern which type of reorganization occurs are largely unknown; however, it is documented that lesion timing, size and location play a significant determining role.[5,7,16,19–23] For example, numerous studies have found that IEHR prevalence decreases with age, indicating that lesions early in life promote IEHR, whilst IAHR is primarily observed in later occurring lesions.[12,19,21,24,25] This age-dependent reorganizational effect suggests that the maturational status of the motor system at the time of injury dictates, in part, the resulting pattern of reorganization.

Other studies have observed a link between lesion size and subsequent reorganization. In short, larger perirolandic lesions are more likely to evoke IEHR, whilst smaller lesions, despite being around the rolandic sulcus, are more likely to evoke IAHR.[12,13] Additionally, other studies have found that lesion size is not a complete predictor of reorganization type, as large but incomplete rolandic lesions showed an increased incidence of IAHR than complete rolandic lesions of similar size.[20] These results demonstrate that IEHR is more likely to occur if the lesion affects the totality of the motor cortex early in life, forcing function to shift to the motor homologues of the contralesional hemisphere.

The severity of damage to descending white matter tracts early in development has also been implicated as a potential driving factor in determining reorganization. Namely, white matter damage has been shown to be positively correlated with the incidence of IEHR whilst negatively affecting motor function.[19] Consistent with these data, it was also found that greater injury to descending white matter tracts coincided with increased ipsilateral motor cortex recruitment and degree of motor reorganization.[26] Reports in regard to motor function are more conflicted, as the levels of functional impairment due to IEHR and IAHR have often been indistinguishable.[17,27]

Although the link between reorganization type, lesion timing and size has been documented, the role of lesion aetiology on induced reorganization type is largely understudied, as only a few case reports or smaller sample sizes ($N \leq 10$) have examined this aspect.[27–29] Further, though studies indicate a shift to contralateral homologues,[6,13] the precise location of reorganized motor cortex in IEHR has never been directly measured. The present study retrospectively examined motor reorganization as indexed by TMS in a cohort of patients presenting with acquired injuries or developmental disorders. We examined the effect of lesion aetiology (acquired versus developmental) on the type of reorganization (IEHR versus IAHR). Moreover, we measured the Euclidean distance between the centre of gravity (COG) of normally located and reorganized motor cortices within subjects to further characterize the extent of reorganization and determine the overlap of motor cortices following IEHR. We also examined the relationship between white matter damage and reorganization, as well as the resulting functional implications of reorganization type, as there are conflicting reports on which type of reorganization yields the best functional outcome.[5,19,23,30] In addition to providing novel information regarding the mechanisms of corticomotor reorganization, this study serves as evidence for the efficacy of TMS in examining motor reorganization in a paediatric cohort.[31,32]

We hypothesized that acquired injuries would be more likely to induce IEHR than developmental disorders and that cortical real estate would be shared in the case of IEHR. We also expected that increased white matter damage would drive IEHR. Finally, we predicted that the best functional outcome would occur following IAHR observed in developmental disorders.

# Materials and methods

## Study cohort

Through a retrospective chart review, we identified 420 patients who underwent TMS motor mapping at Le Bonheur Children's Hospital between July 2012 and May 2019. This study was approved by the institutional regulatory boards of the University of Tennessee Health Science Center and Le Bonheur Children's Hospital. Fifty-two

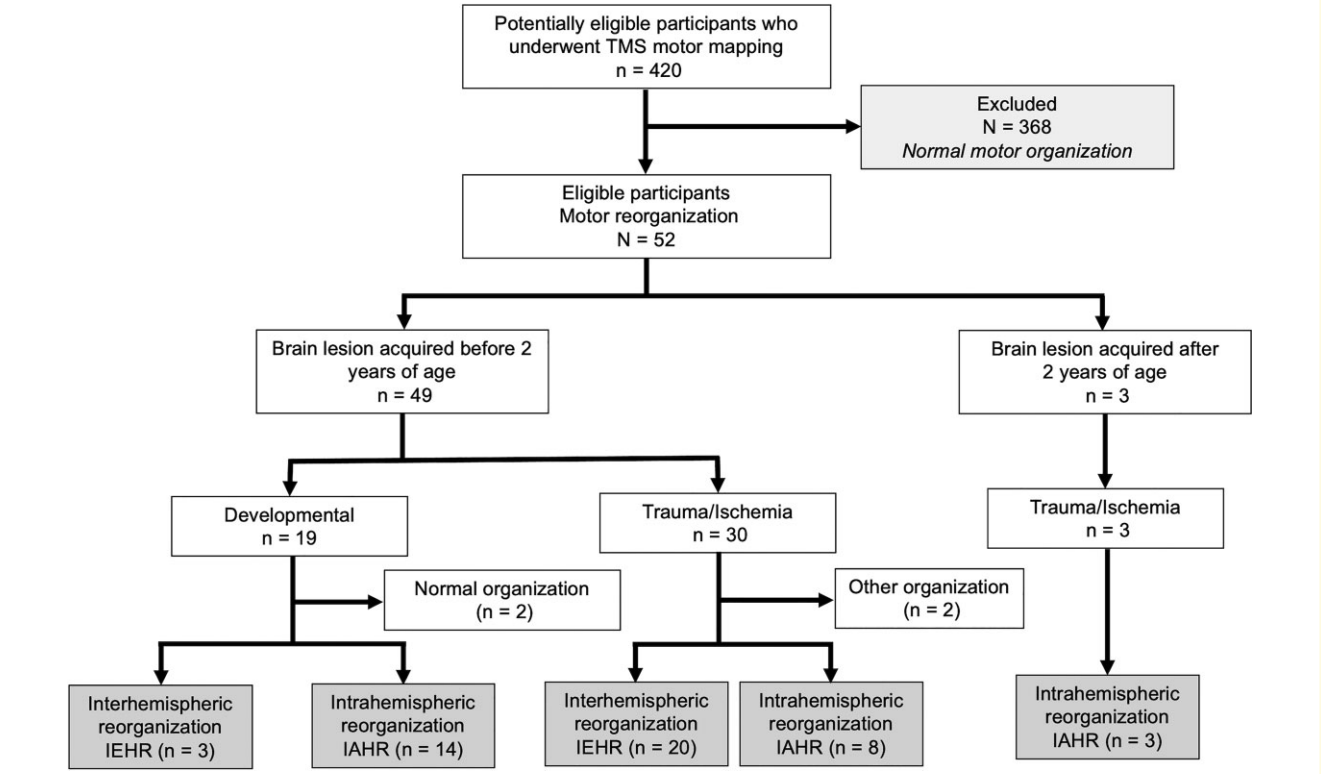


**Figure 1 Flow chart for identifying the study cohort.** IEHR, interhemispheric reorganization; IAHR, intrahemispheric reorganization.

patients were deemed eligible for inclusion in this study (Fig. 1 and Table 1). Eligible patients were those in whom either the cortical motor map of the primary hand motor cortex was displaced from the central sulcus, indicating IAHR, or at least one hemisphere demonstrated abnormal ipsilateral corticospinal projections after the accepted period of ipsilateral projection regression, indicating IEHR. More specifically, IAHR determinations were made based upon previous TMS investigations delineating normal hand motor cortex location and distribution.[33–39] With these studies in mind, IAHR was deemed present if at least one hemisphere exhibited motor cortex representation either within cortical regions known to be associated with the non-hand motor function (i.e. leg or face motor cortex)[39] or anteriorly or posteriorly displaced from the precentral gyrus, outside of the known normal deviation of hand motor cortex area (i.e. anterior to the middle frontal gyrus or posterior to the postcentral gyrus).[33–38] Patients who demonstrated normal motor maps despite lesions in the motor pathway, typically either small or in the subcortical regions, were not included in this study. Eligibility determinations were made using visualized cortical motor maps of the primary hand motor cortices following presurgical and/or clinically indicated TMS motor mapping, as well as a retrospective chart review,

**Table 1 Study cohort demographics**

| | Injury aetiology: developmental | Injury aetiology: acquired injury | Total |
|---|---|---|---|
| Number of patients | 19 | 33 | 52 |
| Age at the time of testing (years, mean ± SD) | 9.7 ± 5.1 | 11.0 ± 8.8 | 10.5 ± 7.6 |
| Age range (years) | 1.7–19.1 | 1.7–50 | 1.7–50 |
| Gender: females/males | 10/9 | 21/12 | 31/21 |
| Lesion acquisition: before age 2/after age 2 | 19/0 | 30/3 | 49/3 |
| Lesioned hemisphere: right/left/bilateral | 12/4/3 | 15/16/2 | 27/20/5 |
| Interhemispheric motor reorganization[a] | 3 | *20** | 23 |
| Intrahemispheric motor reorganization[a] | *14** | 11 | 25 |
| No demonstrable reorganization | 2 | 2 | 4 |

Italics indicate significant difference between the two groups. SD, standard deviation.

[a]Injury aetiology was found to have a significant effect on the resulting type of corticomotor reorganization, with developmental disorders mainly result in intrahemispheric motor reorganization, whilst acquired brain injury primarily results in an interhemispheric motor reorganization.

*$P < 0.01$.

including demographics, clinical history, previous brain imaging, neuropsychological testing and, in some cases, physical and occupational therapy evaluations. For each patient included in the study, the following data were recorded: sex, date of birth, age at the time of motor mapping, type of brain lesion, lesion location, lesion size relative to motor cortex (<50% involvement, >50% but incomplete involvement or complete motor cortex damage), age incurred (before or after 2 years of age), motor cortex reorganization type (IEHR or IAHR), location of resulting reorganization (only recorded for IAHR patients), history of epilepsy and grasp function (non-functional or functional). Antiepileptic medications (AEDs) prescribed at the time of TMS data acquisition were also collected. Based on brain injury aetiology, subjects were placed into two broad groups: developmental brain disorders (i.e. cortical dysplasia, heterotopia, polymicrogyria, etc.) and acquired injuries (i.e. traumatic brain injury, stroke, tumour resection, hemispherectomy, lobectomy, etc.). Groupings were designed to amplify potential links between groups, including type and extent of reorganization and functional outcome patterns. The aforementioned variables and their relationships were further examined via statistical testing (see the Statistical analysis section).

## Transcranial magnetic stimulation

### TMS motor mapping procedure

All individuals underwent TMS motor mapping either as part of their Phase I evaluation for refractory epilepsy, functional mapping prior to brain tumour surgery or to elucidate the functional state of their motor cortex following injury. Motor mapping was performed using a 70 mm figure-of-eight coil integrated into the navigated TMS system (Nexstim Plc., Helsinki, Finland) having a maximum electrical field of 172 V/m at 25 mm from its surface. The high-resolution T1-weighted MRI, the patient and the TMS coil were coregistered using a 3D tracking system. The MEP elicited by TMS was recorded by surface EMG from bilateral abductor pollicis brevis (APB) muscles using disposable electrodes (Neuroline 720, Ambu Inc., MD, USA) and sampled at 3 kHz and band-pass filtered from 10 to 500 Hz. In individuals who could maintain a quiet EMG baseline ($N = 37$), the resting motor threshold (rMT) for both hemispheres were measured at the hotspot for APB using an automated algorithm implemented in the Nexstim software based on the guidelines of the International Federation of Clinical Neurophysiology[40] and expressed as percent maximum stimulator output (% MSO). The extent of the motor cortex was then mapped at a TMS intensity of 110% of rMT; brain areas where an MEP ≥50 μV amplitude was elicited were included in the map and shown as a heat map (example shown in Fig. 2A). In patients who could not maintain a quiet EMG baseline or experienced pain during stimulation ($N = 7$), the MEP amplitudes were visually assessed and the motor cortex was mapped using the TMS intensity that elicited MEP amplitudes ≥50 μV. These patients were not included in the rMT analysis. All patients tolerated TMS without any serious adverse effects. Each patient's TMS session, containing each stimulation location, intensity and resulting MEP, was reviewed. A stimulation was considered to be a valid representation of the hand motor cortex and its corticospinal projection if it elicited a triphasic/polyphasic MEP with an amplitude ≥50 μV. Additionally, corticomotor latencies were measured as time from TMS stimulation to MEP onset for each hemisphere in the IAHR group and for both extremities from the intact hemisphere within the IEHR group. Five patients from the IEHR and eight patients from the IAHR group were excluded from the analysis due to insufficient corticomotor latency data.

### COG of motor maps

Rather than selecting the site where the MEP amplitude was highest, cortical representation for APB was defined by the COG. The COG is largely agnostic to MEP amplitude variabilities and has been shown to be a more accurate representation of the motor cortex.[41] The cortical location where an MEP was elicited in the APB and the MEP amplitude was used to calculate the COGs using the formula:

$$\sum a_i x_i \Big/ \sum a_i;\ \ \sum a_i y_i \Big/ \sum a_i;\ \ \sum a_i z_i \Big/ \sum a_i \qquad (1)$$

where $x_i$ is the mediolateral location; $y_i$ theanteroposterior location; $z_i$ the superoinferior position and $a_i$ the MEP amplitude at that location.[42] A measure of the distance between the normally located and reorganized COGs was necessary to observe the nature of cortical reorganization in the lesioned hemisphere relative to the normally located hand motor area within subjects. The primary hand motor cortex in the contralesional hemisphere acted as a within-subject control. For those in the IEHR group, the COGs of the hemisphere's ipsilateral projections and contralateral projections, both localized within the intact hemisphere, were calculated independently. For those in the IAHR group, the COG for APB representation was calculated independently for the two hemispheres; then, the COG in the lesioned hemisphere was transposed onto the intact hemisphere by mirroring its location around the midline. With the two COGs localized to the same hemisphere, the absolute distance between the COGs of the reorganized motor cortex and the normally located motor cortex was calculated by finding the Euclidian distance (mm) between them using the formula:

$$d = \sqrt{(x_2 - x_1)^2 + (y_2 - y_1)^2 + (z_2 - z_1)^2} \qquad (2)$$

The COG distance values were averaged for each group and the difference between the means was examined to assess the nature of IEHR and IAHR patterns. COG data from five patients were unavailable due to insufficient EMG data.

## Hand function

The hand function status in each patient was derived from a review of the hand motor assessment subsection of the

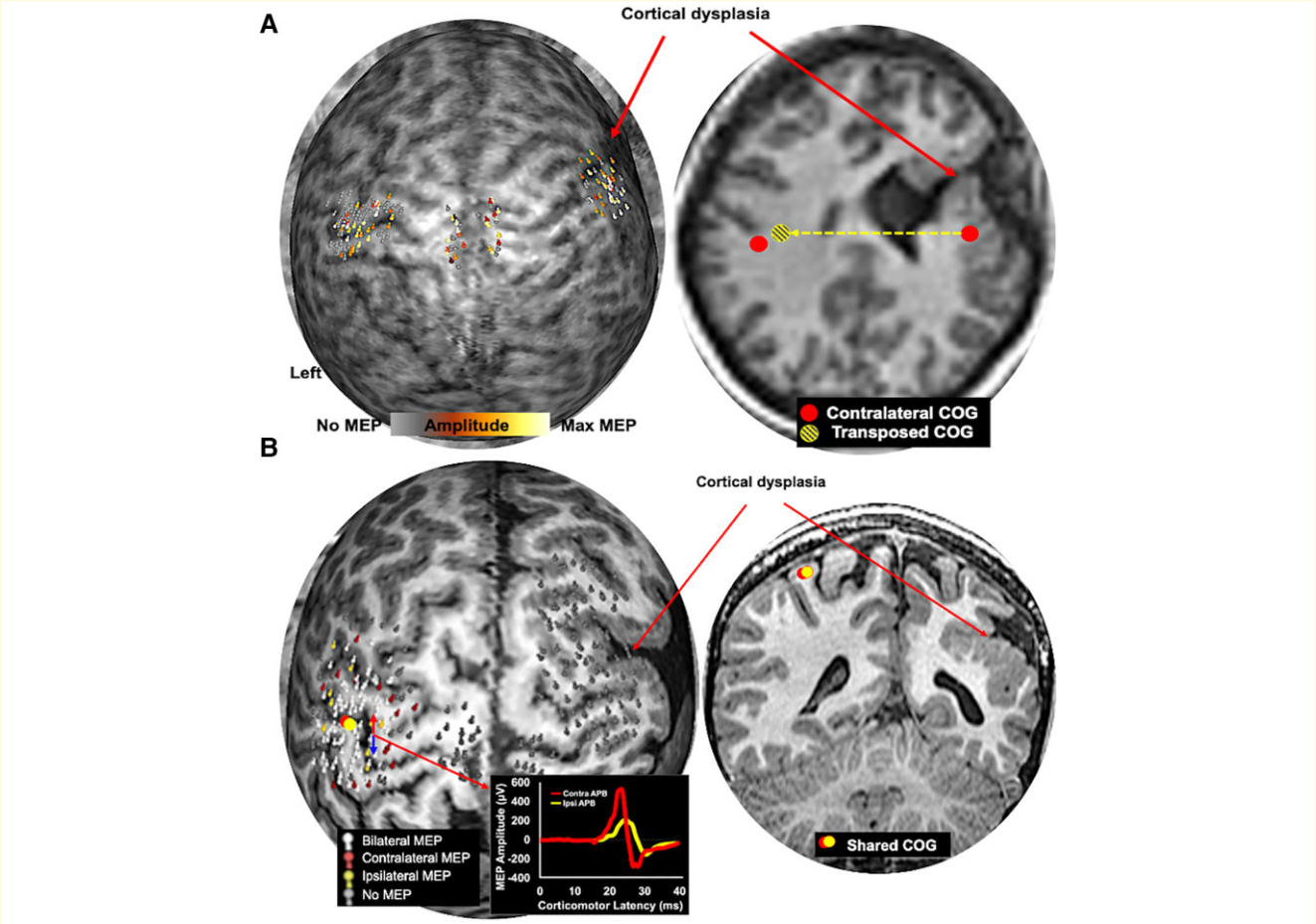


**Figure 2 Examples of motor reorganization in developmental cohort.** (**A**) A 19-year-old female with focal right hemisphere polymicrogyria demonstrating an IAHR pattern. The right hemisphere motor cortex is localized directly over the area of polymicrogyria and was displaced anteromedially when compared with the contralateral motor cortex. (**B**) An 11-year-old male with extensive right hemisphere polymicrogyria demonstrating a rare case of IEHR pattern. The descending white matter tract in the right hemisphere was also affected, making them non-functional. Hence, a shared bilateral corticomotor representation was observed in the left hemisphere. An example of bilateral MEP elicited by stimulation the motor cortex in the left hemisphere is shown.

neuropsychological evaluation. The most commonly used tests to examine the functionality of the affected hand were the Purdue Pegboard, Grooved Pegboard, Bayley Scales of Infant and Toddler Development (3rd edition) and Mullen Scales of Early Learning. The relationship between the time of injury, size of injury, location of injury, aetiology of injury and residual hand function were assessed. Overall, two patients had insufficient data to make an assessment about grasp function.

## White matter tract analysis

The integrity of the white matter tracts in the study cohort was evaluated by visually examining the subjects' high-resolution T1-weighted anatomical MRIs. The hand motor cortex COG coordinates were marked on the MRI. Descending white matter tract viability from the COGs was examined qualitatively. Furthermore, the cerebral peduncle, a region containing descending corticospinal motor neurons,[43] was examined for possible asymmetry.

## Lesion size

The size of each patient's lesion was assessed and documented relative to the amount of lesion involvement within the accepted area of hand motor representation.[33–38] Lesions were qualitatively characterized as <50% involvement, >50% but incomplete involvement and complete motor cortex involvement. Possible effects of lesion size on resulting reorganization and grasp function were examined (see the Statistical analysis section).

## Statistical analysis

All statistical analyses were conducted using SPSS (Release 27.0.1.0; IBM Corporation, Armonk, NY, USA). The effect of injury aetiology on reorganization type was assessed using Fisher's exact test. One-tailed paired *t*-tests were conducted for rMT differences between lesioned and non-lesioned hemispheres for the IAHR group and between contralateral and ipsilateral projections within the same hemisphere for the

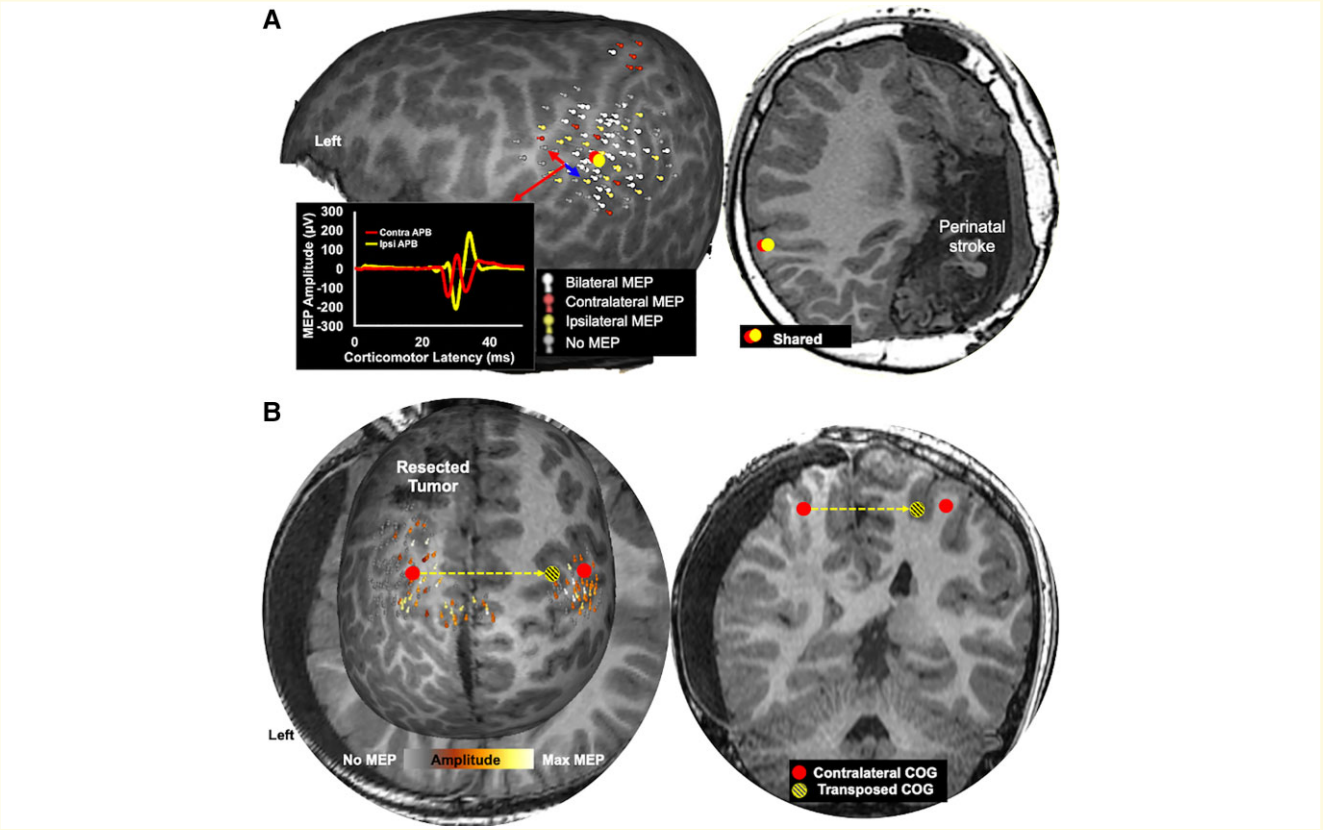


**Figure 3 Examples of motor reorganization in acquired brain injury cohort.** (**A**) A 16-year-old male with a history of intraparenchymal haemorrhage at birth and secondary epilepsy. The brain insult caused complete damage to right hemisphere motor cortex including its white matter tracts. No motor representation was observed in this hemisphere and a shared bilateral corticomotor representation, i.e. IEHR was observed in the left hemisphere. An example of bilateral MEP elicited by stimulation the motor cortex in the left hemisphere is shown. The patient also had severe global developmental delays, including both motor and cognitive deficits. (**B**) An 11-year-old male with a history of left hemisphere frontal lobe tumour located anterior to the primary motor cortex. His seizures began before the age of 2 years, secondary to the tumour. The primary hand motor cortex in the left hemisphere demonstrated an IAHR pattern and was displaced medially when compared with the homologue in the right hemisphere.

IEHR group. Additionally, two-tailed paired *t*-tests were conducted to examine differences in corticomotor latency in both groups. The distance between the COGs of reorganized and normally located APB in the IEHR and IAHR groups was examined using a two-tailed, two-sample *t*-test for unequal variance. Fisher's exact test was conducted to test for an effect of reorganization type on motor function and the effect of lesion aetiology on motor function. Finally, $\chi^2$ testing was also conducted to examine possible effects of lesion size on resulting reorganization and grasp function.

## Data availability

The data that support the findings of this study are available from the corresponding author upon request.

# Results

## Study cohort

The demographic, clinical and motor reorganization patterns observed in the study cohort are tabulated in Table 1 (see Supplementary Tables 1 and 2 for more detailed clinical information). The cohort consisted of 31 females and 21 males with an average age of 10.5 ± 7.6 years. Of the 52 patients in this study, 49 had sustained brain lesion at birth or before 2 years of age (19 presented with developmental disorders and 30 suffered an acquired injury; Fig. 1 and Table 1). The remaining three patients acquired the brain lesion when they were older than 2 years. Twenty-seven individuals had lesions in the right hemisphere, 20 in the left hemisphere and five had bilateral or non-focal lesions. Twenty-five patients demonstrated IAHR and 23 demonstrated IEHR (see Figs 2 and 3 for examples). Four patients (two with developmental and two with acquired lesions) with no clear reorganization were included in the cohort, as they presented with abnormally non-localizable motor cortices. These patients were only factored into analyses relating to effects of lesion aetiology and lesion size on functional outcome. Of those demonstrating IAHR, the majority (56%) had a developmental lesion (Table 1 and Fig. 2A), whilst the majority of patients (87%) in the IEHR group had an acquired injury (Table 1 and Fig. 3A).

**Table 2 Grasp function and TMS parameters in the two injury aetiology groups**

| | Injury aetiology: developmental | Injury aetiology: acquired injury |
|---|---|---|
| Number of patients | 19 | 33 |
| Grasp function: non-functional | 8 (42%) | 24 (73%) |
| Grasp function: functional[a] | 10 (53%) | 8* (24%) |
| Grasp function: insufficient information | 1 (5%) | 1 (3%) |
| TMS intensity: lesioned hemisphere (% MSO)[b] | 87.1 ± 17.3* | 72.4 ± 26.1 |
| TMS intensity: non-lesioned Hemisphere (% MSO)[b] | 75.2 ± 23.5 | 66.3 ± 25.8 |

MSO, maximum stimulator output.
[a]The developmental brain injury was significantly more likely to produce functional grasp when compared with acquired brain injury.
[b]TMS intensity to elicit a motor response was significantly higher in the lesioned hemisphere in developmental brain injury aetiology.
*$P < 0.05$.

See Tables 1–3 for complete cohort description. Of the three patients with brain injury occurring after age 2 years, all were within the acquired group, and all demonstrated IAHR (Supplementary Table 1).

Of the whole study cohort, 44 patients (85%) were prescribed at least one AED. Of those taking AEDs, most (40%) were prescribed two. The most common AEDs were oxcarbazepine and levetiracetam. There were no across-group differences in either the number of patients on AEDs or the number of AEDs prescribed (see supplemental Tables I and II for details).

$\chi^2$ testing conducted to measure an effect of lesion size on resulting reorganization did not achieve significance ($P = 0.611$); however, only incomplete lesions (i.e. lesions with motor cortex involvement of <50% or >50% but incomplete) were included in this analysis, as complete motor cortex lesions ($N = 8$) always resulted in IEHR. Taken together, these results suggest that complete motor cortex lesions significantly contribute to IEHR, whilst any type of incomplete lesion does not significantly contribute an effect on resulting reorganization.

Fisher's exact test conducted to measure injury aetiology's effect on reorganization type, independent of injury timing and overall age, found a significant effect of injury aetiology on resulting corticomotor reorganization. Acquired injuries were significantly more likely to cause IEHR than developmental disorders ($P < 0.01$) whereas occurance of IAHR was signifcantly higher in developmental disorders ($P < 0.01$). Fisher's exact test conducted to measure gender effects on reorganization type was not significant ($P = 0.38$), demonstrating that gender does not play a role in induced corticomotor reorganization.

## Transcranial magnetic stimulation

### Motor threshold

The rMT data were available in 37 patients. rMT in the lesioned hemisphere (87.1 ± 17.3%) was higher than rMT in the non-lesioned hemisphere (75.2 ± 23.5%) in the developmental, but not the acquired injury cohort (Table 2). The average rMTs in the acquired injury group were 72.4 ± 26.1% and 66.3 ± 25.8% for lesioned and non-lesioned hemispheres, respectively. In the IAHR group, the average rMT in the lesioned hemisphere was 81.0 ± 22.17% MSO, compared to 71.5 ± 24.4% MSO in the intact hemisphere (Table 3). In the IEHR group, average rMT for ipsilateral projections was 77.6 ± 21.6% MSO, whilst average rMT for contralateral projections was 71.3 ± 24.6% MSO (Table 3). One-tailed paired *t*-tests conducted for rMT differences between lesioned and non-lesioned hemispheres within the IAHR group found lesioned hemispheres to have significantly higher rMTs than non-lesioned hemispheres ($P = 0.01$). One-tailed paired *t*-tests conducted for rMT differences between contralateral and ipsilateral projections within subjects and within hemispheres for the IEHR group found ipsilateral projections to have significantly higher rMTs than contralateral projections ($P = 0.01$; Table 3).

### Corticomotor latencies

In the IEHR group ($n = 22$), average corticomotor latencies were 21.45 ± 2.12 and 21.02 ± 2.11 ms for ipsilateral and

**Table 3 Grasp function, TMS and COG parameters in the two patterns of motor reorganization**

| | Interhemispheric reorganization | Intrahemispheric reorganization |
|---|---|---|
| Number of patients | 23 | 25 |
| Gender: females/males | 15/8 | 12/13 |
| Grasp function: non-functional | 19 (83%) | 10 (40%) |
| Grasp function: functional[a] | 2 (9%) | ***15*** **(60%)** |
| Grasp function: insufficient information | 2 (9%) | 0 (0%) |
| TMS intensity: lesioned hemisphere (% MSO)[b] | n/a | 81.0 ± 22.2* |
| TMS intensity: non-lesioned Hemisphere (% MSO)[b] | n/a | 71.5 ± 24.4 |
| TMS intensity: contralateral projections (% MSO)[c] | 71.3 ± 24.6 | n/a |
| TMS intensity: ipsilateral projections (% MSO)[c] | 77.6 ± 21.6* | n/a |
| COG Euclidian distance APB (mm)[d] | 2.7 ± 1.7** | 16.0 ± 8.6 |

COG, centre of gravity; MSO, maximum stimulator output.
[a]An intrahemispheric reorganization was significantly more likely to produce functional grasp function.
[b]TMS intensity required to elicit a motor response was significantly higher in the lesioned hemisphere for individuals in the IAHR group.
[c]TMS intensity required to elicit a motor response was significantly higher for ipsilateral projections than for contralateral projections within the non-lesioned hemisphere demonstrating interhemispheric reorganization.
[d]The centres of gravity of the normally located and reorganized representation for APB were significantly closer for persons in the IEHR group than for individuals in the IAHR group.
*$P < 0.05$.
**$P < 0.0001$.

contralateral projections, respectively. In the IAHR group ($N = 19$), corticomotor latencies were $22.16 \pm 4.25$ and $20.96 \pm 2.60$ ms for affected and unaffected hemispheres, respectively. The difference of the mean two-tailed *t*-tests did not reveal differences in corticomotor latency between ipsilateral and contralateral projections or affected and unaffected hemispheres for the IEHR and IAHR groups, respectively.

### COG of motor maps

The average distance between the COGs for APB muscles in the two hemispheres was $16.0 \pm 8.6$ mm in IAHR (Table 3). For the IEHR group, the average distance between the COGs for APB muscles was $2.7 \pm 1.7$ mm. See Tables 2 and 3 for a complete listing of COG and TMS parameters. A two-tailed, two-sample of unequal variance *t*-test examining the average distances between reorganized and normally located APB COGs between the IEHR and IAHR cohorts found that the distances were significantly shorter for the IEHR group than the IAHR group ($P = 5.08E{-}08$), indicating a significant overlap of cortical representation in IEHR. In IAHR, motor cortex was reorganized to juxtalesional areas, including the premotor cortex, leg motor cortex and/or sensory cortex, and thus was not localized within the homologous APB motor area in the non-lesioned hemisphere.

## Hand function

Hand function ranged from non-functional to functional in both the developmental and acquired injury groups (Table 2). Of the developmental lesion group, eight had non-functional grasp function whilst 10 had functional grasp function. In the acquired injury group, 24 had non-functional grasp function, whilst eight had functional grasp function (Table 2). Of the IEHR group, 19 had non-functional grasp function, whilst two had functional grasp function. Of the IAHR group, 10 had non-functional grasp function, whilst 15 had functional grasp function (Table 3). $\chi^2$ testing did not find a significant effect of lesion size on resulting hand function ($P = 0.2$); however, only incomplete lesions (i.e. lesions with motor cortex involvement of $<50\%$ or $>50\%$ but incomplete) were included in this analysis, as complete motor cortex lesions with available hand function data ($N = 6$) always resulted in non-functional hand ability. Fisher's exact test found a significant effect of injury aetiology on functional outcome, indicating poorer functional outcome for acquired injuries ($P = 0.02$) compared to developmental lesions. Fisher's exact test for an effect of reorganization type on functional outcome also found a significant effect, indicating poorer functional outcome following IEHR ($P < 0.001$) when compared with IAHR.

## White matter tracts

In patients exhibiting IEHR, white matter tracts descending from the motor cortex were generally qualitatively non-viable. Additionally, significant asymmetry of pyramidal tracts between affected and unaffected hemispheres at the level of the cerebral peduncle was observed, with the pyramidal tracts in the intact hemisphere being much larger (Fig. 4A–C). The unaffected hemisphere also demonstrated more white matter underneath the motor cortex. In patients exhibiting IAHR, white matter tracts were qualitatively viable, and sufficient symmetry was observed at the subcortical cerebral peduncle level (Fig. 4D). In the four patients who exhibited IAHR with the acquisition of injury before the age of 2 years, the residual cortex connecting to white matter remained, although asymmetry of white matter density between hemispheres was still observed. Resulting motor functions were severely impaired for this sub-group.

# Discussion

The present study demonstrates novel information regarding developmental motor plasticity obtained through the use of an unprecedented clinical cohort size ($N = 52$) analysed with TMS. The results from the current study concur with the currently accepted developmental model of the regression of ipsilateral corticospinal projections by 24 months of postnatal development if significant acquired motor cortex injury does not occur. This is supported by our data, where 67% of children (20 of 30) who presented with an acquired injury before 2 years of age demonstrated IEHR. Although not statistically tested due to the small sample size of this sub-group, all patients with injury after the age of 2 years displayed IAHR (Supplementary Table 1). We also found that motor cortex COG distances in patients with IEHR were significantly shorter ($P < 0.001$) than those with IAHR, indicating bilaterally shared cortex in the case of IEHR. This highly significant difference is likely driven by our exclusion criteria, as only aberrant motor representations were included in the IAHR group; however, the significant amount of overlap between ipsilaterally and contralaterally projecting COGs observed in IEHR (Figs. 2B and 3A) indicates that cortical real estate is likely shared. Furthermore, the results demonstrate that lesion aetiology has an explicit effect on the resulting type of cortical reorganization. That is, acquired injuries are significantly more likely to induce IEHR than developmental disorders ($P < 0.001$). Finally, IEHR and acquired injuries resulted in significantly poorer hand function than IAHR and developmental disorders, respectively ($P < 0.001$ and $P = 0.02$).

The results from this study, namely the finding that cortical real estate is likely shared in the case of IEHR, yields insight into the mechanistic nature of IEHR. Descending corticospinal axon development has been repeatedly shown to be activity dependent.[10,11,22] That is, descending corticospinal axon connections are enhanced by actual axon use. Without axonal activity, the ipsilateral corticospinal axons regress.[22] In the case of complete unilateral motor cortex injury early in life, the use of the injured hemisphere's descending tracts becomes impossible. Therefore, the inherent

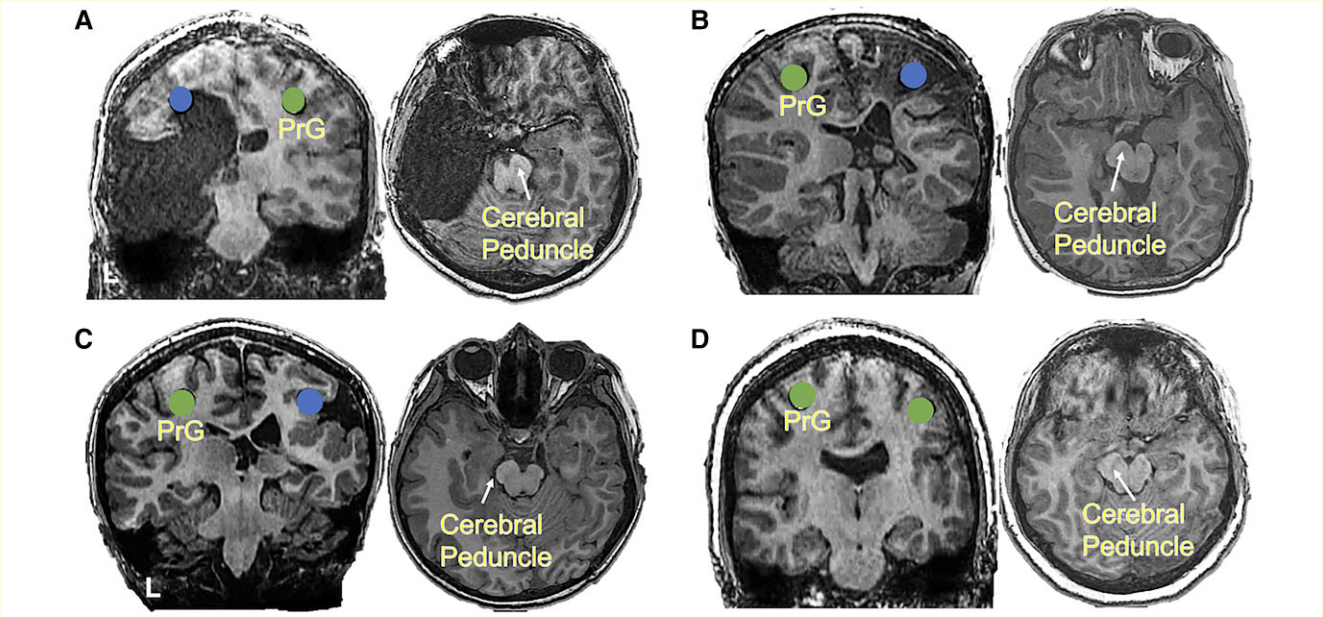


**Figure 4 Case examples of white matter tract viability.** PrG, precentral gyrus; green circles, viable motor cortex; blue circles, homologous inviable motor cortex. (**A**) An 18-year-old female suffering from left hemisphere traumatic brain injury sustained before 2 years of age and resulting IEHR with no remaining left hemisphere motor cortex function. The coronal view of the MRI shows no connection between the cortex and descending spinal tract and the axial view demonstrates the asymmetry of the cerebral peduncle. (**B**) A 6-year-old male suffering from right hemisphere traumatic brain injury before 2 years with no remaining right hemisphere motor cortex function and subsequent IEHR. Coronal MRI demonstrates sparse white matter within the right hemisphere; however, apparent lack of descending white matter and the presence of severely damaged right motor cortex results in non-viable cortex to white matter connectivity. The axial MRI demonstrates significant asymmetry of the cerebral peduncle. (**C**) An 11-year-old male with extensive right hemisphere polymicrogyria, especially affecting the motor cortex. This patient demonstrates a rare case of a developmental disorder resulting in subsequent IEHR. (**D**) A 19-year-old female with focal polymicrogyria who displays resulting IAHR. This patient's white matter tracts appear to be intact in both hemispheres, demonstrate a high degree of symmetry with respect to descending white matter volume.

activity-dependent competition favours the viable ipsilateral projections of the unaffected hemisphere, as contralateral projections are rendered obsolete. In the case of unilateral motor cortex injury involving descending white matter tracts, the activity-dependent nature of development coupled with the competition-free environment for contralesional ipsilateral projections most likely causes increased ipsilateral projection development, ultimately resulting in IEHR. Our results add to the understanding of this mechanism in the sense that it has now been shown that the cortical origins of ipsilateral and contralateral projections appear to be shared following IEHR. It can thus be inferred that the existing ipsilateral projections occurring early in development at least partially share descending corticospinal axons with contralateral projections. To establish bilateral alpha-motoneuron synapses following unilateral motor cortex injury early in life, increased ipsilateral axon activity likely promotes axonal sprouting in the distal muscles ipsilateral to the unaffected hemisphere, concurrent with the earlier postulated mechanistic models and primary findings.[21,26,29] This axonal sprouting establishes more extensive and enhanced connections, resulting in bilateral motor control of single hemispheric origin. Findings from our qualitative white matter tract analysis appear to support this notion. Figure 4 demonstrates that IEHR subjects show descending white matter proliferation of the unaffected hemisphere, especially when the contralateral lesioned cortex is unable to produce viable connectivity. The specifics of ipsilaterally projecting corticospinal networks present during development need further study, as their exact principles of connectivity are largely unknown. Diffusion tensor imaging would provide pertinent information towards a better understanding of mechanistic white matter connectivity following IEHR.

Contralateral and ipsilateral projections appear to share cortical area, implying that ipsilateral and contralateral corticospinal projections stem from the same axons; however, bilateral proliferation by way of axonal sprouting over time must eventually distinguish the laterality of muscle control.[44] This rewiring potentially uncrosses normally crossed neuronal pathways, as well as increases the total number of corticospinal projections.[12,22,45] The way in which cortical activity modulates lateralized muscle control is largely unknown. In healthy controls, differentiation between ipsilateral and contralateral descending pathways was implicated through differing corticomotor latencies.[45] Our population, however, displayed similar latencies for ipsilateral and contralateral innervation, suggesting that injury causes

differentiation through axonal sprouting of the same neurons. Thus, mediation of laterality control after the injury is likely to involve different mechanisms. Our finding that rMTs were significantly higher for ipsilateral than contralateral hand muscles (Table 3) indicates modulation of cortical excitability as a potential mechanism for differentiable control. This may involve enhancement of ipsilateral inhibitory control present in normal populations,[46] but this mechanism has yet to be examined in a patient population. Additionally, our cohort included 47 patients with a prior history of epilepsy and 44 patients with at least one AED prescription (see Supplementary Tables 1 and 2 for more detailed information regarding the history of epilepsy within our cohort). Epilepsy and AED have been shown to be associated with dysregulated cortical excitability, especially within Rolandic cortices.[47–49] This introduces a potential confounding variable within the proposed mechanism, as dysregulated cortical excitability may underlie the differences in rMT between ipsilateral and contralateral innervation. However, the within-subjects design of this study was meant to control for this confound, as subjects acted as their own control. In other words, the same cortical area was analysed against itself when testing for rMT differences, increasing the likelihood that excitability differences between ipsilateral and contralateral innervation are due to the neurophysiology of IEHR rather than comorbid epilepsy. Furthermore, we found no across-group differences in either the number of patients on AEDs or the number of AEDs prescribed, suggesting that our findings are not likely influenced by AEDs. Measuring the factors governing intracortical inhibition and intracortical facilitation in a patient population similar to ours (i.e. with comorbid epilepsy and IEHR or IAHR) in a more purposeful and directed manner may provide insight into the proposed mechanism of differentiating between the laterality of motor control in the event of IEHR.

Injuries to the motor cortex occurring after ipsilateral projection regression (after 2 years of age) almost always induce IAHR. Our finding that motor cortex COG reorganizes to new cortical area during IAHR confirms the implications made by other studies. Motor cortex reorganization to juxtalesional cortex is observed in Fig. 3. This study supports the claim that in the case of IAHR, parallel motor pathways originating from juxtalesional cortices outside of the primary motor cortex such as the premotor cortex, supplementary motor area and cingulate cortex may accept cortical motor control, aiding in functional recovery.[28,44,50] Each of the aforementioned cortical areas contain somatotopic representations and all contribute to the pyramidal tract.[24] These immediate corticomotor changes are most likely modulated by latent synapse unmasking through alterations in GABAergic inhibition, which are then reinforced through activity-dependent reinforcement by way of axonal regeneration, long-term potentiation and axonal sprouting.[2,29] Additionally, the way in which IAHR eligibility determinations were made (i.e. motor reorganization outside of the normally accepted deviation for primary hand motor cortex)[33–39] ensured that IAHR, as observed within our cohort, exemplified significant reorganization and juxtalesional motor acquisition similar to that of the aforementioned studies.[28,44,50]

In order for juxtalesional motor function acquisition to occur, cortical real estate must be readily available. Therefore, lesion size plays an important role in the resulting reorganization type. For example, it has been observed that large and incomplete motor cortex injuries resulted in IAHR, whilst large and complete motor cortex injuries showed a higher prevalence of IEHR.[20] These observations are corrobarated in our study, as every patient with a complete motor cortex injury ($N = 8$) exhibited IEHR, whilst large and incomplete injuries (i.e. >50% but incomplete motor cortex involvement) versus small and incomplete injuries (i.e. <50% motor cortex involvement) had no effect on the resulting type of reorganization ($P = 0.611$). Additionally, the eight patients with injury occurring before the age of 2 years and consequent IAHR demonstrated residual cortex connected to descending white matter tracts following their injury; however, each of these individuals demonstrated severe motor impairments with poor functional recovery. Although lesion size does play a significant role in reorganization type, these results suggest that other factors, such as lesion aetiology and lesion timing, most likely play a more definitive role in the resulting implications of corticomotor reorganization.

Our study found a statistically significant effect of lesion aetiology on resulting corticomotor reorganization, suggesting that acquired brain injuries are far more likely to induce IEHR, whilst developmental brain disorders seem to exhibit a robust tendency to maintain normal hemispheric motor control. Nevertheless, in our study, 3 of the 19 patients presenting with developmental lesion exhibited IEHR (example in Figs. 2B and 4C). This is in parallel to Maegaki *et al.*'s report[29] of a 13-year-old female presenting with extensive unilateral cortical dysplasia and mild hemiparesis exhibiting IEHR, a rare case of cortical dysplasia in which the motor areas failed to develop to functional levels. In these instances, the lack of descending white matter tract integrity due to pervasive developmental lesion is most likely the driving factor for IEHR. The overwhelming majority of children with developmental disorders in our study exhibited IAHR, demonstrating functional dysplastic cortex located within the motor areas. In concurrence with these findings, fMRI activation patterns in a recent study of two children with rolandic-area focal cortical dysplasia type IIb demonstrated functional dysplastic cortex, along with IAHR following surgical lesionectomy.[27] The robust maintenance of normal hemispheric motor control demonstrated throughout the majority of developmental disorder cases in our study and others suggest at least a partial functional role of motor cortex localized within the dysplastic lesion.

When considering the pathologies of the various developmental disorders present in this study, robust maintenance of normal hemispheric motor control appears intuitive. The three main developmental disorders present in this study—cortical dysplasia, polymicrogyria and grey matter

heterotopia—all result from abnormal neuronal migration during development.[51,52] Neurodevelopmental disorders involving neuronal migration abnormalities create fundamentally different anatomical implications than acquired injuries. Acquired injuries ensue blunt damage to key neural structures involved in motor control; developmental disorders, however, affect localization of corticomotor representation and its degree of functionality through abnormal neuronal migration. Specifically, in the case of polymicrogyria, the connection between corticomotor representation and underlying white matter, although altered, is usually not completely severed.[52] This maintenance of the cortex to white matter tract connections indicates at least partial motor control from the affected cortex. In the case of acquired injuries, especially very early on in development, white matter tracts and/or their connections to the cortex can be rendered completely non-viable. Figure 4 investigates this phenomenon in depth. Descending white matter tracts of IEHR patients were universally non-viable, as determined by the lack of MEP from the affected hemispheres, and significant asymmetry of white matter was observed in the cerebral peduncle (Fig. 4A and B). Taken together, the non-viable nature of the white matter tracts and functional consequences are consistent with the occurrence of IEHR due to the lack of viable cortex–white matter connection in the affected hemisphere. The asymmetry of the cerebral peduncle implies action-dependent development of descending ipsilateral motor neurons from the unaffected cortex. In contrast, Fig. 4D shows a patient presenting with right hemispheric focal polymicrogyria. As is evident in this patient's motor map (Fig. 3A), the primary hand motor cortex of the right hemisphere has localized directly over the area of polymicrogyria. Furthermore, this patient's dysgenic motor cortex maintained functional capability, although fine motor functional deficits were observed. A rare instance of IEHR pattern of reorganization in a patient with extensive polymicrogyria is shown in Fig. 4C. In this case, the asymmetry of the cerebral peduncle appears similar to the cases in both Fig. 4A and B. Thus, this case appears consistent with activity-dependent axonal sprouting of the viable hemisphere due to the severe nature of this patient's polymicrogyria producing non-viable cortex to white matter tract connections within the affected hemisphere. The two cases show how acquired injuries alter development through blunt force, whilst developmental disorders are more likely to maintain partial function. Ultimately, this study's findings indicate that developmental disorders of rolandic areas do not typically inhibit hemispheric competition enough to sufficiently recruit consistent activity of contralesional ipsilateral projections, whilst the damage caused by acquired injuries is more likely to irreversibly damage the descending cortex to white matter projections. This corroborates previously held notions[10] and is also concurrent with others' findings regarding the importance of white matter integrity and associated reorganization.[19]

The functional relevance of IAHR versus IEHR is largely unknown. Previous reports indicate that patients with IEHR had variable functional outcomes.[17,53] Some authors have found a positive correlation between ipsilateral MEPs and motor recovery, others a negative one.[54–56] When associated with recovery, the ipsilateral MEPs had low excitability thresholds and large amplitudes; when associated with poorer outcomes, only low amplitude MEPs were elicited at high-stimulation intensities.[53,54] However, it remains unclear if clinical, pathophysiological or methodological differences are responsible for the contrasting observations. In our study, IEHR and acquired injuries were independently associated with poor functional outcome, which is consistent with others.[19] Using our results and building off of previous studies,[11,19,26,57] we propose that acquired injuries, especially those severely affecting descending white matter tract integrity, significantly cause IEHR, which ultimately leads to poor functional outcome due to the difficulty of simultaneously modulating bilateral representation from a common cortical location.

In patients with early hemispherectomy, TMS of the intact hemisphere produced ipsilateral MEPs at latencies similar to contralateral MEPs, with higher amplitudes in proximal rather than distal muscles.[24,30] Patients with late hemispherectomy had ipsilateral MEPs of longer latencies and lower amplitudes with poorer outcome compared to early hemispherectomy patients.[24,30] In our study, 5 of the 52 patients underwent either complete or partial hemispherectomy at some point during their treatment. Each patient demonstrated functional improvement following the procedure. Furthermore, each patient underwent the procedure early enough (i.e. before 2 years of age) that the remaining hemisphere was able to acquire bilateral motor function. The beneficial results of hemispherectomy suggest a release of inhibitory or degrading functions from the affected hemisphere, which in turns leads to improved functional recovery.[20,58] Thus, in the case of IEHR and poor motor function, hemispherectomy may be a viable treatment for motor function recovery in addition to the elimination of seizures.

Additionally, the location of somatosensory cortex following corticomotor reorganization may play a role in the resulting functional outcome. Some have found that in patients with substantial sensorimotor lesions early in life, somatosensory cortex exhibits a robust tendency to maintain hemispheric orientation, even if motor function is reorganized to the opposite hemisphere.[17,59] The same investigators also found that when motor and sensory function are dissociated, the quality of motor function is usually more affected, irrespective of the degree of sensory impairment.[17,59] The link between sensory reorganization and motor reorganization needs further study, as the implications of differing sensory and motor reorganization patterns and their effect on functional recovery are currently not well understood.

Collectively, the novel information gained from this study regarding the underlying neurophysiological principles governing corticomotor reorganization may be useful in developing new and/or improved therapeutic techniques to assist in the recovery of motor function. For instance,

constraint-induced movement therapy (CIMT) has been repeatedly shown to facilitate beneficial neuroplastic changes following unilateral motor cortex injury. Interestingly, CIMT has been shown to elicit functional outcomes linked specifically to the type of reorganization present and the timing of therapeutic intervention relative to an injury.[60–62] Overall, this suggests that knowledge of basic neurophysiological principles regarding corticomotor reorganization type (IAHR or IEHR) is critical to facilitate the optimal level of functional recovery.

Finally, our results provide evidence for the safety and efficacy of TMS in localizing eloquent cortex. Studies comparing TMS to various neuroimaging modalities (e.g. PET, functional MRI and direct cortical stimulation) have revealed substantive TMS accuracy for such purposes, especially in patients with epilepsy, brain tumour and other neurological diseases.[31,32,63–70] Accurate localization of motor cortex is challenging in young and developmentally delayed patients, and many modalities require substantial compliance, natural sleep or sedation. Unlike other methods, TMS is well suited for mapping the motor cortices in children and patients with cerebral palsy or developmental delay. Because TMS directly activates the target neurons and corticospinal tract, it can identify the presence or absence of motor cortex regardless of the patient's motor function or ability, making it uniquely suited for use in those with hemiplegia or paresis. In this cohort, TMS is also useful in mapping treatment-induced changes in motor organization. Our study serves to add to the literature demonstrating the efficacy and safety of TMS in these populations, as well as its utility in studying the impaired motor system.

### Limitations

Due to the retrospective nature of this study, it was at times difficult to find clear measures on each patient. This difficulty stemmed from the broad age range of patients and clinically completed neuropsychological evaluations, resulting in discontinuity of motor tests performed. Ideally, a prospective study would delineate age-specific motor tests for patients with corticomotor reorganization, in order to better compare functional recovery across reorganization types. Another limitation to this study was our inability to compare corticomotor reorganization results across brain imaging modalities. Although TMS has been repeatedly shown to have high accuracy rates in comparison to other neuroimaging modalities, within-subject corticomotor representation accuracy would have benefited from the convergence of multi-modal brain imaging. More generally, retrospective chart review studies have inherent disadvantages, as repeated hospital visits result in data misinterpretation and diagnostic changes over years of evolving medical records. Future prospective longitudinal studies involving corticomotor reorganization, functional outcomes and therapeutic techniques catered to specific neurophysiological changes are needed. Finally, since this study is the first known study of its kind revealing the potential role of injury aetiology in resulting corticomotor reorganization and the nature of IEHR to share cortical real estate, studies seeking to replicate these results are critical.

## Conclusion

The present study examined a largely paediatric clinical cohort of unprecedented size and provided novel data regarding the basic underlying neurophysiological mechanisms of corticomotor reorganization. Key findings included that acquired injuries are much more likely to cause IEHR than IAHR due to the pathological nature of each lesion and that IEHR results in shared cortical representation of ipsilateral and contralateral muscles. Furthermore, IEHR and acquired injuries, respectively, were shown to produce poorer functional motor outcomes. These findings will aid in refining therapeutic techniques using exact neuroplastic principles to optimize functional outcome following injury to the motor cortex in the developing brain.

## Acknowledgements

The authors thank the Neuroscience Institute, Le Bonheur Children's Hospital, for the support.

## Funding

M.B. was funded by the Rhodes College and Le Bonheur Neuroscience Institute.

## Competing interests

The authors report no competing interests.

## Supplementary material

Supplementary material is available at *Brain Communications* online.

## References

1. Binder E, Leimbach M, Pool E-M, *et al*. Cortical reorganization after motor stroke: A pilot study on differences between the upper and lower limbs. *Hum Brain Mapp*. 2021;42:1013–1033.
2. Chen R, Cohen LG, Hallett M. Nervous system reorganization following injury. *Neuroscience*. 2002;111(4):761–773.
3. Pascual-Leone A, Amedi A, Fregni F, Merabet LB. The plastic human brain cortex. *Annu Rev Neurosci*. 2005;28(1):377–401.
4. Choi JT, Vining EPG, Mori S, Bastian AJ. Sensorimotor function and sensorimotor tracts after hemispherectomy. *Neuropsychologia*. 2010;48(5):1192–1199.
5. Dennis M. Margaret Kennard (1899–1975): Not a 'Principle' of brain plasticity but a founding mother of developmental neuropsychology. *Cortex*. 2010;46(8):1043–1059.

6. Krägeloh-Mann I, Lidzba K, Pavlova M, Wilke M, Staudt M. Plasticity during early brain development is determined by ontogenetic potential. *Neuropediatrics*. 2017;48(2):66–71.
7. Staudt M, Grodd W, Gerloff C, Erb M, Stitz J, Krägeloh-Mann I. Two types of ipsilateral reorganization in congenital hemiparesis: A TMS and fMRI study. *Brain*. 2002;125(10):2222–2237.
8. Inguaggiato E, Sgandurra G, Perazza S, Guzzetta A, Cioni G. Brain reorganization following intervention in children with congenital hemiplegia: A systematic review. *Neural Plast*. 2013;2013:1–8.
9. Ismail FY, Fatemi A, Johnston MV. Cerebral plasticity: Windows of opportunity in the developing brain. *Eur J Paediatr Neurol*. 2017;21(1):23–48.
10. Eyre JA, Taylor JP, Villagra F, Smith M, Miller S. Evidence of activity-dependent withdrawal of corticospinal projections during human development. *Neurology*. 2001;57:1543–1554.
11. Eyre JA. Development and plasticity of the corticospinal system in man. *Neural Plast*. 2003;10(1–2):93–106.
12. Sebastianelli L, Versace V, Taylor A, *et al*. Functional reorganization after hemispherectomy in humans and animal models: What can we learn about the brain's resilience to extensive unilateral lesions? *Brain Res Bull*. 2017;131:156–167.
13. Staudt M. (Re-)organization of the developing human brain following periventricular white matter lesions. *Neurosci Biobehav Rev*. 2007;31(8):1150–1156.
14. Staudt M. Reorganization after pre- and perinatal brain lesions. *J Anat*. 2010;217(4):469–474.
15. Narayana S, Gibbs SK, Fulton SP, *et al*. Clinical utility of transcranial magnetic stimulation (TMS) in the presurgical evaluation of motor, speech, and language functions in young children with refractory epilepsy or brain tumor: Preliminary evidence. *Front Neurol*. 2021;12:650830.
16. Fiori S, Guzzetta A. Plasticity following early-life brain injury: Insights from quantitative MRI. *Semin Perinatol*. 2015;39(2):141–146.
17. Gupta D, Barachant A, Gordon AM, *et al*. Effect of sensory and motor connectivity on hand function in pediatric hemiplegia. *Ann Neurol*. 2017;82(5):766–780.
18. Payne BR, Lomber SG. Reconstructing functional systems after lesions of cerebral cortex. *Nat Rev Neurosci*. 2001;2(12):911–919.
19. Holmström L, Vollmer B, Tedroff K, *et al*. Hand function in relation to brain lesions and corticomotor-projection pattern in children with unilateral cerebral palsy. *Dev Med Child Neurol*. 2010;52(2):145–152.
20. Irle E. Lesion size and recovery of function: Some new perspectives. *Brain Res Rev*. 1987;12(3):307–320.
21. Maegaki Y, Maeoka Y, Ishii S, *et al*. Mechanisms of central motor reorganization in pediatric hemiplegic patients. *Neuropediatrics*. 1997;28(3):168–174.
22. Martin JH, Kably B, Hacking A. Activity-dependent development of cortical axon terminations in the spinal cord and brain stem. *Exp Brain Res*. 1999;125(2):184–199.
23. Staudt M, Gerloff C, Grodd W, Holthausen H, Niemann G, Krägeloh-Mann I. Reorganization in congenital hemiparesis acquired at different gestational ages. *Ann Neurol*. 2004;56(6):854–863.
24. Hallett M. Plasticity of the human motor cortex and recovery from stroke. *Brain Res Rev*. 2001;36(2–3):169–174.
25. Jankowska E, Edgley SA. How can corticospinal tract neurons contribute to ipsilateral movements? A question with implications for recovery of motor functions. *Neuroscientist*. 2006;12(1):67–79.
26. Reddy H, De Stefano N, Mortilla M, Federico A, Matthews PM. Functional reorganization of motor cortex increases with greater axonal injury from CADASIL. *Stroke*. 2002;33(2):502–508.
27. Barba C, Montanaro D, Frijia F, *et al*. Focal cortical dysplasia type IIb in the rolandic cortex: Functional reorganization after early surgery documented by passive task functional MRI. *Epilepsia*. 2012;53(8):e141–e145.
28. Duffau H. Acute functional reorganisation of the human motor cortex during resection of central lesions: A study using intraoperative brain mapping. *J Neurol Neurosurg Psychiatry* 2001;70(4):506–513.
29. Maegaki Y, Yamamoto T, Takeshita K. Plasticity of central motor and sensory pathways in a case of unilateral extensive cortical dysplasia: Investigation of magnetic resonance imaging, transcranial magnetic stimulation, and short-latency somatosensory evoked potentials. *Neurology*. 1995;45(12):2255–2261.
30. Benecke R, Meyer B-U, Freund H-J. Reorganisation of descending motor pathways in patients after hemispherectomy and severe hemispheric lesions demonstrated by magnetic brain stimulation. *Exp Brain Res*. 1991;83(2):419–426.
31. Narayana S, Mudigoudar B, Babajani-Feremi A, Choudhri AF, Boop FA. Successful motor mapping with transcranial magnetic stimulation in an infant: A case report. *Neurology*. 2017;89(20):2115–2117.
32. Narayana S, Papanicolaou AC, McGregor A, Boop FA, Wheless JW. Clinical applications of transcranial magnetic stimulation in pediatric neurology. *J Child Neurol*. 2015;30(9):1111–1124.
33. Ahdab R, Ayache SS, Brugières P, Goujon C, Lefaucheur JP. Comparison of "standard" and "navigated" procedures of TMS coil positioning over motor, premotor and prefrontal targets in patients with chronic pain and depression. *Neurophysiol Clin Neurophysiol*. 2010;40(1):27–36.
34. Ahdab R, Ayache SS, Brugières P, Farhat WH, Lefaucheur J-P. The hand motor hotspot is not always located in the hand knob: A neuronavigated transcranial magnetic stimulation study. *Brain Topogr*. 2016;29(4):590–597.
35. Kantelhardt SR, Fadini T, Finke M, *et al*. Robot-assisted image-guided transcranial magnetic stimulation for somatotopic mapping of the motor cortex: A clinical pilot study. *Acta Neurochir (Wien)*. 2010;152(2):333–343.
36. Niskanen E, Julkunen P, Säisänen L, Vanninen R, Karjalainen P, Könönen M. Group-level variations in motor representation areas of thenar and anterior tibial muscles: Navigated transcranial magnetic stimulation study. *Hum Brain Mapp*. 2010;31:1272–1280.
37. Diekhoff S, Uludağ K, Sparing R, *et al*. Functional localization in the human brain: Gradient-echo, spin-echo, and arterial spin-labeling fMRI compared with neuronavigated TMS. *Hum Brain Mapp*. 2011;32(3):341–357.
38. Julkunen P, Ruohonen J, Sääskilahti S, Säisänen L, Karhu J. Threshold curves for transcranial magnetic stimulation to improve reliability of motor pathway status assessment. *Clin Neurophysiol*. 2010;122:975–983.
39. Roux F-E, Niare M, Charni S, Giussani C, Durand J-B. Functional architecture of the motor homunculus detected by electrostimulation. *J Physiol*. 2020;598(23):5487–5504.
40. Rossi S, Antal A, Bestmann S, *et al*. Safety and recommendations for TMS use in healthy subjects and patient populations, with updates on training, ethical and regulatory issues: Expert Guidelines. *Clin Neurophysiol*. 2021;132(1):269–306.
41. Wilson SA, Thickbroom GW, Mastaglia FL. Transcranial magnetic stimulation mapping of the motor cortex in normal subjects. *J Neurol Sci*. 1993;118(2):134–144.
42. Karl A, Birbaumer N, Lutzenberger W, Cohen LG, Flor H. Reorganization of motor and somatosensory cortex in upper extremity amputees with phantom limb pain. *J Neurosci*. 2001;21-(10):3609–3618.
43. Kwon HG, Hong JH, Jang SH. Anatomic location and somatotopic arrangement of the corticospinal tract at the cerebral peduncle in the human brain. *Am J Neuroradiol*. 2011;32(11):2116–2119.
44. Fries W, Danek A, Scheidtmann K, Hamburger C. Motor recovery following capsular stroke: Role of descending pathways from multiple motor areas. *Brain*. 1993;116(2):369–382.
45. Ziemann U, Ishii K, Borgheresi A, *et al*. Dissociation of the pathways mediating ipsilateral and contralateral motor-evoked

potentials in human hand and arm muscles. *J Physiol*. 1999;518(3): 895–906.
46. Chen R, Yung D, Li J-Y. Organization of ipsilateral excitatory and inhibitory pathways in the human motor cortex. *J Neurophysiol*. 2003;89(3):1256–1264.
47. Pawley AD, Chowdhury FA, Tangwiriyasakul C, *et al*. Cortical excitability correlates with seizure control and epilepsy duration in chronic epilepsy. *Ann Clin Transl Neurol*. 2017;4(2):87–97.
48. Andreasson A-C, Sigurdsson GV, Pegenius G, Thordstein M, Hallböök T. Cortical excitability measured with transcranial magnetic stimulation in children with epilepsy before and after antiepileptic drugs. *Dev Med Child Neurol*. 2020;62(7):793–798.
49. Hamed SA, Tohamy AM. Mohamed KO, el Mageed Abd el Zaher MA. The effect of epilepsy and antiepileptic drugs on cortical motor excitability in patients with temporal lobe epilepsy. *Clin Neuropharmacol*. 2020;43(6):175–184.
50. Dum R, Strick P. The origin of corticospinal projections from the premotor areas in the frontal lobe. *J Neurosci*. 1991;11(3): 667–689.
51. Desikan RS, Barkovich AJ. Malformations of cortical development. *Ann Neurol*. 2016;80(6):797–810.
52. Squier W, Jansen A. Polymicrogyria: Pathology, fetal origins and mechanisms. *Acta Neuropathol Commun*. 2014;2(1):80.
53. Caramia MD, Iani C, Bernardi G. Cerebral plasticity after stroke as revealed by ipsilateral responses to magnetic stimulation. *NeuroReport*. 1996;7(11):1756–1760.
54. Turton A, Wroe S, Trepte N, Fraser C, Lemon RN. Contralateral and ipsilateral EMG responses to transcranial magnetic stimulation during recovery of arm and hand function after stroke. *Electroencephalogr Clin Neurophysiol Mot Control*. 1996; 101(4):316–328.
55. Hendricks HT, Hageman G, van Limbeek J. Prediction of recovery from upper extremity paralysis after stroke by measuring evoked potentials. *Scand J Rehabil Med*. 1997;29(3):155–159.
56. Netz J. Reorganization of motor output in the non-affected hemisphere after stroke. *Brain*. 1997;120(9):1579–1586.
57. Eyre J. Corticospinal tract development and its plasticity after perinatal injury. *Neurosci Biobehav Rev*. 2007;31(8):1136–1149.
58. Chiricozzi F, Chieffo D, Battaglia D, *et al*. Developmental plasticity after right hemispherectomy in an epileptic adolescent with early brain injury. *Childs Nerv Syst*. 2005;21(11):960–969.
59. Guzzetta A, Bonanni P, Biagi L, *et al*. Reorganisation of the somatosensory system after early brain damage. *Clin Neurophysiol*. 2007;118(5):1110–1121.
60. Walther M, Juenger H, Kuhnke N, *et al*. Motor cortex plasticity in ischemic perinatal stroke: A transcranial magnetic stimulation and functional MRI study. *Pediatr Neurol*. 2009;41(3):171–178.
61. Matusz PJ, Key AP, Gogliotti S, *et al*. Somatosensory plasticity in pediatric cerebral palsy following constraint-induced movement therapy. *Neural Plast*. 2018;2018:1–14.
62. Okabe N, Himi N, Nakamura-Maruyama E, *et al*. Very early initiation reduces benefits of poststroke rehabilitation despite increased corticospinal projections. *Neurorehabil Neural Repair*. 2019; 33(7):538–552.
63. Wassermann EM, Wang B, Zeffiro TA, *et al*. Locating the motor cortex on the MRI with transcranial magnetic stimulation and PET. *NeuroImage*. 1996;3(1):1–9.
64. Thickbroom GW, Byrnes ML, Mastaglia FL. A model of the effect of MEP amplitude variation on the accuracy of TMS mapping. *Clin Neurophysiol*. 1999;110(5):941–943.
65. Krieg TD, Salinas FS, Narayana S, Fox PT, Mogul DJ. PET-based confirmation of orientation sensitivity of TMS-induced cortical activation in humans. *Brain Stimul*. 2013;6(6):898–904.
66. Forster M-T, Hattingen E, Senft C, Gasser T, Seifert V, Szelényi A. Navigated transcranial magnetic stimulation and functional magnetic resonance imaging: Advanced adjuncts in preoperative planning for central region tumors. *Neurosurgery*. 2011;68(5):1317–1325.
67. Uy J, Ridding MC, Miles TS. Stability of maps of human motor cortex made with transcranial magnetic stimulation. *Brain Topogr*. 14(4):293–297.
68. Mäkelä JP, Vitikainen A-M, Lioumis P, *et al*. Functional plasticity of the motor cortical structures demonstrated by navigated TMS in two patients with epilepsy. *Brain Stimul*. 2013; 6(3):286–291.
69. Vitikainen A-M, Lioumis P, Paetau R, *et al*. Combined use of noninvasive techniques for improved functional localization for a selected group of epilepsy surgery candidates. *NeuroImage*. 2009; 45(2):342–348.
70. Vitikainen A-M, Salli E, Lioumis P, Mäkelä JP, Metsähonkala L. Applicability of nTMS in locating the motor cortical representation areas in patients with epilepsy. *Acta Neurochir (Wien)*. 2013; 155(3):507–518.